ATOMISTIC MODELING OF ENVIRONMENTAL AGING OF EPOXY RESINS

A Dissertation
Presented to
The Academic Faculty

by

YAO LI

In Partial Fulfillment
of the Requirements for the Degree
Doctor of Philosophy in the
School of Materials Science and Engineering

Georgia Institute of Technology
May 2012

ATOMISTIC MODELING OF ENVIRONMENTAL AGING OF EPOXY RESINS

Approved by:

Dr. Karl Jacob, Advisor
School of Materials Science and Engineering
Georgia Institute of Technology

Dr. Yonathan Thio
School of Materials Science and Engineering
Georgia Institute of Technology

Dr. Steven Johnson
School of Materials Science and Engineering
Georgia Institute of Technology

Dr. Donggang Yao
Materials Science and Engineering
Georgia Institute of Technology

Dr. David McDowell
School of Mechanical Engineering
Georgia Institute of Technology

Date Approved: Feb 24 2012

ACKNOWLEDGEMENTS

First of all, I would like to thank NASA Langley research center for providing financial support to conduct this work. I really appreciate Dr. Jeffery Hinkley and Dr. Kristopher Wise serving as great collaborator and excellent mentor.

Special thanks go to my PhD advisor Dr. Karl Jacob, without whom this work would not be possible. Dr. Jacob provided me invaluable guidance throughout my journey as a graduate student not only in research but also in my personal development and career.

I would like to thank members of my dissertation committee: Dr. Steven Johnson, Dr. David McDowell, Dr. Donggang Yao and Dr. Yonathan Thio for their valuable feedback and the time they spent reading my thesis.

Thanks to all the previous and current group members and friends I met here for making my life easier, enjoyable and full of fun.

Last, but not the least, I would like to express my special gratitude to my wife Ying Cao. Without her love, encouragement and support, I would certainly not be here today and for that I am extremely grateful. I also would like to thank my parents and parents-in-law for their unconditional support and patience.

TABLE OF CONTENTS

LIST OF TABLES

LIST OF FIGURES

LIST OF SYMBOLS AND ABBRIVATIONS

Å	angstrom
atm	atmospheric pressure
DDS	4,4'-diaminodiphenylsulphone
DETDA	diethyltoluenediamine
DGEBA	diglycidyl ether of bisphenol A
fs	femtosecond
MD	Molecular dynamics
nm	nanometer
PA	primary amine
ps	picosecond
SA	secondary amine
TA	tertiary amine
T_g	glass transition temperature
TGDDM	tetraglycidyl-4,4'-diamino-diphenylmethane

SUMMARY

Epoxy resins are finding widespread applications in a variety of structural applications, including demanding aerospace structures. Thus, understanding the behavior of epoxy is very important to design structures and to understand the reliability of them. Polymers undergo aging with time, diminishing their properties. Therefore understanding the effective life span of such epoxy structures, during which the material is safe, is a very important design criterion. Exhaustive experimental studies are costly and time consuming. Thus, computational approaches are attractive to at least in identifying promising candidates for further experimental studies. In this work, nanoscale epoxy resins were modeled using all atom representations in a simulation box, to understand their behavior. Tetrafunctional epoxy and corresponding multifunctional amine were chosen as model materials, since they are used widely in the industry. Algorithms of constructing interconnected network structures were developed to accurately incorporate the chemical structures and geometrical aspects of epoxy with minimum cost. Monomers were generated in a diamond lattice and crosslinked to model complex epoxy multifunctional network. These initial polymer structures were relaxed and equilibrated using molecular dynamics and a suitable potential function, known as force field, representing interactions between molecular units. Physical, thermal and mechanical properties obtained from equilibrated epoxy samples are found to be in good agreement with experimental results.

Possible impact of chemical degradation was studied by incorporating oxidation and hydrolysis in the simulation process. Mechanism of degradation was based on bond

reaction probabilities and chemical structures of epoxies. Network structures have different architectural aspects, the chain length between cross-links, number of cross-links per unit volume, the chemical structure of the chains, etc. Both oxidation and hydrolysis were found to decrease materials' performances by reducing the number of crosslinking points. Elastic modulus of materials was directly related to crosslinking density. Hydrolysis has a more severe effect on degrading materials properties since chain scission only takes place at network nodes.

Interfaces between two types of epoxies were constructed to study interactions at interfaces. Covalent bonds linking two components play an important role in interfacial strength. Free volume calculation, representing a measure of the unoccupied volume, helps to identify and monitor generation of crazes and voids within materials. It was found that voids and cracks initiate and grow at interfaces and lead to materials failures. Compatibilizer layers can improve overall composite performances by preventing void growth at interfaces.

Water absorption and diffusion in epoxy matrix was also examined. Diffusion pattern of water in epoxy resins was studied by tracking displacements of single molecules in specific time intervals. The typical jump-diffuse pattern seems to agree for epoxy system and is consistent with other properties of epoxy systems. The characteristic pattern of water diffusion in epoxies was interpreted by a free volume theory. A large number of small voids in epoxy confine water molecules' ability of movement. Meanwhile, hydrogen bonds between polymer and water also constrain mobility of water. Formation of water clusters increases diameters of penetrants and affect the jump dynamics. Mechanical modulus of wet epoxy resin was found to be higher than neat epoxy due to the presence of hydrogen bonds.

A reactive force field was introduced to study thermal degradation behavior of epoxy resins. Variation of different types of covalent bonds and number of effective chains were tracked during heating processes and analyzed to uncover the degradation mechanism of epoxy resins. Order-of-bond scission obtained from simulation agrees well with experimental results. Effects of chemical environments were studied by adding water or oxygen molecules into the nanoscale material. It was found that oxygen reacted with epoxy continuously but did not destroy network structures. Water molecules decreased decomposition temperature of epoxy by swelling network structures.

CHAPTER 1

INTRODUCTION

1.1 Polymer Network

Polymer network is generally referred to as an interconnected structure of polymer chains, connecting various nodal points known as cross-links. The composition and length of polymer chains can be varied, and the number of chains connected with a specific cross-linking point can be designed using an appropriate cross-linking agent. Highly crosslinked polymer networks have very good physical and mechanical properties due to extensive presence of covalent bonds, entanglements and other interactions between chains. Cross-linking tends to increase glass transition temperature (T_g), and strength. Rubber and epoxy polymers are the two commonly used types of polymer networks. Hydrogels are another category of polymer networks interconnected by hydrogen bonds.

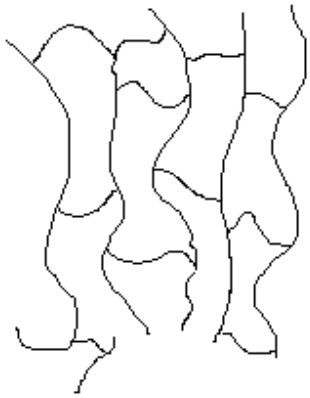

Figure 1-1. A scheme of polymer network.

To synthesize a polymer chain, monomers must have functional groups to create linkages with other monomers. Usually linear or branched chain will result from such polymerization. To construct a network, monomers should have higher degree of functionality to form junctions, where other chains can connect, different from linear polymers. A network can be defined and characterized by several parameters: the average junction functionality, the molecular weight of chains between two junctions, the number of junctions per unit volume, and the number of chains per unit volume as well as the degree of cross-linking. The number of functional groups in monomers, which is larger than two, boosts the complexity of network structures. Researchers have been trying to investigate the detailed structures of polymer networks and how they are related to macroscopic properties. Experimental approach basically involves trying to synthesize various network structures in a systematic fashion, and characterizing them to identify the basic parameters that maximize properties. Once that is identified, polymer network with optimal properties can be synthesized. However, this is a time consuming procedure. The reason is that chemical linkages are not totally predictable between multi-functional reactive groups. In addition, side reactions always take place and reaction rate coefficients depend on several factors (such as temperature, chemical environment). For example, the reaction rate coefficients of primary amine and secondary amine may fluctuate significantly when the viscosity of a reaction system prevents heat from spreading and molecules from moving at a high degree of crosslinking [1].

1.1.1 Epoxies

Epoxies are a class of polymers with a network structure. Epoxies are formed from two components, which are referred as epoxide resins and curing agents. Epoxide resins are chemicals with two or more epoxide groups at the ends of monomer backbones. Figure 1-2 shows the chemical structure of an epoxide monomer. Most common epoxy resins are produced from a reaction between epichlorohydrin and bisphenol-A, though the latter may be replaced by similar chemicals. Bisphenol-A brings benzene rings into chemical structures of epoxy network, which can improve mechanical strength and thermal stability of epoxies. Curing agents of epoxy resins are a category of chemicals with varying functional groups which can react with epoxide groups to form covalent bonds. A majority of curing agents are amines.

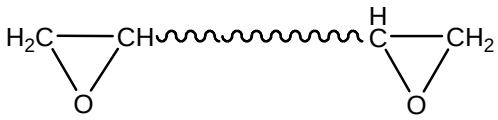

Epoxide

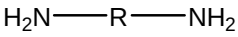

Amine

Figure 1-2. Chemical structures of an epoxide molecule and an amine curing agent.

Reaction mechanism between epoxide and amine to form network structure is shown in Figure 1-3. The reaction process is often called “curing”. Curing is always carried out at a temperature range from 100℃ to 20 0℃. Curing involves (1) an epoxide group reacts with a primary amine group to link secondary carbon atom with nitrogen atom and yield a hydroxyl group and a secondary amine group. Also (2), another epoxide group reacts with a secondary amine to yield a tertiary amine. After reactions (1) and (2), network structure is built as tertiary amine atoms serve as crosslinking points.

The third reaction takes place between epoxide groups and hydroxyl groups produced before. The exact mechanism of this step is still under debate. The question is whether the secondary carbon or the tertiary carbon in epoxide group will connect to oxygen atom in hydroxyl group. No matter what the mechanism is; oxygen atoms in hydroxyl groups will also serve as interlinking points in epoxies.

The kinetics of three reactions can be described as given in Figure 1-4. In Figure 1-4, the paired square bracket [ ] means concentrations of certain groups in reaction system. SA refers secondary amine; PA is primary amine; EP stands for epoxide; TA is tertiary amine; O refers ether oxygen and OH is hydroxyl group. k_i is reaction rate constant.

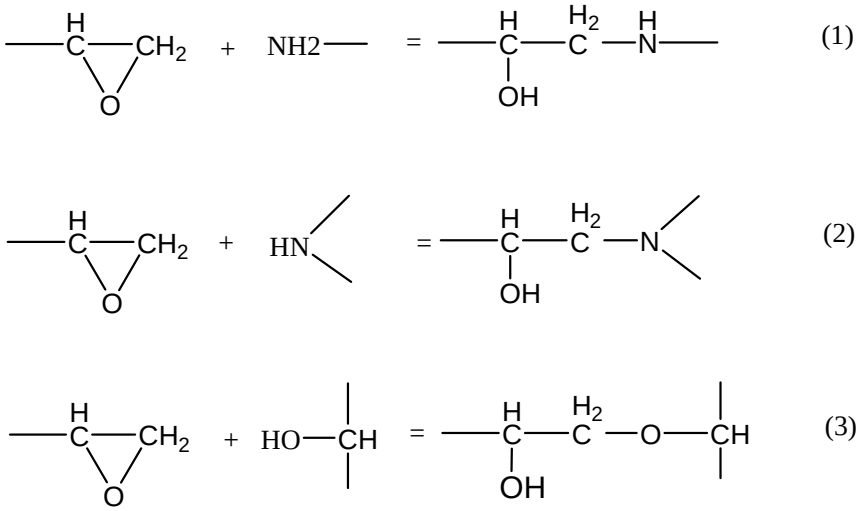

Figure 1-3. Chemical reactions take place in a curing process of epoxide and amine.

$$[SA] = k_1 \cdot [PA] \cdot [EP]$$

$$[TA] = k_2 \cdot [SA] \cdot [EP]$$

$$[O] = k_3 \cdot [OH] \cdot [EP]$$

Figure 1-4. Kinetics of chemical reactions between epoxide and amine.

Reaction rate constant of each reaction is related to specific structures of epoxide and amine and temperature dependent. Etherification is known to occur only at high temperature and advanced degrees of cure, so reaction (3) is always neglected [2, 3]. The ratio of k_1/k_2 varies from systems to systems and has been well investigated in the past decades [4]. If there is no substitution effect, k_1 should be the same as k_2. However, because of spatial hindrance or electron arrangement imposed by substitution groups, the ratio of k_1/k_2 always does not equal to one. A general rule k_1 is greater than k_2. Figure 1-5 lists values of k_1 and k_2 for different curing systems. Change of either the epoxide monomer or the curing agent will lead to variation of k_1/k_2.

System	$k_1/10^{-3}$ ($kg^3\ mol^{-2}\ min^{-1}$)	$k_2/10^{-3}$ ($kg^3\ mol^{-2}\ min^{-1}$)	k_2/k_1
TGDDM/DDS	10.2	2.15	0.21
TGDDM/DETDA	13.4	11.3	0.84
TGDDM/DMTDA	2.75	2.75	1.00
TGAP/DDS	12.5	2.55	0.20
TGAP/DETDA	15.8[a]	8.48[a]	0.53
TGAP/DMTDA	3.8	3.8	1.0
DGEBA/DDS	15.5	3.5	0.23
DGEBA/DETDA	43.4[a]	8.34[a]	0.19
DGEBA/DMTDA	10.6	4.5	0.42

[a] Calculated from the activation energy.

Figure 1-5. Reaction rate coefficients at 160℃ for different epoxy/amine systems. [4]

1.1.2 Properties of epoxies

Because of exceptional properties of epoxies, epoxy-based materials are widely used as adhesives, coatings, composite materials, electronic packaging materials,

aerospace structural materials and so on. Its properties are related primarily to chemical compositions, and commonly used epoxies are known for their excellent adhesion, chemical and heat resistance, excellent mechanical properties and very good electrical insulating properties. More importantly, as a composite matrix, some properties of epoxies can be modified while maintaining the other properties, giving additional flexibility to the system. For example, metal particle/epoxy composites can be electrically conductive with retaining its excellent adhesion and moisture resistance properties.

Pre-cured epoxide and amine blends are viscous liquid and gradually become semi-transparent solid during curing process. Cured epoxy may be red, yellow or colorless depending on chemical compositions. Table 1-1 lists typical properties of two epoxy adhesive materials. It is worth mentioning that these properties are related to the specific curing steps involved, curing temperature and the amount of other additives. Generally, epoxies show outstanding overall performance compared to other polymers of similar weight and geometry.

Table 1-1. Properties of some epoxy adhesives. [5-8]

Properties	TGDDM/DDS	DGEBA/DETDA
Density (g/cm^3)	1.23	1.08
Young's modulus (GPa)	5.0	2.7
Volumetric CTE (ppm/℃)	150	240
Maximum water absorption (wt%)	4 ~ 7	5 ~ 8
T_g (℃)	260	217
Degradation Temperature (℃)	390	360

1.2 Simulation of polymers

Instead of an experimental approach, that involves making samples and characterizing them, computational methods offer a less expensive route at least to eliminate several candidates for further experimental studies. In addition, computational methods provide a way to study material systems such as polymers with complex architecture and components. Compared to metals, small molecular liquids and crystals of small molecules, the length scales of polymers in melts, blends and solutions can vary from nanometer to microns, millimeters and larger. The corresponding time scales associated with the dynamic processes relevant for different materials properties span an even wider range, from femtoseconds to milliseconds, even seconds or hours in glassy materials or for large scale ordering processes such as phase separation in blends. No single model or simulation algorithm can cover this range of length and time scales. Therefore, simulation models at different scales for polymeric materials range from those including quantum effects and electronic degrees of freedom; chemically realistic, classical models; to coarse-grained, particle-based mesoscale models that retain only the most essential elements of the polymer system to be simulated; to field-theoretic models that describe the polymer system in terms of density or composition variables [9]. One of the most important and challenging problems in computational materials research is bridging of length and time scales and the linking of computational methods to predict the behavior and the associated properties of the materials from fundamental molecular levels. Here, a brief overview of these simulation methods will be given in this dissertation. The overview will be organized roughly in the order of the length and time scales where these methods are applicable.

1.2.1 Overview of multi-scale simulation methods

The modeling and simulation methods at molecular level usually deal with electrons, atoms, molecules or their clusters as the basic units considered. The most popular methods include molecular mechanics (MM), molecular dynamics (MD) and quantum mechanics (QM). Modeling of polymers at this scale is predominantly directed toward understanding the underlying fundamental thermodynamics and kinetics of the formation of bonds, molecular structure and interactions. Among these methods, MD and MM are two major tools used in this research. Details of MM and MD will be discussed later.

The modeling and simulation at microscale aim to bridge molecular methods and continuum methods and avoid their shortcomings. For instance, in nanoparticle–polymer composite systems, the study of structural evolution (i.e., dynamics of phase separation and particle aggregation) involves the description of bulk flow (i.e., hydrodynamic behavior) and the interactions between nanoparticles and polymer matrix. Note that hydrodynamic behavior is relatively straightforward to handle by continuum methods but is very difficult and relatively expensive to treat by atomistic methods. In contrast, the atomic specific interactions between components can be examined at an atomistic level modeling but are usually not easily incorporated at the continuum level. Therefore, various simulation methods have been used alone and in combination with other methods to link hierarchical scales to study the microscopic structural and phase separation behavior of polymers and polymer composites, including Brownian dynamics (BD), dissipative particle dynamics (DPD), lattice Boltzmann (LB) and dynamic density functional theory (DDFT). In these methods, a polymer system is usually treated with a

field description or as microscopic particles that incorporate molecular details implicitly. Therefore, they are able to simulate the phenomena on larger length and time scales currently inaccessible by the classical MD methods.

Macroscale methods ignore the discrete atomic and molecular structure and assume that the material is continuously distributed throughout its volume. The continuum material is thus assumed to have an average density and can be subjected to body forces such as gravity and surface forces. Generally speaking, the macroscale methods account for the fundamental laws of: (i) continuity, derived from the conservation of mass; (ii) equilibrium, derived from momentum considerations and Newton's second law; or the impulse - momentum relation, (iii) the moment of momentum principle, based on the model that the time rate of change of angular momentum with respect to an arbitrary point is equal to the resultant moment; (iv) conservation of energy, based on the first law of thermodynamics. These laws provide the basis for continuum models and must be coupled with the appropriate constitutive equations and the equations of state to provide all the governing equations necessary for solving a continuum problem. The continuum method relates the deformation of a continuous medium to external forces or fields acting on the medium and the resulting internal stresses and strains. Computational approaches range from simple closed-form analytical expressions to systems with well defined geometry, ranging from beam, plate and shell theory to numerical methods for systems with complex geometry. While closed form micromechanics solutions can be applied to a range of problems in polymer composites, such as Halpin–Tsai model[10] and Mori–Tanaka model[11], other methods such as equivalent-continuum model, self-consistent model and finite element analysis can also be used. Although these methods can be used in understanding the behavior of

epoxy composites, this category of simulation methods is not the scope covered in this investigation.

1.2.2 Molecular mechanics

Molecular Mechanics (MM) method refers to the use of Newtonian mechanics to model molecular systems at zero degree Kelvin. In MM the potential energy within the system resulting from the interactions between atomic units is calculated using what is known as force fields that approximate atomic interaction potential as a function of atomic positions or charge interactions. The MM deals with atomic units or particles. In general particles can be single atoms or virtual particles containing a group of atoms. Therefore, molecular mechanics can be used to study small molecules as well as large biological systems or material assemblies with many thousands to millions of atoms. When every atom is treated as a particle, this is called all-atom model. As a comparison, if a union of several atoms is seen as a basic particle, then a united-atom assumption is made. For example, many simulations have historically used the united-atom assumption in which methyl and methylene groups were represented as a single particle, and large protein systems are commonly simulated using a "bead" model that assigns two to four particles per amino acid. Molecular mechanics methods usually have the following features:

- Each particle is assigned a mass, coordinate, radius (typically the van der Waals radius), polarizability, and a constant net charge (generally derived from quantum calculations and/or experiment);

- Interactions between particles are defined by a series of equations representing the potential energy as a function of particle positions, which are known as force fields.

Potential functions or force field as it is generally called are used in both MM and MD, with which the interactions between atoms and total energies in simulation system are computed. The parameters associated with the functional forms of potentials in a force field can be empirical, semi-empirical or ab initio. The criteria for selecting a force field include accuracy, transferability and computational speed. A typical interaction potential *U* for polymers may consist of a number of bonded and nonbonded interaction terms:

$$U(\vec{r}_1,\vec{r}_2,\ldots,\vec{r}_N)=\sum_{i_{bond}}^{N_{bond}}U_{bond}(i_{bond},\vec{r}_a,\vec{r}_b)+\sum_{i_{angle}}^{N_{angle}}U_{angle}(i_{angle},\vec{r}_a,\vec{r}_b,\vec{r}_c)$$

$$+\sum_{i_{torsion}}^{N_{torsion}}U_{torsion}(i_{torsion},\vec{r}_a,\vec{r}_b,\vec{r}_c,\vec{r}_d)+\sum_{i_{inversion}}^{N_{inversion}}U_{inversion}(i_{inversion},\vec{r}_a,\vec{r}_b,\vec{r}_c,\vec{r}_d)$$

$$+\sum_{i=1}^{N-1}\sum_{j>i}^{N}U_{vdw}(i,j,\vec{r}_a,\vec{r}_b)+\sum_{i=1}^{N-1}\sum_{j>i}^{N}U_{electrostatic}(i,j,\vec{r}_a,\vec{r}_b) \quad (1\text{-}1).$$

The first four terms represent bonded interactions, i.e., bond stretch U_{bond}, bond-angle bend U_{angle} and dihedral angle torsion $U_{torsion}$ and inversion interaction $U_{inversion}$, while the last two terms are non-bonded interactions, i.e., van der Waals energy U_{vdw} and electrostatic energy $U_{electrostatic}$. In the equation, $\vec{r}_a$, $\vec{r}_b$, $\vec{r}_c$ and $\vec{r}_d$ are the positions of the atoms or particles specifically involved in a given interaction; N_{bond}, N_{angle}, $N_{torsion}$ and $N_{inversion}$ stand for the total numbers of these respective interactions in the simulated

system; i_{bond}, i_{angle}, $i_{torsion}$ and $i_{inversion}$ uniquely specify an individual interaction of each type; *i* and *j* in the van der Waals and electrostatic terms refer to the pair of specific atoms involved in the interaction. Equation 1-2 gives a detailed description of AMBER force field, which was developed and widely applied for simulation of biological and organic molecules.

$$U_{total} = \sum_{bonds} K_r \left(r - r_{eq}\right)^2 + \sum_{angles} K_\theta \left(\theta - \theta_{eq}\right)^2 +$$

$$\sum_{dihedrals} \frac{V_n}{2} [1 + \cos(n\emptyset - \gamma) + \sum_{i<j} \left[\frac{A_{ij}}{R_{ij}^{12}} - \frac{B_{ij}}{R_{ij}^{6}} + \frac{q_i q_j}{\epsilon R_{ij}}\right] \quad (1\text{-}2).$$

Different force fields differ depending on the functional form of the potential function. In addition to the functional form of the potentials, a force field defines a set of parameters for each type of atom. For example, a force field would include distinct parameters for an oxygen atom in a carbonyl functional group and in a hydroxyl group. The typical parameter set includes values for atomic mass, van der Waals radius, and partial charge for individual atoms, and equilibrium values of bond lengths, bond angles, and dihedral angles for pairs, triplets, and quandruplets of bonded atoms, and values corresponding to the effective spring constant (linear or non-linear) for each potential. Although many molecular simulations involve biological macromolecules such as proteins, DNA, and RNA, the parameters for given atom types are generally derived from observations on small organic molecules that are more tractable for experimental studies and quantum calculations. Popular force fields include: AMBER [12] -widely used for proteins and DNA; CHARMM [13]-widely used for both small molecules and macromolecules; CVFF [14]-broadly used for small molecules and macromolecules; QCFF [15] -for conjugated molecules; CFF [16] - adapted to a broad variety of organic compounds, includes force fields for polymers and metals.

The classical MM approach is energy minimization. That is, the force field is used as an optimization criterion and the minimum of U_{total} searched by an appropriate algorithm (e.g. steepest descent). Molecular mechanics potential energy functions have been used to calculate binding constants [17, 18], protein folding kinetics , protonation equilibria [19], active site coordinates, and to design binding sites, etc.

MM and MD are related but different. Main purpose of MD is modeling of molecular motions, although it is also applied for optimization, for example using simulated annealing or stretching. Thus, as opposed to MM, MD has a specific non-zero temperature associated with it. MM implements more "static" energy minimization methods to study the potential energy surfaces of different molecular systems. However, MM can also provide important dynamic parameters, such as energy barriers between different conformers or steepness of a potential energy surface around a local minimum. MD and MM are usually based on the same classical force fields. But MD may also be based on quantum chemical methods such as DFT. MM is also loosely used to define a set of techniques in molecular modeling.

1.2.3 Molecular dynamics

Molecular Dynamics (MD) is a simulation methodology based on the well-familiar Newton's law, relating force with the rate of change of momentum, namely:

$$\vec{F} = m\vec{a} \qquad (1\text{-}3).$$

All the atoms and/or molecules in the simulation box are treated as classical particles obeying Newton's equations, and the positions and velocities of each atom can be calculated knowing the positions and velocities at the current time knowing the position

and velocity of the particles at a short time interval before, once the forces acting on each atom are computed. Forces are derived from a conservative potential function as described before, also known as force fields, arising from the interactions between the units of the material present in the simulation box.

Assuming that we have *N* particles in the system, we have *6N* independent variables: positions $\vec{r}_1, \vec{r}_2, \ldots, \vec{r}_N$ and velocities $\vec{v}_1, \vec{v}_1, \ldots, \vec{v}_N$. Derived from the classical dynamics, positions and velocities of particles are related as

$$\frac{d\vec{r}_i}{dt} = \vec{v}_i \qquad (1\text{-}4).$$

and $$\frac{d\vec{v}_i}{dt} = \frac{\vec{f}_i}{m_i} = \frac{d^2\vec{r}_i}{dt^2} \qquad (1\text{-}5).$$

where $\vec{f}_i$ is the force vector acting on particle *i* . In order to implement Equations 1-4 and 1-5 in a simulation algorithm, and numerical integration is employed instead of analytical integration. If the position of particle *i* at time *t* is known as $\vec{r}_i(t)$, using the Taylor's expansion, the position of the particle at time *t+Δt* is given by

$$\vec{r}_i(t+\Delta t) = \vec{r}_i(t) + \Delta t \cdot \dot{\vec{r}}_i(t) + \frac{(\Delta t)^2}{2}\ddot{\vec{r}}_i(t) + \frac{(\Delta t)^3}{6}\dddot{\vec{r}}_i(t) + O((\Delta t)^4) \qquad (1\text{-}6).$$

Substituting Equation 1-4 and 1-5 into Equation 1-6,

$$\vec{r}_i(t+\Delta t) = \vec{r}_i(t) + \Delta t \cdot \vec{v}_i(t) + \frac{(\Delta t)^2}{2} \cdot \frac{\vec{f}_i(t)}{m_i} + \frac{(\Delta t)^3}{6}\dddot{\vec{r}}_i(t) + O((\Delta t)^4) \qquad (1\text{-}7).$$

Thus, the position of atoms at time *t+Δt* can be calculated by knowing the position at *t* and the forces at *t*, provided the time interval *Δt* is short. A similar relation can be derived

for calculating the velocity at a given time, knowing the velocity at a short interval prior to that time. Similarly the new positions can also be calculated knowing previous positions and current velocities.

Another assumption made by MD is the reversibility of time, i.e. if we trace particles' trajectories in the reverse time direction, all particles will follow their original trajectories. Under this assumption, we can obtain the particle's position at time *t-Δt* as

$$\vec{r}_i(t-\Delta t) = \vec{r}_i(t) - \Delta t \cdot \vec{v}_i(t) + \frac{(\Delta t)^2}{2} \cdot \frac{\vec{f}_i(t)}{m_i} - \frac{(\Delta t)^3}{6} \dddot{\vec{r}}_i(t) + O((\Delta t)^4) \qquad (1\text{-}8).$$

Adding the Equations 1-7 and 1-8 and omitting the higher order derivatives will give us

$$\vec{r}_i(t+\Delta t) + \vec{r}_i(t-\Delta t) = 2\vec{r}_i(t) + (\Delta t)^2 \cdot \frac{\vec{f}_i(t)}{m_i} \qquad (1\text{-}9).$$

Thus, as long as we know the positions at least at time *t* and preferably at *t-Δt* as well as the net force acting on the particles at time *t*, we can compute the positions at time *t+Δt*. Equation 1-9 is the widely used Verlet algorithm in MD simulation, which is similar to the finite difference numerical procedure.

Since higher order terms are neglected, a requirement for Equation 1-9 to be useful is to have very small time interval *Δt*, comparable to the characteristic time scale of actual atoms' movement. A typical time step of 1-10 femtosecond is adopted in most MD simulations.

The remaining unknown in Equation 1-9 is $\vec{f}_i(t)$, which is the gradient of the potential energy field *U*, given by

$$\vec{f}_i(t) = -\nabla_i U(t) \qquad (1\text{-}10).$$

U(t) is the same total energy used in MM and can be computed using Equation 1-1 at every time step.

Subtracting Equation 1-8 from Equation 1-7 will give the following equation:

$$\vec{r}_i(t+\Delta t) - \vec{r}_i(t-\Delta t) = 2\Delta t \cdot \vec{v}_i(t) + O((\Delta t)^3) \quad (1\text{-}11).$$

Neglecting the last term and dividing the Equation 1-11 by 2*Δt* leads to

$$\vec{v}_i(t) = \frac{\vec{r}_i(t+\Delta t) - \vec{r}_i(t-\Delta t)}{2\Delta t} \quad (1\text{-}12).$$

The total kinetic energy then can be calculated as

$$\vec{E}_{kinetic}(t) = \sum_{i=1}^{N} \frac{1}{2} m_i \vec{v}_i^{\,2}(t) \quad (1\text{-}13).$$

Many thermodynamics properties (temperature, pressure, etc.) of the simulated system can also be calculated from the time dependent position and velocity data of atoms based on statistical mechanics. For an isolated system, the total energy and linear momentums are conserved.

MD simulations are generally carried out within the framework of an appropriate ensemble, such as microcanonical ensemble (*NVE*), canonical ensemble (*NVT*) and isothermal-isobaric ensemble (*NPT*), depending upon which thermodynamic variables are fixed. For example in the isothermal-isobaric ensemble, the number of moles of the substance (*N*), pressure (*P*) and temperature (*T*) are kept constant. There are many subtle procedures involved in keeping the average value of these variables fixed during the simulation, which is achieved through various “thermostats”. Since the number of interactions between atoms increase non-linearly with the number of atoms present in the system, for a system containing *N* particles it was found that the number of times

forces are calculated at a given time step vary at least with N^2. [20] This will limit the number of particles one could simulate and the simulation time one can afford, even with the availability of larger and faster massively parallel clusters. Although there are many exceptions, the highest number of particles or atoms generally studied in MD is in the order of millions of atoms and the simulation time frame has been within nanosecond duration. Even with a very large number of atoms in a system, many of those atoms will reside on the surface of the simulation box, giving rise to significant influence of surface energy in the simulation of such nanosystems. Thus, if the interest is to study the bulk properties, the surface effects must be removed, which is achieved by using the periodic boundary condition (Figure 1-6). For periodic boundary conditions, the same simulation box or unit cell is repeated in every direction from the primary simulation box to fill the entire domain. When periodic boundary conditions are applied, an atom that move from the primary simulation cell to the next cell will reappear appear like an atom entering from the opposite side of the primary simulation cell as all cells are images of the same cell.

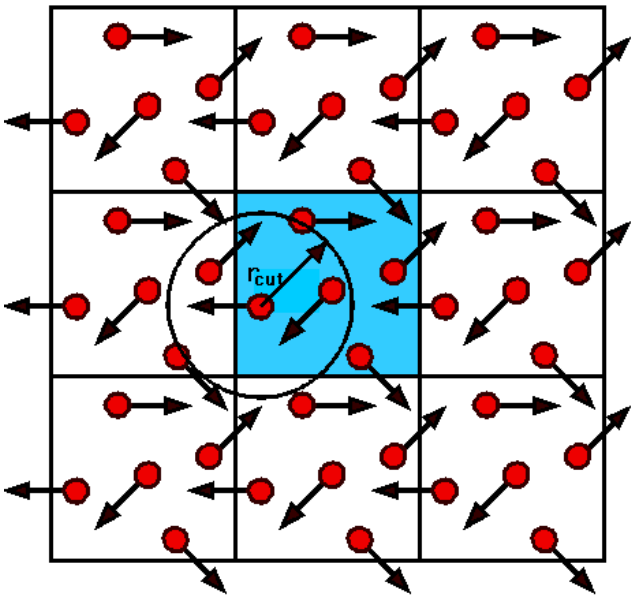

Figure 1-6. A scheme of periodic boundary conditions.

In Figure 1-6, r_{cut} is the cutoff radius that is normally applied when calculating the force between two atoms in order to save computing time. Thus, atomic units outside the cutoff radius are assumed to have an insignificant contribution to the overall potential, thus can be ignored in the calculations. It can be seen that an atom may interact with one in the neighboring cell (which is an image of one of the atoms in the simulation cell) because it is within the cutoff radius. It ignores the equivalent atom in the simulation cell because it is too far away. In other cases the interaction comes from an atom in the simulation cell itself. Thus the interaction that is calculated is always with the closest image. This is known as the minimum image convention. Note that the cutoff radius is always chosen so that an atom can interact with only one image of any given atom. This means that r_{cut} cannot be greater than half the width of the cell.

MD is a convenient tool to study the static and dynamic attributes of materials. Researchers have been applying MD to most materials science areas, including metals, small molecules, polymers, biomaterials, etc. Useful results can be extracted from MD simulations to help predict behaviors of materials, design possible structures and save expensive experiment costs. MD does have some limitations. First, due to the necessity of large number of atoms involved in macroscopic system, it is computationally expensive and technically demanding to study large scale problems using MD. Second, the time steps employed in solving equations of motion for atoms are on the time scale of femtosecond. The typical relaxation time of polymers is many orders of magnitude larger than the time scale of atomic movements, depending on the temperature. So, many new techniques are incorporated into MD to enhance its capability to address phenomena that spans larger time and length scales.

Some of the pioneering simulations in polymers emerged as early as 1970s. At the beginning, MD served as an important tool in protein structure determination and refinement based on X-ray data. The first published macromolecular MD simulation paper in 1977 [21] studied the dynamics of a folded globular protein (bovine pancreatic trypsin inhibitor). The results provided the magnitude, correlations and decay of fluctuations about the average structure. The results suggested that the protein interior is fluid-like in that the local atom motions have a diffusional character. Since then, MD was extended to general polymer area to uncover the structure-property relationship. The use of MD simulation techniques to study the dynamic properties of polymeric materials using chemically realistic models has a long and successful history [22-24]. In particular, our understanding of the conformational relaxation of polymers has profited greatly from this approach. Recently, the development of quantitatively accurate force fields has led to the possibility of a parameter-free quantitative prediction of the relaxation behavior and properties of polymers. Dreiding force field [25] was first introduced in 1990s. Although this force field is much more general than many other force fields, its latest version is equally or even more effective for protein and polymer simulations. COMPASS [26, 27] is another powerful force field that supports atomistic simulations of condensed phase materials. It is an ab-initio force field that has been parameterized and validated using condensed-phase properties in addition to various ab-initio and empirical data for molecules in isolation. Both of these two force fields have been implemented in a commercial simulation software package. These force fields coupled with classic and modified MD methodologies have been shown to have a fair enough agreement, most often qualitative and many cases quantitative, with experiments. MD simulations performed on polyethylene with united atoms assumption were reported by many authors [28-31]. On stepwise cooling of the system under a constant pressure, the temperature coefficient of specific volume changes abruptly at a temperature (T_g)

mimicking the glass transition phenomenon observed in laboratory. The results of the simulation runs, lasting for nanoseconds, were analyzed to investigate the short time dynamics of bond reorientation [30]. Besides T_g, various energy components at different temperatures of the polymers were investigated and their roles in the glass transition process were analyzed [31]. The calculated distribution of the decomposition products was compared with the experimental results of gas mass spectrometry and secondary ion mass spectrometry (SIMS) under the main assumption of thermal decomposition process for the cleavage of polymer bonds [29]. The simulation cell can also be uniaxially stretched by using the constant tension MD method. Mechanical moduli are other parameters can be extracted from MD. During the deformation, one can observe the void growth, fiber formation, and chain scission [28]. It also turned out that the strain of amorphous region is relaxed by the chain scissions with a consequent acceleration of the void growth. Based on the validated results of MD on PE, researchers turned their interest to more complex polymeric materials. The glass transition temperatures, Young's moduli, yield stresses and strain-hardening moduli of tactic polystyrene (PS) and bisphenol A polycarbonate (PC) were calculated and they compared well with the experimental data [32]. Establishing this kind of excellent agreement between simulation and experiment is evidence that the force field employed is able to capture not only the static thermodynamic and physical properties of the specific polymer but also its transport properties. The detailed comparison between simulations and experiments performed on identical materials (microstructure, average degree of polymerization, temperature, density, etc.) yields insight into the mechanisms of molecular motion underlying the materials behavior. Such models using carefully validated force fields are for specific polymeric material in the range of thermodynamic parameters where they can be studied in thermal equilibrium have been shown to be quantitatively predictive. MD can also be used as a tool to study diffusion of small molecules [33], polymer blends

[34], composites [35] and single chains behavior [36], etc. In all these work, polymers modeled are linear which simplify the generation of initial configurations.

1.2.4 Generation of initial Structures

The generation of the initial state of a polymer system is one of the most complex aspects of atomistic modeling of polymers. Typical polymer systems of interest are generally neither ordered enough to generate simplistic crystalline-like configurations nor random enough to create completely arbitrary configurations (Figure 1-7). The “random order” of the polymer systems must be correctly captured in order for atomistic simulations to yield reasonable and relevant results. Entanglements, amorphous and crystalline phases of semi-crystalline polymers are other differences from small systems.

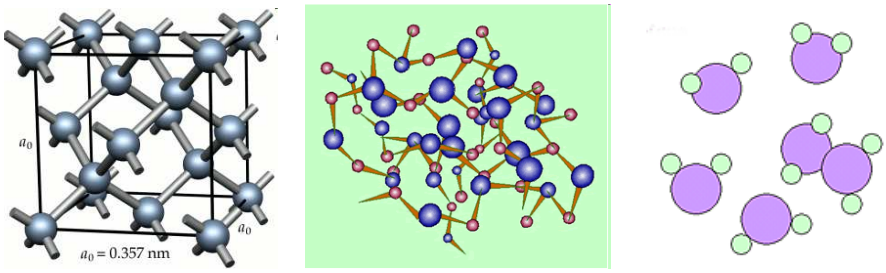

Figure 1-7. “Random order” structure of polymer systems (middle) compared to ordered structure of crystals (left) random structure of gases (right).

To avoid the necessity of long times required for polymer chains to achieve the energy-favorable state from a state far away from equilibrium, an initial configuration should be generated as close to the final state as possible. Lattices are always utilized as a guide to position the atoms in order to limit the degrees of freedom in the system and efficiently track volume exclusion (Figure 1-8). Commonly used lattice models are cubic lattice and diamond lattice. The lattice does have the disadvantage of constraining

the configurations available to the molecules to be grown on the lattice. This limitation can become significant if the lattice topology does not closely resemble the topology of the polymer molecules to be modeled. However, implementation of a suitable lattice (such as a diamond lattice) can capture main characteristics of polymer molecules and improve computational efficiency as well.

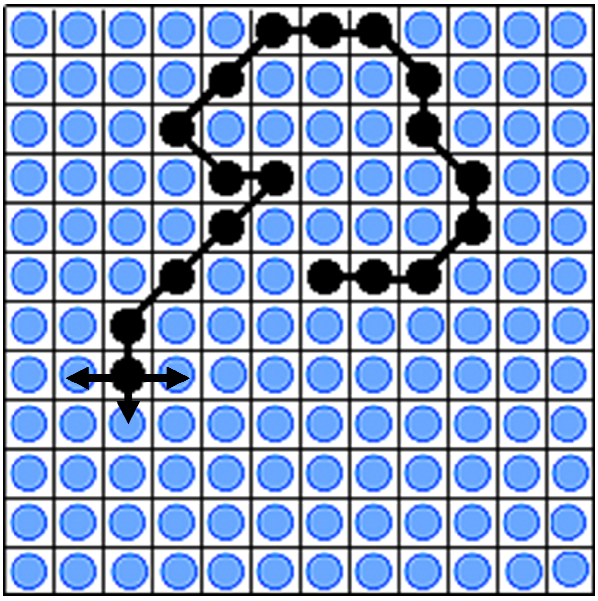

Figure 1-8. Generation of polymer structures with the aid of lattices.

Recently, some algorithms emerged to build the initial configurations of polymer networks reasonably at different scales. Figure 1-9 shows three schemes of generating polymer structures. The first category of these methods adopt “step growth” algorithm to create networks from basic repeating units. The assumption made here is that those repeating units are identical and therefore can be replicated and extended in three dimensions. Starting from one central unit, surrounding units are grown from the reactive points of the central unit while each head atom should be linked to a tail atom. The advantage of this category of methods is that they are relatively straightforward and easy

to be implemented into computer programs. However, these procedures are only suitable for certain networks. Sometimes the network produced is too regular and flawless to be realistic. Spatial hindrance may be another problem if the repeating unit is short or spatially compact.

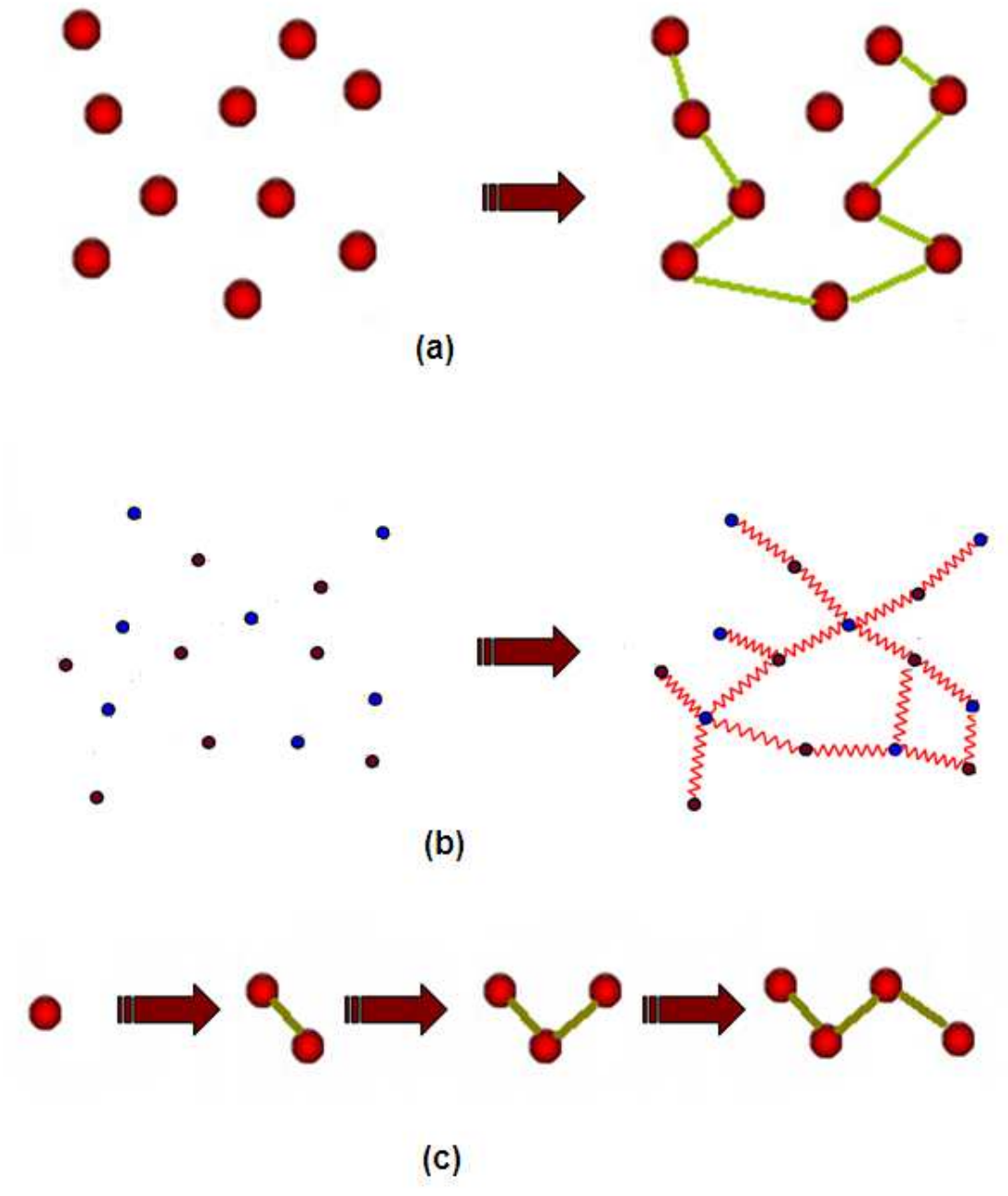

Figure 1-9. Schemes of initial structures generation of polymers.

The second type of methods creates segments between fixed crosslinking junctions, which are generated first according to the length-to-length distance of segments between them. These methods are appropriate for networks with uncertain number of repeating units. If the atoms at crosslinking points are the same and branches growing from the crosslinking points are chemically identical, efficiency of the second type of simulation methods can be within an affordable range. Linkages at each crosslinking point should be determined while the structures of each branch are different. The computational cost is expected to be very high when the network is complex and large. Another problem may arise is similar to as addressed in the first type of methods. Polymer networks with defects and unreacted functional groups, which are common experimentally, are not easy to simulate using this method.

The last class of methods to simulate polymer networks mimics the actual polymerization process. Generally, monomers are created in simulation box, and a following equilibrium step is always performed to blend and relax monomers. Then, some crosslinking criteria (the distance between nearby atoms is a commonly used criterion) are adopted to generate bonds between possible reactive groups. This type of methods can build either all-atom models or coarse grain models. They are able to simulate networks with multi-functional groups and capture the complexity of these networks. Usually, an imperfect network will be generated.

Overall, the network configurations obtained with all these simulation methods are more or less unfavorable structures and/or unrealistic bond and angle parameters, therefore a final energy minimization process is necessary to equilibrate and optimize the structures.

Many reports have addressed different means to simulate polymer networks. Hamerton et al. [37] used a program from Molecular Simulations, Inc. to predict mechanical and physical parameters of polycyanurate network polymers. Later Doherty et al. [38] reported a methodology to build network of poly(methacrylates) by means of crosslinking monomers based on a polymerization molecular dynamics scheme. They proposed an algorithm to create crosslink upon a cutoff distance criterion, which was frequently used by later researchers. Yarovsky et al. [39] then developed another way to construct low molecular weight water soluble epoxy resins. Recently, Xu et al. [40] conducted atomic simulation of epoxy resins using an alternative MM (energy minimization)/MD method. In summary, a four-step procedure (monomer construction, monomer equilibrium, crosslinking and the final network equilibrium) was employed in these papers. Reasonable agreements between computational results and experimental results have shown the validity of these methods. Meanwhile, together with the development of commercial software, some other authors [41] employed the molecular simulation package Cerius2 from Accelrys to predict material properties. However, the size of studied systems is limited and control of the detailed crosslinking process is also lacking in this approach. In the last several years, researchers tried to combine and modify previous methodologies to build polymer networks, using efficiency and robustness as criteria. Komarov et al. [42] and Varshney et al. [43] both successfully deployed different mechanisms to construct highly-crosslinked, relatively large scale polymer networks with fairly comparable properties with experiments. However, until now, none of these papers gained detailed insight into the chemical linkages and moieties percentages of complex networks because side reactions were either nonexistent or neglected in their models. On the other hand, network connectivity was shown to play an important role on mechanical properties [44].

1.4 Aging of materials

Applications of materials heavily depend on the properties and reliability of materials. As the properties degrade in time, it is important to estimate the active life span of materials in specific applications. Thus aging usually reduces materials' properties. Physical and chemical aging are two types of aging constituting different mechanisms. For polymers, physical aging is mainly referred to as the change of configurations of chains and evolution of free volumes in time. Normally, it will not change the chemical linkages and compositions of chains. Physical aging may be initiated by light, stress, diffusion of small molecules and other factors. On the other hand, chemical aging usually involves chemical reactions and the original chemical structures would be destroyed. This may lead to fatigue and final failure of materials. Chemical aging is always accompanied by physical aging. The breaking of bonds can be induced by long time internal stress and diffusion of oxygen and/or water molecules inside polymers. Researchers study aging of materials always under more intensive conditions than those in normal situation to expedite aging using experimental facilities; and by using the results of such accelerated aging, actual aging can be calculated.

1.4.1 Physical aging

Mechanical, physical or electrical properties of polymers changes as a function of time. For polymers, physical aging takes place in a form of chain relaxation. Since the aging is “physical”, the change of state is reversible. In other words, physical aging does not involve permanent modification of chemical structures of polymers. The microscopic explanation is polymer chains have a local or global transition of phase, state or position. Considering the manufacturing process of polymers, rapid melting and cooling

procedures do not allow polymer chains to relax. As a result, polymers generally start their state at non-equilibrium conditions. The thermodynamic drive of physical aging is the trend of achieving a state with lower energy by local movement of segments. In a steady environment, the course of physical aging may be slow; while temperature or chemical factors can accelerate aging. For a polymer with a T_g higher than room temperature, physical aging undergoes over a long time frame since polymer chains are at glassy state and have limited mobility. For polymers with a T_g lower than room temperature, chains can move more freely and aging proceeds fast. Physical aging can be observed even in an isolated environment. The kinetics of aging is mainly related to temperature. Polymer chains have long segments and the energy barrier of chain rotation and bond rotation is relatively low. Also there are some unoccupied spaces in polymers allowing bond rotation of segments. The unoccupied volume, also called the free volume, exists in polymers particularly due to its disordered structure as amorphous polymers. Figure 1-10 shows a void near the end of a polymer chain.

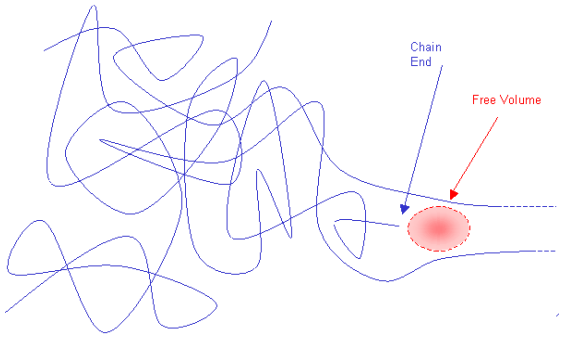

Figure 1-10. Free volume near chain end in polymer system.

Free volume can occupy several percentages of total volume of the polymer systems. This concept and the experimentally verified concept make the physical interpretation of chain relaxation possible. Positron Annihilation Lifetime Spectroscopy (PALS) is an effective technique utilized in determining the polymer free volume size and

size distribution. When measuring evolution of free volume as a function of time, Cangialosi [45] showed the variation of free volume along with aging for polycarbonate system (Figure 1-11).

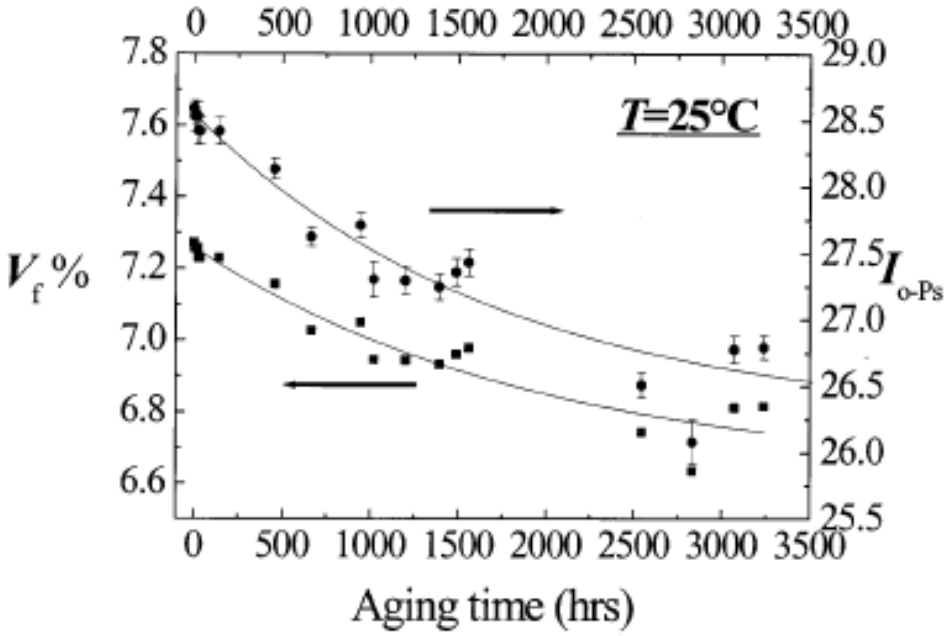

Figure 1-11. Evolution of free volume of polycarbonate during aging. [45]

It can be seen from Figure 1-11 that free volume fraction decreases as aging goes on. A mathematical model relating free volume to time was also proposed in the paper. A number of theories and models were also developed to explain physical aging.

Aging of semi-crystalline polymers was also studied by many researchers. Almost every physical property of polymers will change during the physical aging. Liao et.al [46] researched the effects of aging on T_g of poly(lactide). As aging time increased, the starting and ending temperature as well as peak of glass transition shifted to higher temperatures. Figure 1-12 shows the change of stress-strain curves for glassy PET at room temperature for varied aging time [47]. An increase of yield stress was observed as

aging time increased. This was contributed to a higher degree of tacticity of PET chains. An increase in modulus and a decrease in impact strength were found for polypropylene films due to aging.

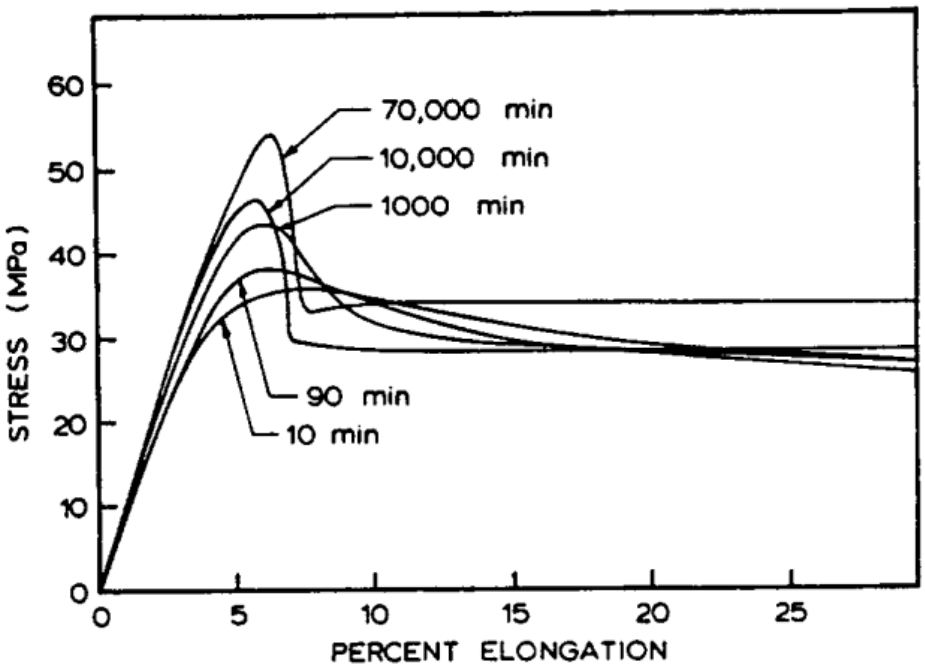

Figure 1-12. Tensile stress–strain curves for glassy PET at room temperature. [47]

1.4.2 Chemical aging

As discussed in previous section, the main difference between physical and chemical aging lies on if there are changes of chemical bonds. Chemical aging is usually irreversible and leads to a larger change in properties. Like physical aging, chemical aging in a commonly encountered environment is slow. However, heat, radiation, chemicals and moisture can make polymers more sensitive to aging. The dominant chemical aging mechanism depends on chemical structures of polymers and environment. Normally, end-use polymers are blends of polymer chains of different

monomers, unreacted monomers, catalysts and other additives. Any unsaturated or reactive groups may initiate reactions in certain conditions. However, only the aging of polymer chains will be discussed here.

Radiation and elevated temperature may initiate scission of weak bonds. Rupture of bonds can decrease the degree of polymerization, break linkage between crosslinking points and emit small molecules. Experimentally, one can use spectroscopy to analyze bond breaking mechanism at a high temperature. Here, we will give a brief summary of typical chemical aging mechanisms.

When no external molecules are present, bond scission at room temperature can be neglected. At high temperature, several mechanisms are possible. Figure 1-13 shows some mechanisms of degradation of a carbon-carbon bond. Elimination, depolymerization and random scission were shown and observed for different types of polymers. Substitutions will influence bond scission mechanism in many ways. PMMA is believed to degrade from depolymerization while PVC will take the form of elimination. Since activation energies of all these three reactions are high, it takes significantly long time for polymers to totally depolymerize.

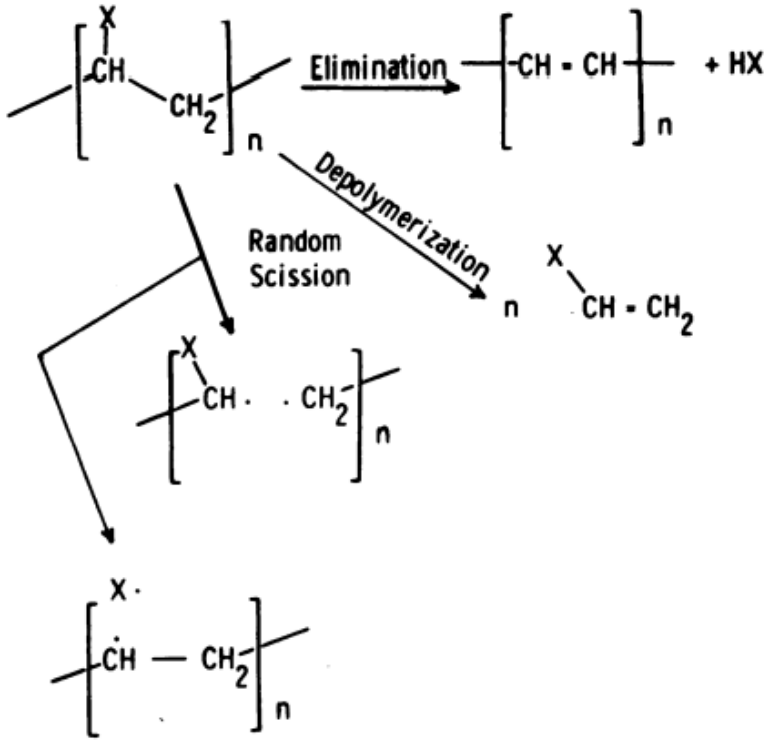

Figure 1-13. Various energy-induced processes of degradation. [48]

Oxidation of polymers is a more common way of chemical aging than depolymerization. Studies showed that oxidation starts with reaction between oxygen and a radical, which may be produced by losing a hydrogen atom (Figure 1-14). Unsaturated double bonds are also susceptible to oxygen. Oxidation will break backbones of polymers and leave oxygenated functional groups. It can also affect side groups and generate small molecules. Although oxygen has a high chemical activity, oxidation at room temperature is still slow. High temperature and ultraviolet radiation can significantly accelerate oxidation. A broad range of polymer types such as poly(olefins), PVC, PVA and PAN are vulnerable to oxidation. Polymers with photo-sensitive groups have weaker resistance to radiation than temperature. In reality, both oxygen and

radiation reach materials surface at first, so efforts of improving polymer durability focus on surface region of materials.

$$R\cdot + O_2 \rightarrow RO_2\cdot$$

Figure 1-14. Initiation of polymer oxidation.

The third mechanism of chemical aging is hydrolysis. From the name, one can infer the reaction involves water molecules. Different from oxidation, hydrolysis is always associated with certain types of bonds within polymers. Esters, amides as well as acetals are common victims of hydrolysis. Mechanisms of hydrolysis of three model polymers are given in Figure 1-15. Hydrolysis can lead to production of small molecules and cleavage of backbones depending on the location of reaction. Temperature is still an acceleration factor of hydrolysis. Temperature can make hydrolysis faster in two ways. First, temperature can accelerate water diffusion. Second, temperature reduces the energy barrier of hydrolysis. Water can diffuse into polymer faster than oxygen and the saturated uptake amount of water is larger than that of oxygen. Behavior of water diffusion and uptake will be discussed later.

The effect of chemical aging on properties of polymers includes weight loss, decrease of strength, initiation of crack and failure of materials.

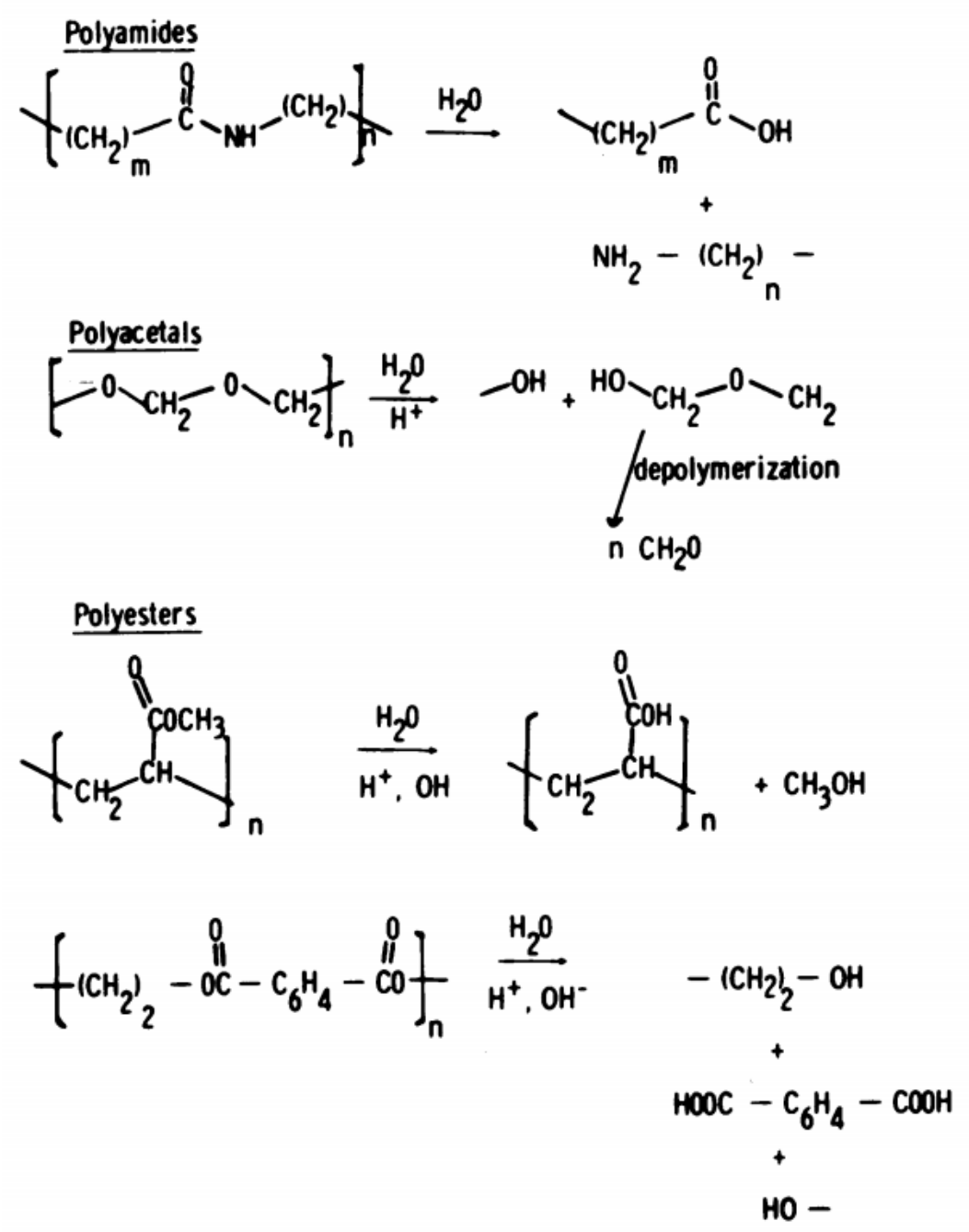

Figure 1-15. Hydrolysis reactions of representative polymers. [48]

1.5 Composites and interfaces

1.5.1 Composites

To improve some properties of polymers, one can blend two or more types of polymers or add fillers into polymer matrix. Materials consist of two or more components are always called composites. Considering the extreme difficulty in synthesizing new polymers, composites are excellent candidates that can be engineered for materials with desired properties. The majority of applied materials are composites in many areas because single component materials cannot satisfy combination of properties that are needed.

Based on components of composites, polymer composite materials can be divided into two categories. The first category consists of two or more polymer components and small additive molecules; no inorganic fillers are added. This type of composites is also called polymer blend or alloy. The second category of composites includes reinforcement inorganics such as particles, clays and nanotubes. These fillers are stronger and stiffer than polymers providing a boost of properties for matrix materials. In composites, the major component in volume percentage is referred as matrix and the minor component is called dispersed phase. The dispersion and morphology of minor component plays an important role in performance of composite materials. Generally speaking, a well dispersed filler distribution will lead to optimum overall performance. For nonsphere fillers such as nanotubes and clays, orientation of tubes or layers also has a significant impact on properties. A well orientated and well dispersed distribution of fillers still remains as a challenge task.

In aerospace industry, when replacing metal structure with composite, weight reductions of 20% or better are possible. Weight reduction is the greatest advantage of

using composite materials, and is one of the key items to influence decisions regarding materials selection. Other advantages over conventional materials include its high corrosion resistance, and its resistance to damage from cyclic loading (fatigue).

1.5.2 Interface strength

Composites have significant advantages over conventional materials; however added fillers also bring new problems to materials. Due to different surface properties of matrix and fillers, the interfaces between them can be weak. Interface is the contact region between the two components. In Figure 1-16, an interface is illustrated to highlight the difference between a sharp and diffused interface. From a macroscopic view on the left, it seems there is a sudden change in component at the boundary. This is true when two well-polished perfect surfaces are brought to a seamless contact. When tensile or shear forces are applied to each component, this “interface” has zero strength, unless the two sides are connected with bonded or strong non-bonded interactions at the interface. A better interface then should have an interface region by a boundary of finite size as shown on the right in Figure 1-16. In other words, there is a gradual change in component composition at interfaces. The transition from pure component A to pure component B decides the strength of interfaces.

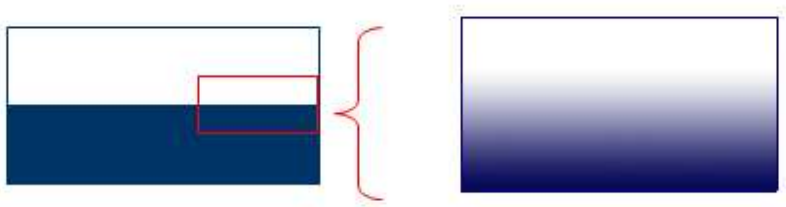

Figure 1-16. Scheme of interfaces between two components.

In ancient times, people had discovered the migration phenomenon at interfaces when a piece of copper and silver were put together for a long time. Experimental approaches suggested that metal atoms can diffuse cross the boundary into the other component. As time goes on, the depth of interface will increase which means the two components are more difficult to be separated at the interface. The same phenomenon was observed when two polymers at rubber-like state were placed together. The interactions between two components at interface can be physical entanglement, non-bonded van de Waals forces, ionic interaction, hydrogen bond interaction, electrostatic forces and covalent bonds. Morphology of an actual interface between two polymers is shown in Figure 1-17. The interface between epoxy and PBT has a thickness of about tens of nanometers. Generally, depth of interfaces is smaller than 1 micrometer. If the interfaces were generated when thermosets were not fully cured, strength of interfaces can be enhanced because of deeper penetration of monomers in another component.

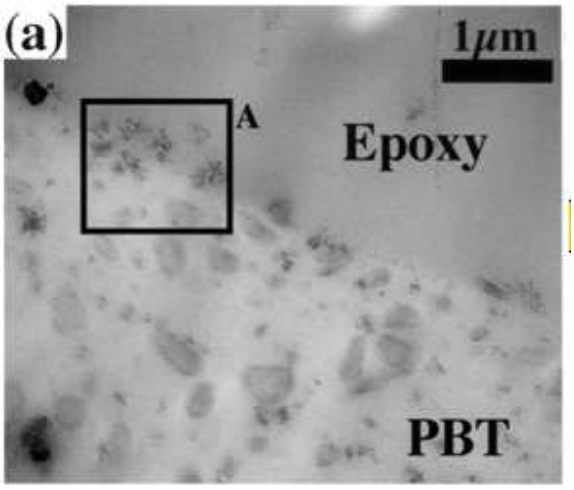

Figure 1-17. Interfaces between two polymers. [49]

However, actual manufacturing process is not long enough for chain inter-diffusion. Lack of strong interactions between fillers and matrix and different surface

energies are two main origins of weak interfaces. To overcome the problem of wetting, Gorga et.al [50] deposited a PMMA conformal coating layer on carbon nanotubes and mixed them with PMMA matrix. It was found that the surface treated CNT had a better reinforcement effect than CNT without coating. Compatibilizer also can modify interfacial properties and stabilize two immiscible components. Typical compatibilizers are block or graft copolymers for polymer blends. Block or graft copolymers have two segments, which are chemically identical to the components of polymer blends. When added into polymer blends, each segment can self-assembly itself to come to contact with the same component in blends as shown in Figure 1-18. As a result, total interfacial energies are reduced and interfaces are blurred. For the polymer/filler composites, compatibilizers can improve surface wetting by wrapping particles or nanotubes with polymer chains. Tensile strength of the compatibilized fiber/SEBS composite was found to increase when compatibilizer was used [51]. Another advantage of polymer compatibilizer for polymer/filler composites is fillers can get a better dispersion due to the repulsive forces between polymer coils.

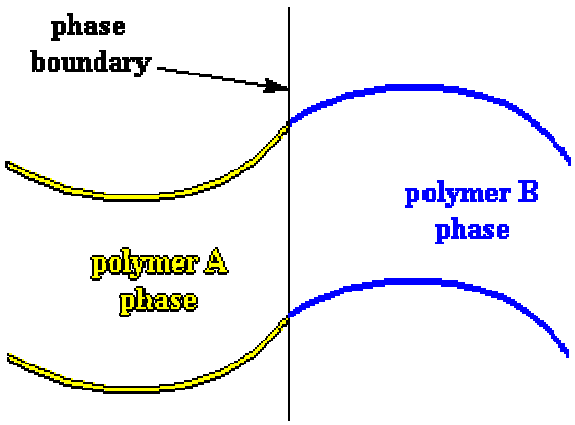

Figure 1-18. Block copolymer compatibilizer at interfaces between two polymers.

Stronger interactions at interfaces are introduced intentionally by different techniques. Surface treatment is an effective way to introduce functional groups to material surfaces while keeping the mechanical strength intact. Particles, fibers, nanotubes and substrate surfaces can be chemically modified quickly using different chemical reactants. A number of experiments done starting from last century have shown that silane coupling agents can change surface of inorganic materials to a variety of chemical groups and yield the best properties. More importantly, the modification process is fast, simple and cost effective. Silane coupling agents have broad applications in many areas. Figure 1-19 shows the steps of surface modification of a substrate ended with hydroxyl groups using silane coupling agents. Y groups in Figure 1-17 can be vinyl, amino, methacryl, epoxy and etc.

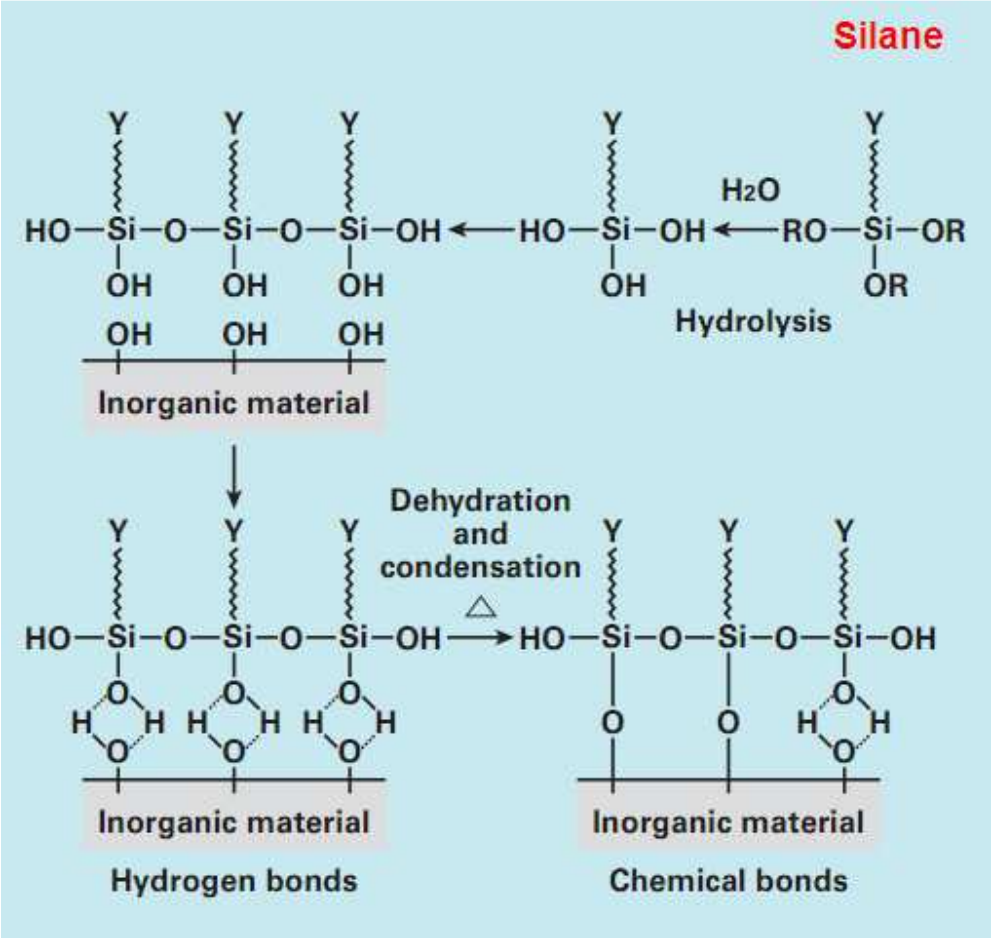

Figure 1-19. Steps of surface modification using silane.

Some other techniques such as plasma treatment, oxidation layer deposition were also employed to modify interfaces between polymer and inorganics. With the emerging of nano materials, polymer nanocomposites had become a research hotspot for promising applications. Properties of nanocomposites heavily depend on interfaces and distribution of fillers.

1.5.3 Crack and failure

Study of crack propagation and failure mechanisms has an important meaning in materials design, preparation and test. After a long service time, materials will lose their designed function due to fatigue, environmental aging and degradation. A complete understanding of failure mechanisms of materials will help predicting materials lifetime, preventing accident and designing structures. For different materials, failure mechanisms depend on materials characteristics, external stress, environment and many other factors. In Section 1.4, we have reviewed molecular level origins of failures of polymers. It is of great importance to failure mode analysis of pure polymers. In actual applications, when used as adhesives or composite matrix, failure mechanism of materials is not only related to polymers but also interfaces. As discussed above, interfaces are always a weak part in composite materials. Here, we will focus on the mechanism of crack initiation, propagation and failure of composites especially on interfaces. Previous studies have discovered two failure modes of adhesive joints as shown in Figure 1-20. When crack was initiated and propagated along interfaces, it was called an adhesive failure. If crack tips formed and developed in bulk of adhesives or adherents, it was referred as a cohesive failure. There are some factors that could contribute to failure mode of a composite. In some case, some modes may interface and interchange.

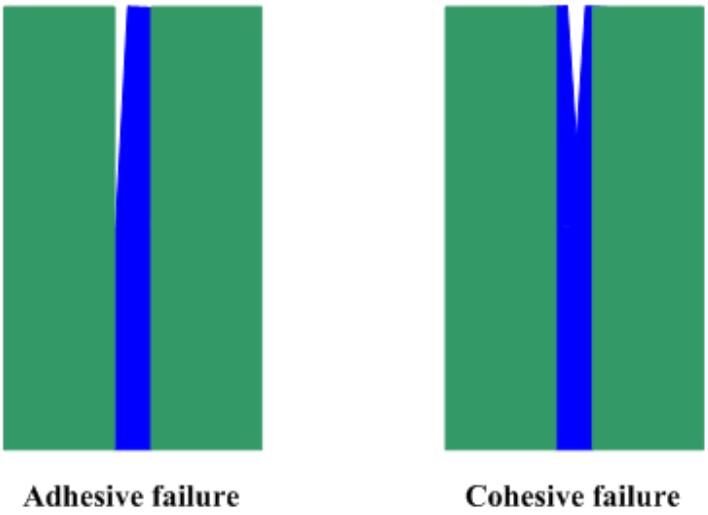

Figure 1-20. Failure mechanisms of adhesive bonding.

Experimentally, one can often identify the failure mode by examining surfaces of failed materials. Theoretical studies also shed some light on failure mechanism of polymer adhesives. It is believed that if adhesives totally wet substrate surface or the interactions between adhesives and substrate are strong, cohesive failure may take place. Otherwise, adhesive failure is likely to happen. The advantage of molecular modeling over experimental methods is its ability of varying surface properties arbitrarily to study patterns of interface behavior. A number of modeling studies on interfacial failure were reported in the literature. Kulmi et.al [52] studied the failure mechanisms of a thin linear polymer layer between two substrates using MD. The effects of interactions between united atoms in polymers and substrates and lengths of polymer chains were investigated. Thickness of adhesive layers was also found to have an effect on joint strength [53]. Most of these researches focused on adhesion strength between polymers and inorganic substrates such as metals, silicon and glass. Interactions between polymers and inorganics were simulated using non-bonded Van de Waals interactions

(Figure 1-21). Polymers are always approaching inorganic surface to minimize overall energies of simulation systems. One problem of this type of simulations is that interfaces have zero thickness, which is not consistent with experiments.

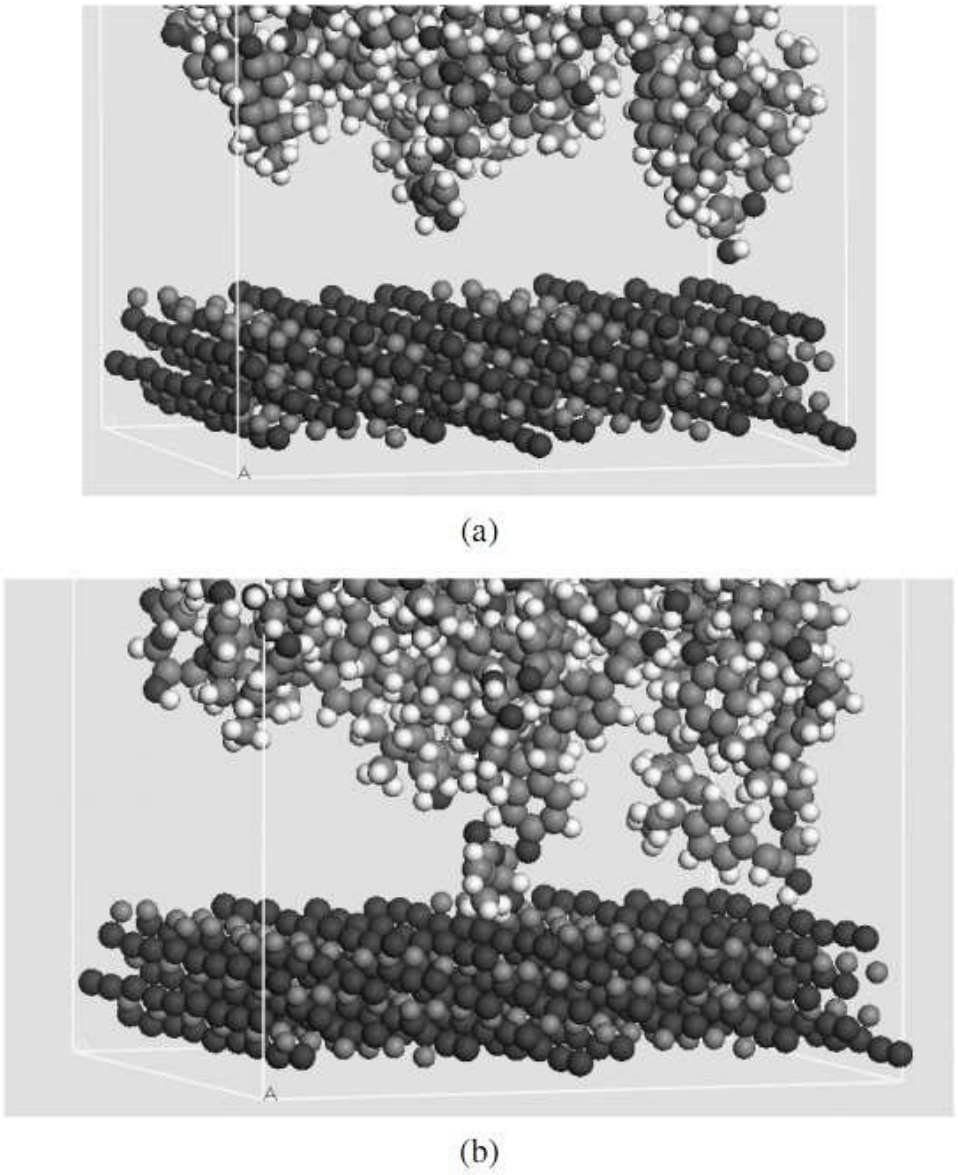

Figure 1-21. Conformational changes in the macromolecules after interaction with the metal surface, (a) before and (b) after Molecular Dynamics. [54]

1.6 Water uptake of polymers

Moisture environment is a major challenge epoxy resins will face while being used as structural adhesives. While the humidity levels change significantly from lower to upper level of atmosphere, environmental temperature is also changing. It is commonly believed that water molecules can invade into polymer bulks and result in certain physical and/or chemical changes to polymer. In this section, the interest is primarily in studying diffusion and transportation behavior of water molecules and factors associated with these behaviors.

1.6.1 Diffusion Law

Diffusion of small molecules has been described by Fick's law. Fick's first law relates the concentration gradient of diffusant to the diffusion flux by a linear relationship, which is defined by the following equation.

$$\vec{J} = -D\nabla c \qquad \text{(1-14).}$$

,where $\vec{J}$ is diffusion flux, ∇ is the gradient operator, c is the concentration of diffusing particles, D is the negative slope of the linear relationship, called diffusion coefficient.

Diffusion coefficient is a measurement of how fast molecules or particles travel. In room temperature, molecules of gases, small organic molecules in dilute solutions or ions in solutions have a diffusion coefficient in the range of 10^{-10}-10^{-8} m^2/s. The diffusion coefficients of gas or water molecules in solids are measured to vary from 10^{-10}-10^{-13} m^2/s depending on characteristics of particles, voids in the solids, temperature and some other factors. Experimentally, it is relatively easy to measure the diffusion coefficient of

small molecules through bulk material once the material is synthesized, although for interfaces it may pose some difficulties. Using computational method, calculating diffusion coefficient is also relatively straightforward. Compared to experiments, MD is an effective approach to get insight into the diffusion behavior at a fundamental level describing the motion of diffusing molecules, if such materials are unavailable for diffusion experiments or one wants to design and synthesize a new material with certain moisture transport properties. In this case the power of MD is more on narrowing down the candidate materials with specific properties that needs to be synthesized for further experimental verification. The theoretical foundation of computational method is discussed here. Conservation of mass gives:

$$\frac{\partial c}{\partial t} + \nabla \cdot \vec{J} = 0 \qquad \text{(1-15).}$$

Combining Equations (1-14) and (1-15), one can get

$$\frac{\partial c}{\partial t} = D\nabla^2 c \qquad \text{(1-16).}$$

Solution diffusion equation in three dimensions is given by

$$c(\vec{r},t) = (2\pi Dt)^{3/2} \exp[-\frac{r^2}{2Dt}] \qquad \text{(1-17).}$$

The approach first used by Einstein will lead to the following equation:

$$\langle r^2(t)\rangle = 6Dt \qquad \text{(1-18).}$$

If we define $\Delta\vec{r}_i(t) = \vec{r}_i(t) - \vec{r}_i(0)$, then

$$\langle \Delta r^2(t)\rangle = \frac{1}{N}\sum_{i=1}^{N}\langle \Delta r_i^{\,2}(t)\rangle = \frac{1}{N}\sum_{i=1}^{N}\langle [\vec{r}_i(t) - \vec{r}_i(0)]^2\rangle \qquad \text{(1-19).}$$

Substituting Equation (1-17) into Equation (1-18) gives

$$D = \lim_{t\to\infty} \frac{1}{6N} \sum_{i=1}^{N} \langle [\vec{r}_i(t) - \vec{r}_i(0)]^2 \rangle \qquad (1\text{-}20).$$

This equation can be applied to get the diffusion coefficient D, using the positions of diffusing molecules in a medium. For the problem of interest, in Equations (1-19) and (1-20), *N* is the number of penetrating water molecules in the epoxy; $\vec{r}_i(t)$ is the position vector of water molecule *i* at time *t*; $\langle\rangle$ means an ensemble average.

1.6.2 Water uptake of polymers

Diffusion of water molecules in polymers was studied by many researchers [55-60]. Diffusion coefficient is mainly related to temperature, relative humidity and the structure of materials. In MD, one can compute mean square displacement (MSD) and plot it as a function of time. From this plot, diffusion coefficient can be derived from the slope of a linear fitting to data points according to Equation (1-18). Although the principle is fairly straightforward, the implementation and analysis of the result can be involved when using this method. Since there are various regions in the mean-squared displacement-time plot, one has to be careful in picking the appropriate region for calculating the diffusion coefficient. For example, diffusion coefficient calculated from the initial ballistic region may not be any significance. In addition, many diffusion processes are non-Fickian, thus care must be taken in the interpretation of data to obtain meaningful results.

For polymers, the total amount and the distribution of free volume cavities will directly influence how fast small molecules can diffuse. Diffusion coefficient of same

penetrant molecules in polydimethylsiloxane (PDMS) is three times larger than in amorphous polyethylene (PE) due to larger free volume fraction and the broader free volume distribution in PDMS [60]. Since most polymers stay in a glassy state at room temperature, the diffusion of small molecules always take a much longer time than in a simple liquid. Interactions with water molecules, such as hydrogen bonding, can significantly alter the diffusion process. This procedure is very useful in obtaining various parameters associated with the diffusion of water molecules, as shown by E. Dermitzaki *et al* [61], who by systematically changing the structures of epoxy resins found out that the polarity is the dominant factor for water uptake.

Size effect of materials also plays a role in water transport. Penetrating capabilities of small molecules through bulky materials are believed to differ from that in thin films or membranes. A comparison between interface and bulk models of simulated rubbery and glassy polymers addressed by D. Hofmann *et al.* [57] revealed an experimentally important pervaporation feature of membranes, which means a combination of membrane permeation and evaporation. Comparison between EMC bulky samples and EMC/Cu interfaces [55] shows that water molecules are more prone to penetrate in thin interfaces. The diffusion coefficient of moisture through interfaces increased by one magnitude compared to that in bulk. Such behavior demands researchers to pay more attention to study and prevent moisture diffusion particularly at thin interfaces, and this is becoming an important issue as electronic devices are miniaturized.

Some small penetrants (such as water) in a polymer have aggregative attributes and intend to form large clusters. In one of the earliest papers in this field, Yoshinori Tamai *et al.* [60] studied the mechanism of small molecules diffusing through an amorphous polymer membrane. Diffusion studies of different penetrants (water,

methane and ethanol) in different polymers (PE and PDMS) were conducted. Diffusion coefficient of non-aggregated penetrant species coincided with experimental value; however, aggregation of water and ethanol in PDMS reduced diffusion coefficient by more than one magnitude. It suggested that water clusters forming in polymers played an important role in diffusion. Results by Fukuda *et al.* [56] also validated this observation. This study was also performed with MD simulation with a simulation time of about 10 nanoseconds. The diffusion coefficient of a water cluster containing 10 molecules in polyethylene was detected to be 7.1×10^{-7} cm^2/s. Relevant to the topic on aggregation, the relative humidity affects the diffusion behavior through the formation of water aggregates. At a low moisture concentration, the number of water clusters in polymer was believed to be few. Higher relative humidity leads to a low moisture concentration gradient and more water aggregates. These two results will contribute to a low diffusion coefficient [55].

The result from water uptake can be divided into two categories: change in physical properties and loss of mechanical strength. It was discussed earlier that water uptake by epoxy will decrease glass transition temperatures [61]. Lager amount of moisture in epoxies means a larger reduction of glass transition temperature, which can change the state of some materials from glassy to rubbery. It was observed experimentally that the joint strength of epoxy adhesives was substantially weakened when exposed to moisture above a critical relative humidity for a long time [62]. However, the influence of moisture exposure on the mechanical properties of epoxies has not been adequately captured through MD simulation.

1.7 The need and Objectives of the proposed research

1.7.1 The need of proposed research

The rapid growth of aerospace adventures and missions puts forward an urgent need of property-elevated, environment-resistant materials. Light-weight epoxy resins serve as the main adhesive for the demanding aerospace application. Particularly, those epoxy resins with high functionalities are required to have high temperature capability. The other challenge that aerospace materials undergo is the hot-wet environment. For example, the currently favored aerospace structural material is tetraglycidyl-4,4'-diamino-diphenylmethane (TGDDM) /4,4'-diaminodiphenylsulphone (DDS) resin. Researchers have shown water uptake values for this system of the order of 5%, suggesting a reduction in glass transition temperature of up to 100 ℃ if a highly moist atmosphere were to be encountered [63]. Diffusion of water molecules into the epoxy network may lead to chemical and physical aging. Mechanical properties based on the network structures would also inevitably suffer under these circumstances. Horrible accidents took place several times due to the loss of adhesive functions of epoxy resins in the past years. These potential hazards increase the pressure to investigate the mechanism of water uptake at molecular level. The solution may be either reducing the amount of water uptake or modifying epoxy structures.

Molecular simulation is a powerful tool to illustrate the factors governing structural evolution. However, until now the underlying physical and chemical mechanisms of reactions between diffusing water molecules and epoxy resins have not been elucidated clearly. So a microscopic study of this problem is required to predict and design long-term durability of aerospace materials.

1.7.2 Objectives

The primary objective of this research is to build a reliable nanoscale model capturing most of the main physical, chemical and mechanical features of the epoxy polymer network. This model is the basis for the diffusion and degradation simulations under realistic conditions. Modeling of adsorption and transportation of small molecules through polymers is the second main step of this work. Finally, chain scission during aging will be studied. Overall, a methodology to investigate the main issue and sub-aspects of epoxy resin degradation will be addressed at the end of this study.

CHAPTER 2

GENERATION OF POLYMER NETWORKS FOR ATOMISTIC SIMULATIONS

2.1 Modeling and simulation details

As addressed in Chapter 1, a reliable and efficient way of generating initial structures of polymers is a prerequisite for molecular level simulations. The need to study structure-property relationship and aging behavior of epoxies from a fundamental level requires a realistic model to represent all aspects of the problem, such as chemical composition, and physical and mechanical properties, etc. In this chapter, TGDDM epoxy cured with DDS was used as the model system to demonstrate the methodology of generating realistic initial polymer networks. The chemical structures of TGDDM and DDS were shown in Figure 2-1. For TGDDM and DDS systems, both epoxy and curing agent have a short branch structure. At the same time, high polarity of TGDDM and DDS suggests that hydrogen bonding and electrostatic forces play an important role in the inter-molecular and intro-molecular interactions. Since the purpose of this work is to investigate the relationships between structures and properties of polymer networks at an atomistic level, all-atom models of polymeric systems are adopted. This implies the generation of every atom for the polymeric material included in the simulation boxes according to their chemical structures.

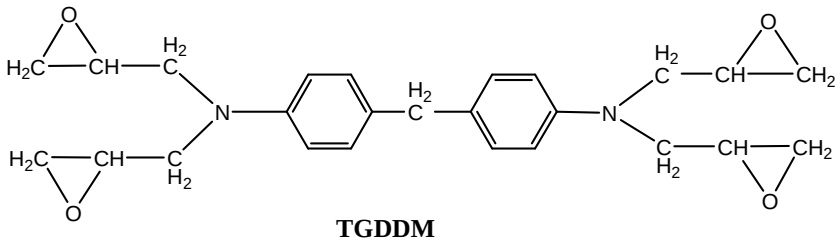

TGDDM

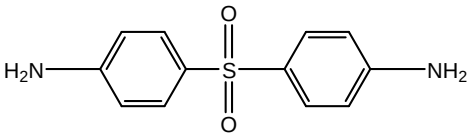

DDS

Figure 2-1. Chemical structures of epoxy TGDDM and amine DDS.

While the structures of single epoxy and polyamine molecules are fairly simple, the final architectures of cured epoxy resins are so complex that they cannot be represented in the usual repeating unit form. This is primarily due to the multi-functionality of both epoxy and curing agent. Possible chemical reactions taking place in a curing process were already discussed in the previous chapter, especially in Figure 1-3. For each epoxy group, competing reactions take place during the curing process. Besides the primary amines present in the initial stage of curing, secondary amines and hydroxyls produced during curing reaction also can react with epoxy group. The percentages of each moiety of epoxy and amine after curing vary depending on the system. It is difficult to define a repeating unit for a crosslinked epoxy network, as for a linear polyolefin.

The complex characteristics of epoxy resin make it difficult to generate its initial structure compared to linear polymers with a repeating unit. Here, a newly developed methodology to mimic the actual process of curing and obtain final structures close to

real structures was found to be very effective. There are three steps in this methodology: generation of monomers, crosslinking and finally energy minimization.

2.1.1 Generation of monomers

TGDDM and DDS with equivalent stoichiometric amounts were simulated in this research. No catalysts or additives were added into epoxy systems for the sake of simplicity. United atom assumption was used in this stage, while all atom representation was used while carrying out the MD simulations. The basic algorithm used to build the initial structures on a diamond lattice in this research was taken from the basic methodology developed by James Shepherd [64]. As a summary of this methodology, the bond length and bond angle between two adjacent carbon atoms in a diamond structure are close to those of carbon-carbon bonds in a linear polymer such as polyethylene. The advantage of generating polyethylene in diamond lattice is that it will not bring significant stress in the initial structure. A more important reason comes from the fact that it significantly reduces the possible positions of one atom within the neighborhood of another atom from infinity to a finite known lattice sites. As a result, computational time and cost is also reduced significantly. In practice, the simulation box has to be mapped with a diamond lattice first. The bond length of the diamond lattice is set to be 1.53 Å and the bond angle is 109.5 degree. Atoms are added successively to available neighboring lattice sites, starting with the least dense site in the diamond lattice. A possibility matrix based on several criteria including least density, closest, lowest energy, RIS and random is used for the path selection. Side atom positions of existing atoms are reserved to exclude other atoms. Until a molecule is successfully completed with the desired structure, the routine switches to the next molecule. Different from commonly used linear polyethylene, TGDDM and DDS have short, compact structures with two benzene rings in them. Therefore monomers are only considered completed

until the exact backbone atoms except hydrogen atoms are built. No further delete-and-add procedure for segments is needed. In order to make the chain generation process more effective for aromatic molecules, several overlaps near benzene rings are allowed. Uncompleted segments will be removed to free the lattice sites. The random order is used to generate TGDDM and DDS to assure that the box contains a well-dispersed polymer system before the curing step. The whole simulation box is created with a density lower than the realistic density for computational efficiency, as compressing these systems to represent actual density is fairly straightforward. After all molecules were generated in simulation box, united atom assumption was replaced with all-atom representation by restoring hydrogen atoms in the system. Figure 2-2 shows the structure of a TGDDM molecule in a diamond lattice and after energy minimization. Now we have a box of TGDDM and DDS molecules to be cured.

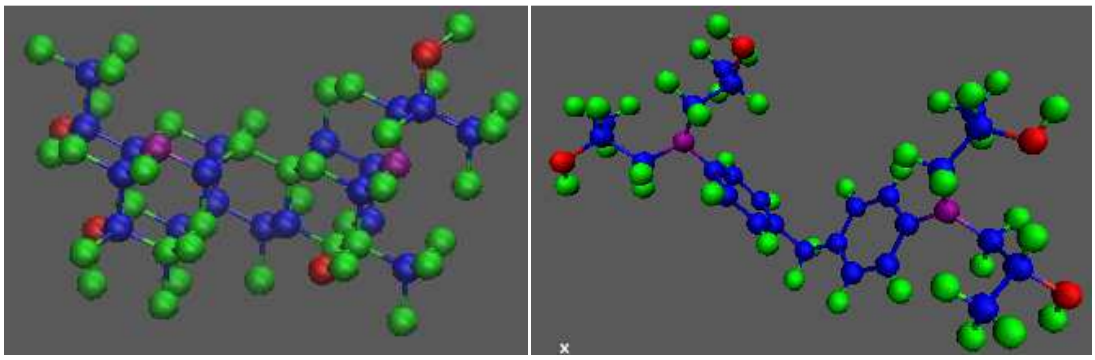

Figure 2-2. A TGDDM molecule generated in diamond lattice (a) and after energy minimization (b).

2.1.2 Crosslinking

The algorithm for crosslinking epoxy and amine was shown in Figure 2-3. A maximum value of cutoff distance and desired degree of polymerization were set at first. To cure the blend of epoxy and curing agent, one need to identify all reactive atoms in

the system, which are oxygen atoms in epoxides and hydroxyl groups, and nitrogen atoms in primary and secondary amines. In each reaction iteration, all possible reactive atoms were found and the distances between reactive sites were computed. For each epoxide group, possible reactive sites within a certain cutoff distance were found. Certain pairs of reactive sites were crosslinked according to the possibility list. If no such pairs existed, cutoff distance was increased for the next iteration. The curing reaction step for this site will stop when either the maximum cutoff distance was reached or the desired degree of polymerization was obtained.

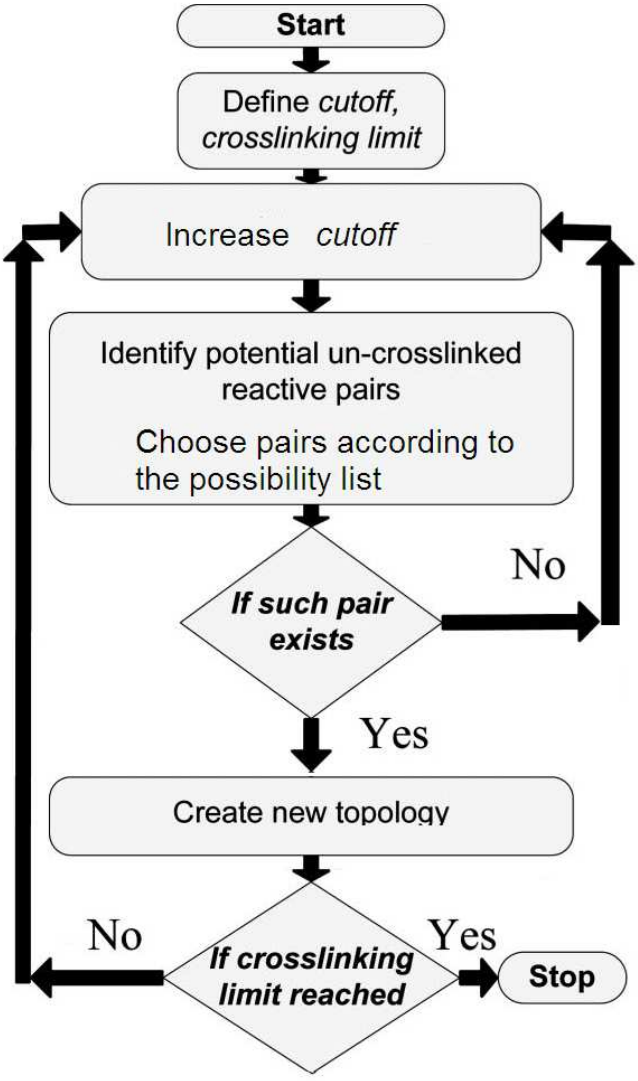

Figure 2-3. Algorithm of crosslinking epoxy and amine.

The methodology of computing the possibility list of each epoxide group was illustrated in Figure 2-4. For one epoxide group, there may be several reactable groups with a certain cutoff distance. As such, an algorithm must be used to pick one from all reactable groups to react with epoxide group.

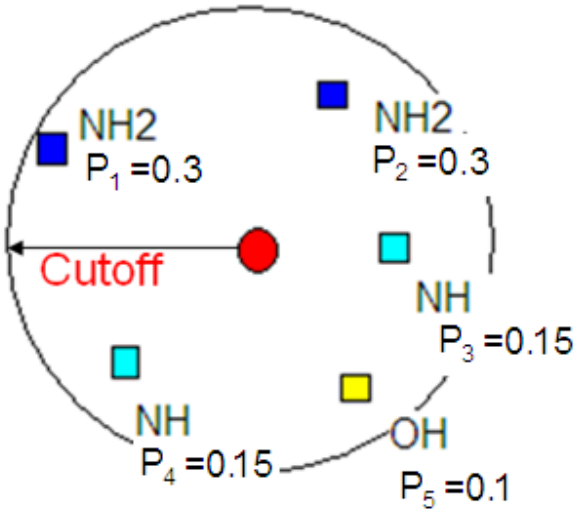

Figure 2-4. Algorithm of picking the reactive site according to the possibility.

In Figure 2-4, for instance, five reactive sites were on the neighboring list of the red site which stands for an epoxide group. The possibility of each reactive site was calculated using the following equation.

$$P_i = \frac{r_i}{\sum_i r_i},\ r_i = k_i \cdot [A] \qquad (2\text{-}1).$$

In Equation 2-1, P_i is the possibility of a reactive site; r_i is the reaction rate; k_i is the reaction rate coefficient and *[A]* is the concentration of a reactive site. Real kinetic reaction rate coefficients (160 ºC) [4] were used to calculate the reaction rate according to the type of each reactive site, despite their distance away from the epoxide site. Then

another random number *p* between 0 and 1 is generated. If *p* satisfies Equation 2-2, the *k*th reactive site was selected to react with the epoxide group. This is essentially the well-known Metropolis rule.

$$\sum_{i=1}^{k-1} P_i < p \leq \sum_{i=1}^{k} P_i \quad (2\text{-}2).$$

A single cross-linking bond will be created between the epoxy group and selected reactive site from the neighboring list, one at a time. After the establishment of every crosslinks, the concentrations of each reactive group were updated. As a result, the reaction possibilities of each kind of reactive groups vary during the entire cross-linking process, which will lead to a more realistic network. The cutoff distance chosen to build the neighboring list of each epoxy group will determine the topology and conversion of the epoxy network. During the crosslinking process, the cutoff distance was gradually increased by 1 Å (starting from 0) with each cycle until the desired conversion was reached. This approach was introduced to reduce the percentage of unrealistically long bonds. A maximum cutoff distance of 18 Å was adopted in this research, which assured that more than 99% of bond lengths in the system could be corrected by relaxing the system. Repeating the crosslinking process sequence showed that the final structure of the epoxy network is mainly dependent on the initial positions of monomers and the cutoff distance. The randomness of distribution of the monomers before cross-linking was also thought to have an important impact on the final cross-linked structures. A simulation box consisting of a larger number of monomers can increase the randomness. Since after the crosslinking process, most of the epoxy groups had been consumed, the network structures were not strongly dependent on the exact cycle time at which the cross-links were established.

2.1.3 Charge distribution of epoxies

The number of atoms with high polarities in TGDDM and DDS is not neglectable, therefore charge equilibrium is essential for determining columbic interactions. Oxygen and nitrogen have a high value of eletronegativity while hydrogen, carbon and sulfur have a relatively low value of electronegativity. Commonly, charges of oxygen and nitrogen will be negative since they have a stronger ability to attract electrons from carbon or hydrogen atoms. As a comparison, hydrogen atoms will be positively charged since they are likely to lose electrons to other more electronegative atoms. The total charge for an isolated epoxy system should be zero. The actual charge value of one specific atom depends not only on the electonegativity of the atom but also the charge environment around it. An accurate method to determine the actual charge distribution is critical to describe interactions between non-bonded atoms. Until now several methods were put forward to estimate charge equilibrium for polymer systems. The standard of a good approach is (a) if the results agree well with experimental dipole moments and with ab initio calculations; (b) whether it is easy to be implemented in computer language and computationally efficient. Here two widely used approaches for charge equilibration are implemented to compare results and efficiency. Rappé's method [65] used electronegativity, radius and idempotential of an element as input to dynamically assign atomic charges. By solving linear equations, one equation for each atom, one can obtain environmentally sensitive atomic charges for the model system chosen for the study. Iterative partial charge equalization of orbital electronegativity model proposed by Gasteiger [66] is another way to distribute charge for molecular dynamics simulation. It is based on some parameters associated with every element and only takes account of connected atoms.

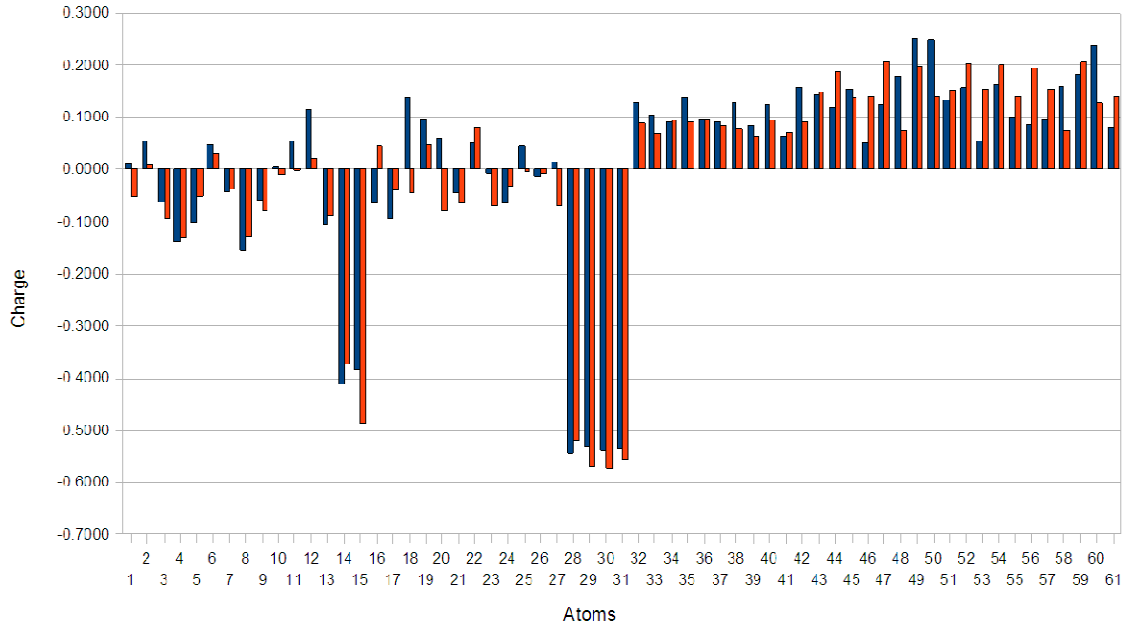

Figure 2-5. Comparison of atomic charges calculated by two methods. (red): Rappé; (blue): Gasteiger.

Figure 2-5 compares charges of all atoms in a TGDDM molecule computed by Rappé and Gasteiger's methods. Net charges of oxygen atoms are around -0.55 eV; atomic charges of nitrogen atoms are about -0.4 eV; hydrogen atoms have a charge range from 0.1 to 0.2 eV; charges of carbon atoms fluctuate from -0.1 to 0.1 eV depending on atoms connected. Results from two methods agree fairly well and are consistent with ab initio results. However, Rappé's method needs to solve a large linear sparse matrix, which is very time consuming. This problem is worse when the size of simulation box is increased. On the other side, Gasteiger's method will converge in ten steps to an equilibrated charge state. For the sake of computational cost, Gasteiger's iterative method was adopted for charge equilibration of epoxy system.

2.1.4 Energy minimization

The crosslinking and diamond lattice leaded to high energy and stress of the epoxy system. Energy minimization of the crosslinked system was conducted to adjust atom positions. Lattice constraints were removed at this stage. Dreiding force field was used to conduct a molecular mechanics simulation. A mathematical expression of Dreiding force field is given in Figure 2-6.

$$E = E_B + E_A + E_T + E_I + E_{vdW}$$
$$E_B = k_1(r - r_0)^2$$
$$E_A = k_2(\cos\theta - \cos\theta_0)^2$$
$$E_T = k_3\{1 - \cos[n(\varphi - \varphi_0)]\}$$
$$E_I = k_4(\phi - \phi_0)^2$$
$$E_{vdW} = k_5((\frac{r_0}{r})^{12} - (\frac{r_0}{r})^6)$$
$$E_Q = \frac{Cq_iq_j}{\varepsilon r}$$

Figure 2-6. Dreiding force field.

In Figure 2-6, E is the total energy; E_B is the energy of bond stretching, where r is bond length; E_A is the energy of bond bending, where θ is the bond angle; E_T is the dihedral torsion energy, where φ is the dihedral angle; E_I is the inversion energy for atoms bonded to exactly three other atoms, where Φ is the inversion angle; E_{vdW} is the LJ potential, where r is the distance between non-bonded atoms and r_0 is the cutoff distance; E_Q is Coulombic pairwise interaction, where C is an energy-conversion constant, q_i and q_j are the charges on the two atoms, ε is the dielectric constant and r is

the distance between the two atoms. All other parameters with a *0* subscript stands for the equilibrium value. All the "*k*"s are specific energy parameters to be determined for every system. All the parameters were obtained from published literature. The mixing rules of parameters for all LJ potentials were to use the geometric formulas. For non-bonded LJ parameters, a general mixing rule was used to calculate interactions between dissimilar atoms when those coefficients are not explicitly known. A general cutoff distance of 10Å was set for pairwise interactions. Side length of simulation box was always larger than 20Å. We assumed periodic boundary condition in the simulation. The Polak-Ribiere version of conjugate gradient (CG) algorithm was used for minimization. Molecular mechanics was conducted at 0K and with fixed volume. Figure 2-7 gives a snapshot of an energy minimized structure of cured TGDDM epoxy resin.

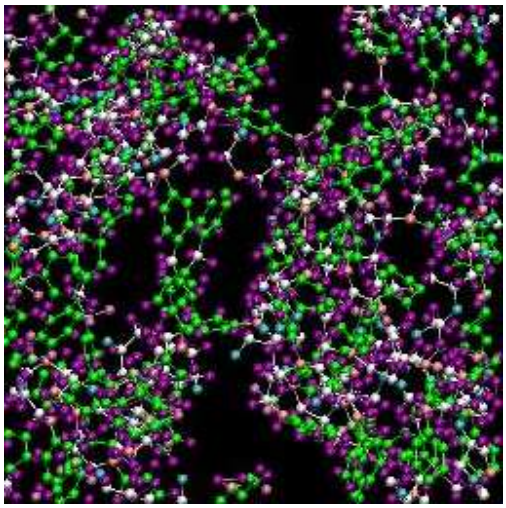

Figure 2-7. A crosslinked TGDDM network formed as discussed in text.

2.1.5 Molecular dynamics

After system relaxation but before any MD runs, a bond length check routine was conducted to remove unrealistically long bonds and crosslinks that lead to catenation

and numerical instability. After molecular mechanics simulation, the system achieved a configuration that generally was shown to be within the vicinity of the minimum potential energy. The next step is to run dynamics at certain temperature and pressure to approach a realistic state. MD simulations were conducted using LAMMPS under NPT ensemble. Time step was set to 1 fs throughout this chapter. The Velocity-Verlet algorithm was used for integration in all the MD simulations. The temperature and pressure were maintained by the Nose-Hoover thermostat.

The material within the simulation box underwent a compression to bring the density to the desired level and then a relaxation to achieve an equilibrium state. The box was gradually compressed to 2500 atm pressure (applied isotropically) and then decompressed to 1 atm gradually. At each pressure, a time interval of 100ps was adopted to allow equilibrate. The whole compression-decompression process was repeated three times. The structures obtained at the after these cycles were used as the starting structures for other studies.

An annealing process was conducted from 700K to 300K at a rate of 10 K/300 ps. This process was also repeated for three times. The annealing was well tuned to get a stabilized state at each temperature. Figure 2-8 shows an equilibrated structure of TGDDM epoxy cured with DDS.

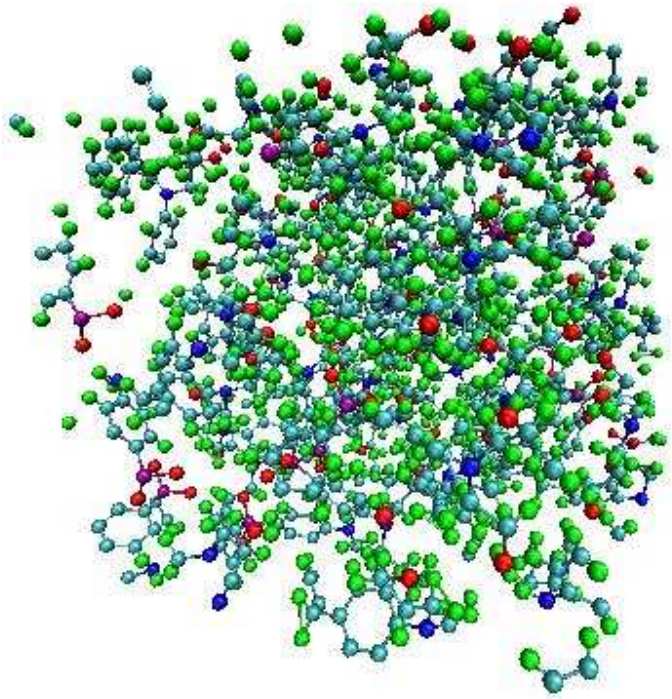

Figure 2-8. A crosslinked TGDDM epoxy resin after equilibration. Color code: green(hydrogen); cyan(carbon); blue(nitrogen); red(oxygen); purple(sulfur). Bonds across boundaries are not shown.

2.2 Adjustment of parameters

Until now, only the selection of force field was described in detail. In addition to having proper force fields, other simulation parameters must also be adjusted to get reliable simulation results. In this section, the effect of varying several key parameters is provided.

First of all, energy, volume and pressure evolutions were examined.

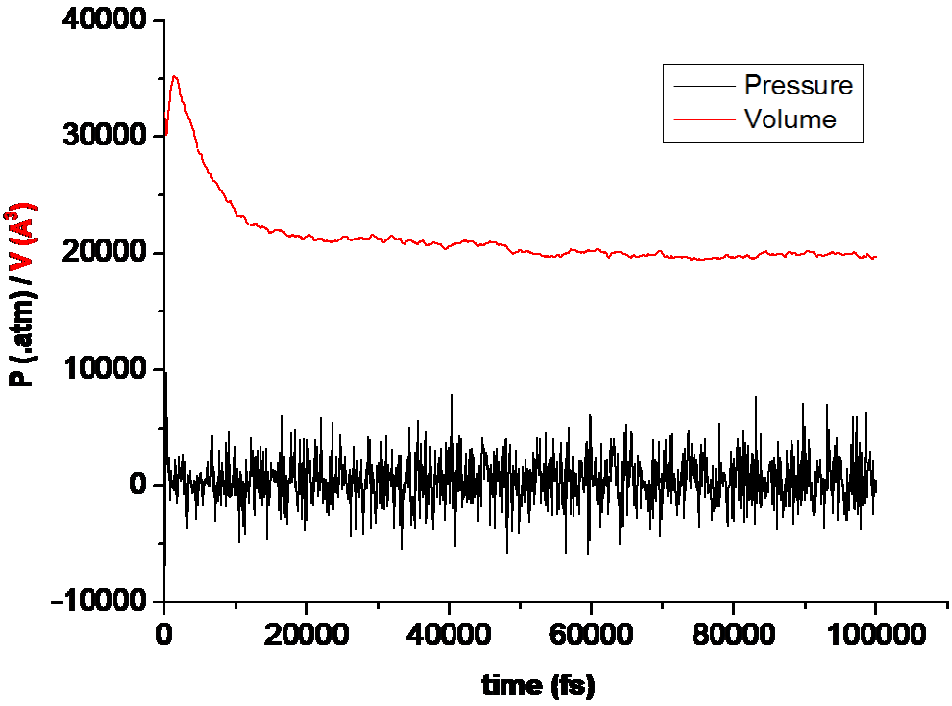
40000
30000
20000
10000
0
-10000
P (,atm) / V (A³)
0
20000
40000
60000
80000
100000
time (fs)
Pressure
Volume

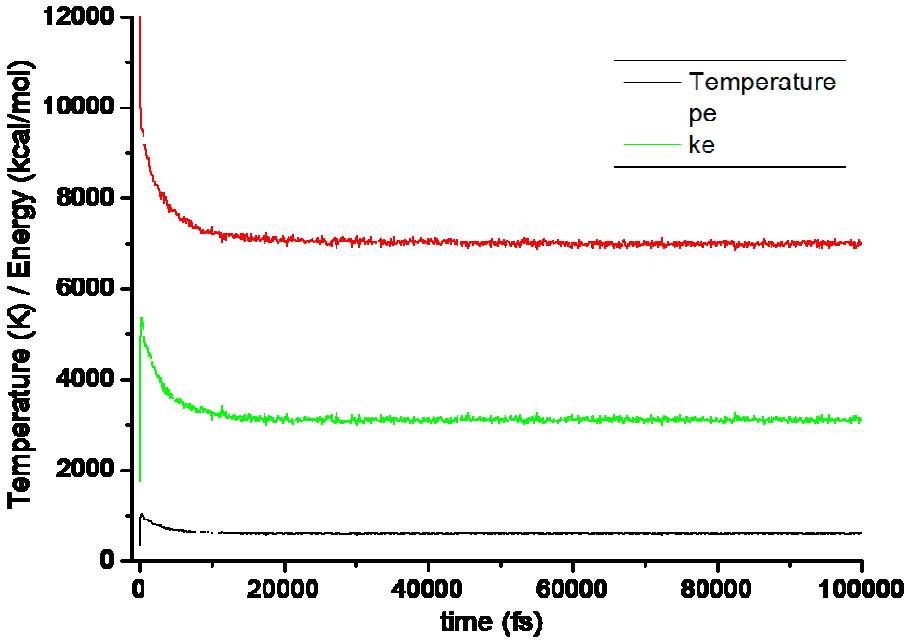
12000
10000
8000
6000
4000
2000
0
Temperature (K) / Energy (kcal/mol)
0
20000
40000
60000
80000
100000
time (fs)
Temperature
pe
ke

Figure 2-9. Evolution of (a) volume and pressure (b) temperature and energies in a compressing process.

Figure 2-9 shows time evolution of pressure, energy, temperature as well as volume in a compressing process. Fluctuation of all these terms was small after 50ps, which suggests the existence of an equilibrium state. In other words, the 100ps time interval between every dynamic run was long enough to let the system equilibrate. Damping factor is another parameter influencing MD runs. If the damping factor is small, system will fluctuate wildly; while the damping factor is large, system may take a long time to equilibrate. Figure 2-10 compares system behavior with varied temperature and pressure damping parameters.

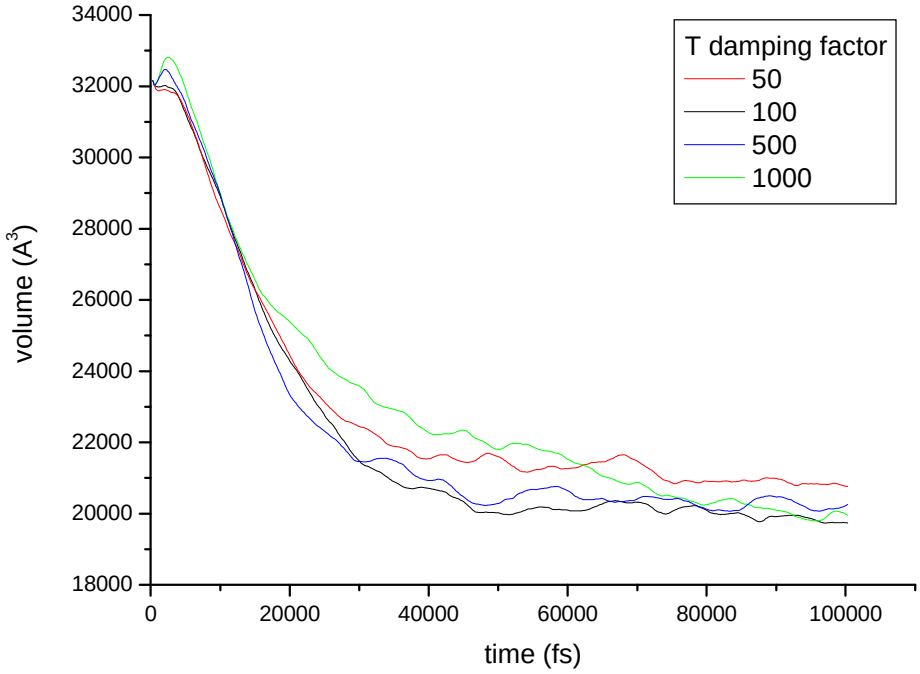
T damping factor
50
100
500
1000
volume (A3)
time (fs)
34000
32000
30000
28000
26000
24000
22000
20000
18000
0
20000
40000
60000
80000
100000

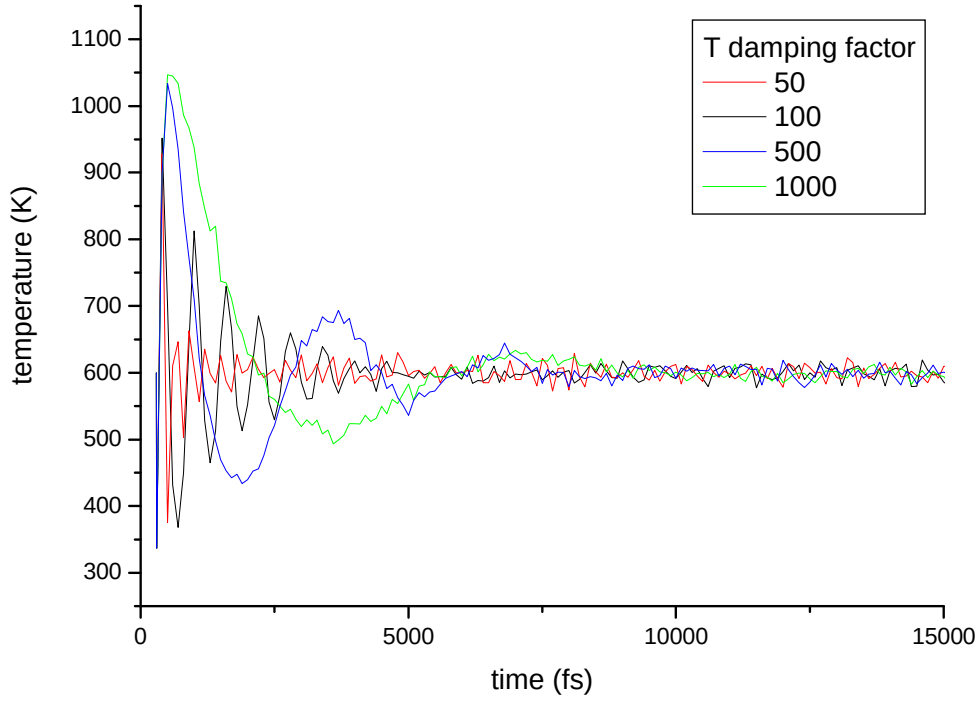
T damping factor
50
100
500
1000
temperature (K)
time (fs)
1100
1000
900
800
700
600
500
400
300
0
5000
10000
15000

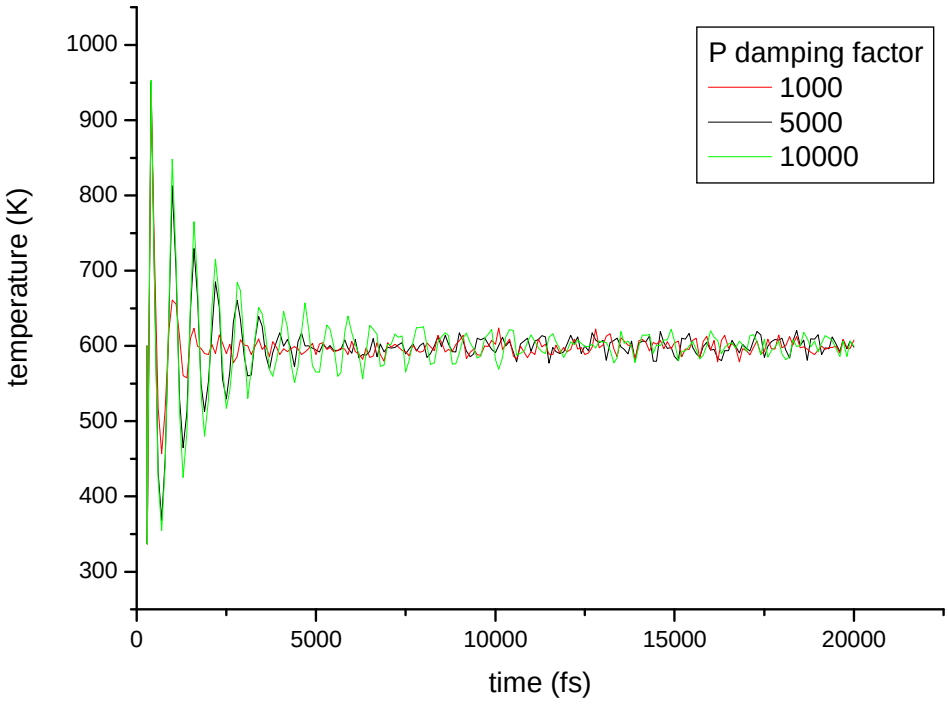
P damping factor
1000
5000
10000
temperature (K)
1000
900
800
700
600
500
400
300
0
5000
10000
15000
20000
time (fs)

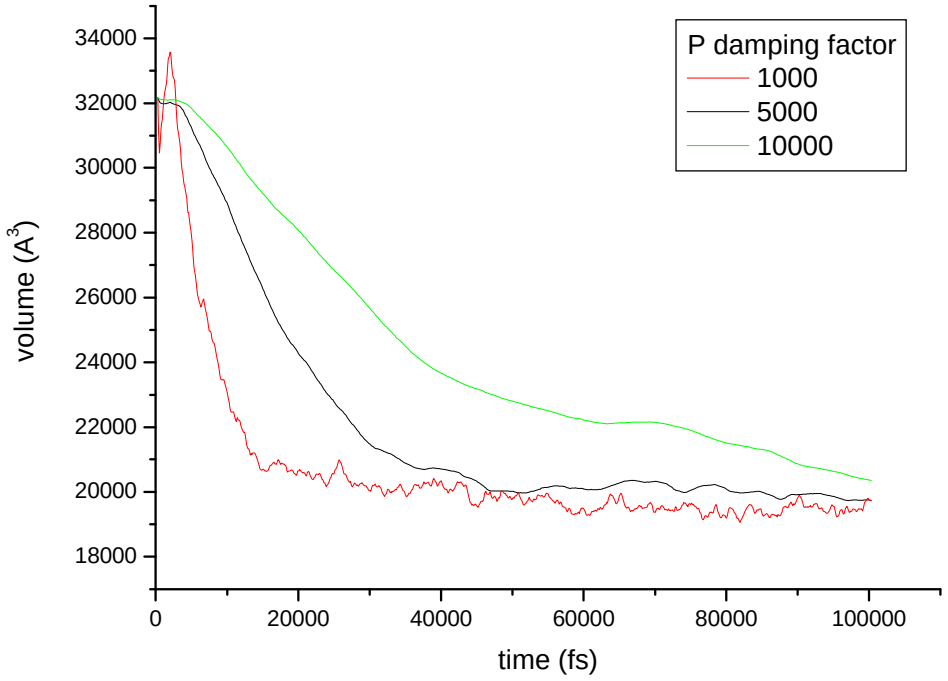
P damping factor
1000
5000
10000
volume (A3)
34000
32000
30000
28000
26000
24000
22000
20000
18000
0
20000
40000
60000
80000
100000
time (fs)

Figure 2-10. Effects of temperature and pressure damping factor on temperature and volume of system during a compressing process.

It was obvious that the influence of damping factors on system equilibrating is the same as expected. A temperature damping factor of 100 and a pressure damping factor of 5000 were chosen for following studies to leverage speed of equilibration and oscillation of physical parameters for such systems.

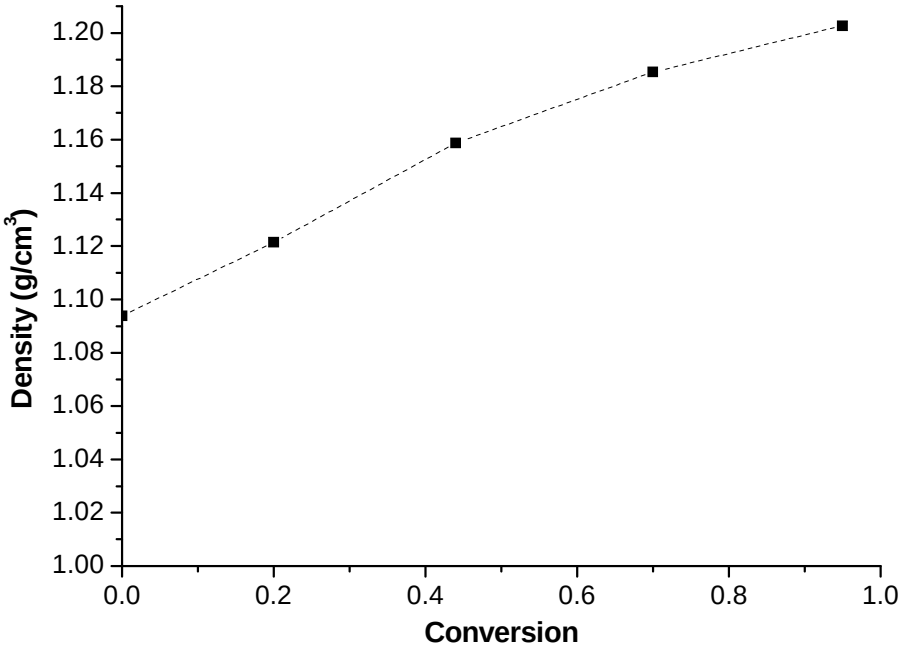

Figure 2-11. Densities of networks with varied conversions. ■: simulation data; dash line is for eye guide.

Density of the simulated epoxy network is related to conversion, primary sample size and the random seed used at the beginning for generating structures. First of all, TGDDM/DDS networks with different conversions were investigated. The densities of these networks are shown in Figure 2-11. It is obvious that a network with higher

crosslink density will have a more contracted configuration, which leads to a larger density. In non-cured TGDDM/DDS blends, molecules prefer stretched configurations. Density increases linearly with network conversions when conversion is lower than 0.6, and it achieves a steady value when conversion is larger than 0.8. The simulation box size is also believed to have an impact on the density. The larger the simulation box is, the closer the density is to actual value. Figure 2-12 illustrate the trend when the number of monomers in simulation box was increased. Different from the epoxy conversion, box size was shown to have less influence on the density of cured network. The variation of densities of different boxes was less than 2%, within experimental error range. Also, neither the increasing nor a decreasing trend suggested a suitable box size larger than 40 monomers, where box size effects will be eliminated.

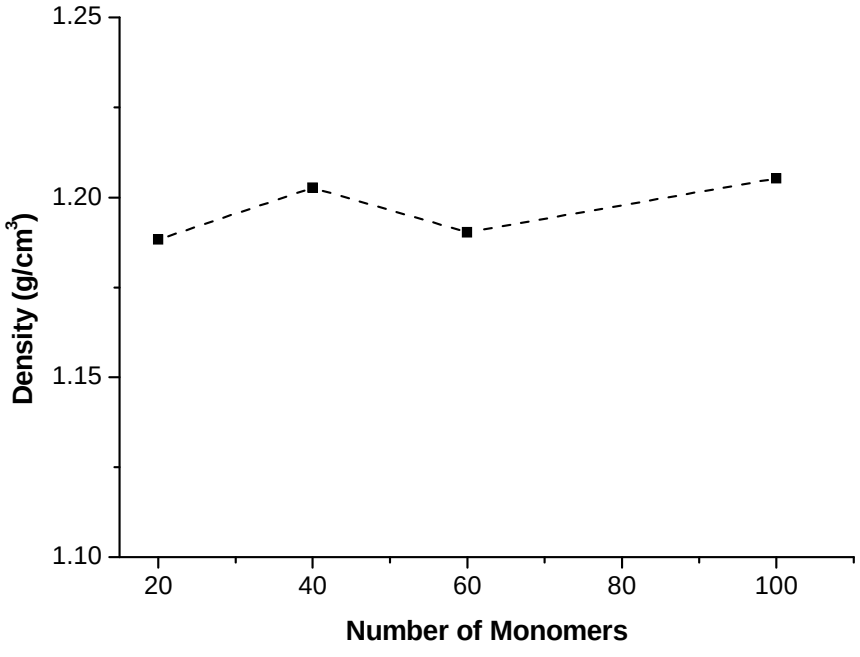

Figure 2-12. Densities of system with different size. ■: simulation data; dash line is for eye guide.

As mentioned in the previous sections, the Dreiding force field was employed to characterize forces and energies in the system. Dreiding is generic force field with a small number of equations and parameters. The advantage of the Dreiding force field is that it can predict and reproduce properties of organic systems fairly well although it may not be very accurate. A more complex force field COMPASS was invented exclusively for polymers. The mathematical expression of COMPASS is much more complex than Dreiding and has a large number of parameters. To compare Dreiding and COMPASS, we collected parameters from published literatures and implemented in LAMMPS. When applied to the same molecule, no obvious difference was observed. Figure 2-13 compares the structure of a BPA epoxy molecule using two force fields.

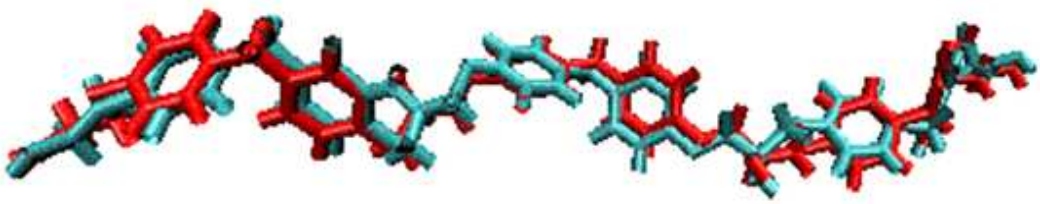

Figure 2-13. Structures of a linear epoxy obtained with two force fields. Blue: Dreiding, Red: COMPASS.

2.3 Properties derived from simulation

2.3.1 Physical and chemical properties

The density of the material in the simulation box shown in Figure 2-8 is 1.21 g/cm^3, while experimental value is close to 1.23~1.29 g/cm^3 [67] . The conversion of epoxy group is 0.91 when using a maximum cutoff distance of 18 Å. It should be pointed out that the maximum cutoff distance depends on the nature of the epoxy system, cross-

linking method and lattice parameters. Crosslinking the reactive sites within a cutoff distance of 18 Å may create some bonds with very high bond lengths, which are unrealistic and increase the local potential energies. Too many too long crosslinks would lead to a configuration with high energy. However, the advantage of a large cutoff distance is that it helps increase the conversion of network and overcome the lack of mobility of monomers in the system. Long bonds and associated high energies can be fixed when force field is effectively used. Therefore the percentage of long bonds after crosslinking was examined and shown in Figure 2-14.

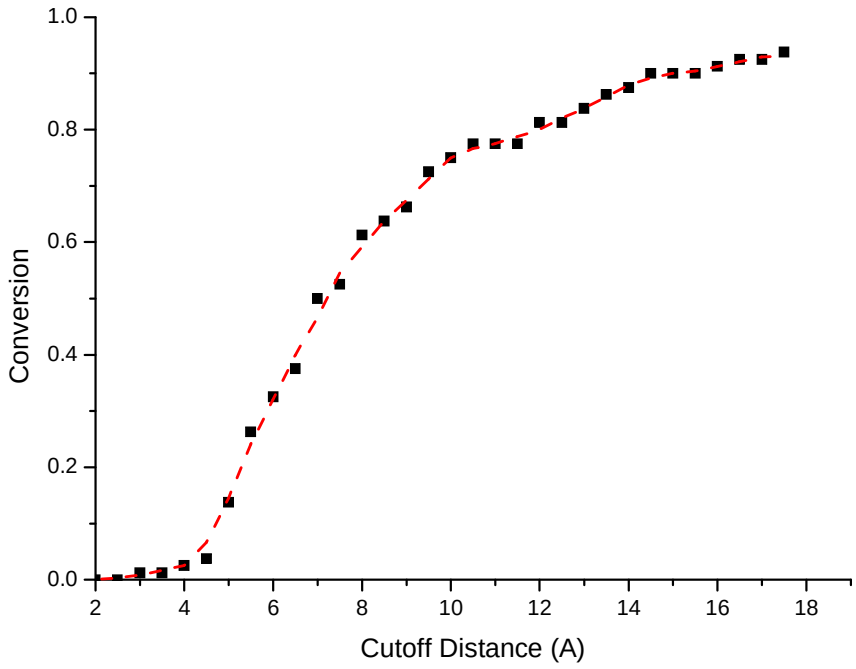

Figure 2-14. Conversion of epoxy as a function of cutoff distance.

As seen from Figure 2-14, about a conversion of 70% could be reached when the cutoff distance was increased to 10 Å, which means 70% of the total crosslinks were less than 10 Å. After minimizing energy, the other 30% long crosslinks would be

corrected. Bond energy per unit after crosslinking and energy minimization verified that all the crosslinks were adjusted to equilibrium length. The bond length check routine also showed that the maximum cutoff distance was acceptable in our research. Varying the cutoff distance for crosslinking could adjust the conversion from 0 to 1, although a conversion of 1 is unreachable experimentally. This is due to the fact that conversions of epoxy group to hydroxyl groups in TGDDM occurs before curing in reality, which were not designed to be happening in our simulation.

Table 2-1. Number of reacted functional groups in the major components

	TGDDM		DDS
4	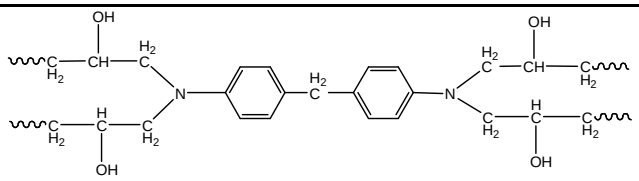	3	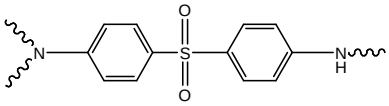
5	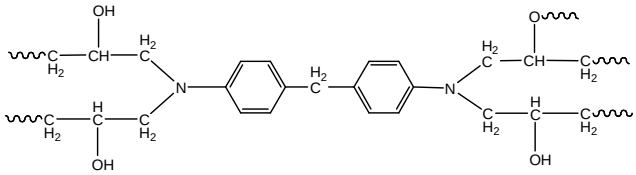	4	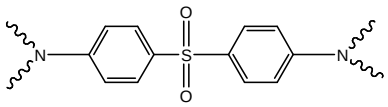

Since the numbers of functional groups in TGDDM and DDS is four and epoxy group can react with hydroxyl group, the types of moieties of both components after crosslinking are larger than four. Despite the complexity of these moieties, there are two major moieties in both components, as shown in Table 2-1. The percentages of the major moieties of TGDDM and DDS were given in Table 2-2. The percentages of two main moieties of TGDDM and DDS existing in the system after crosslinking were in a roughly agreement with experimental results. The difference can be attributed to adopting cutoff besides reaction rate as criteria to crosslink monomers. In addition, high

crosslinking conversion will turn more secondary amine groups to tertiary amine, which leads to a higher percentage of fully reacted DDS moieties. For epoxy system in which more than one types of crosslinking are expected to take place, our methodology provides a way to analyze chemical connectivity after crosslinking. In addition, for most diamine cured epoxy, the primary amine and secondary amine have different reaction rate coefficients due to dimensional and chemical environment. From the literature search, it was observed that this is the first time uncover the chemical connectivity of polymer networks was uncovered via MC/MD simulation.

Table 2-2. Percentages of major moieties of epoxy and amine after curing.

Epoxy			Amine		
n	MD	Exp [68]	n	MD	Exp [68]
4	42	38	3	44	45
5	36	39	4	40	32

The thermal dependence of volume and density of the simulation box was also investigated by means of MD. The detailed MD routines were discussed in the previous part. The glass transition temperature (T_g) of crosslinked epoxy resin can be determined as the slope change point in a plot of density versus temperature. T_g is sensitive to cooling rate, thermal history and measurement method. In atomic simulation, T_g may also fluctuate time to time due to different initial configurations. Figure 2-15 is a plot of densities at varied temperatures. Linear fitting to MD results illustrated that density decreased linearly when the system is cooled down both above and below T_g. The cross point of the two fitted line indicated T_g as 557 K, in a good agreement with experimental T_g of 533~563 K [67]. Another way to calculate T_g is looking at the temperature dependence of volume as shown in Figure 2-16. The kink point of volume change

fraction versus temperature curve gave the same T_g. Another physical parameter that can be obtained from the curve is the volume thermal expansion coefficient (VTEC). VTEC is defined as

$$\alpha = \frac{1}{V}(\frac{\partial V}{\partial T})_P \qquad (2\text{-}3).$$

VTEC is three times the linear thermal expansion coefficient (LTEC) for small values of VTEC,

$$\beta = \frac{1}{3}\alpha \qquad (2\text{-}4).$$

Computed from the slope of linear fitted line, VETCs above and below T_g were found to be 394 ppm/ºC and 272 ppm/ºC for our system. Compared with literature results [43, 67] of similar systems, the the values calculated from the present simulations are fairly accurate. A larger VTEC above T_g than the one below T_g is obviously due to the higher mobility of polymer segments above T_g.

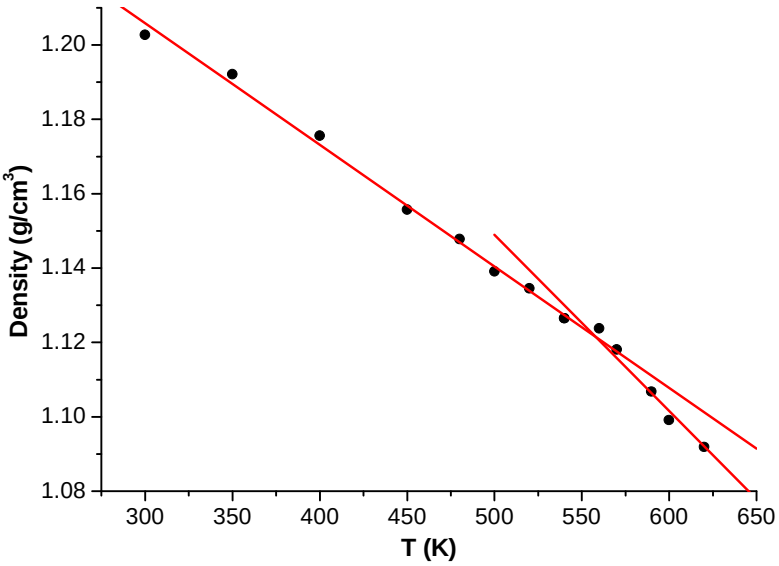

Figure 2-15. A plot of density versus temperature of TGDDM/DDS system. ●: simulation data; red lines are linear fitting to the simulation data points.

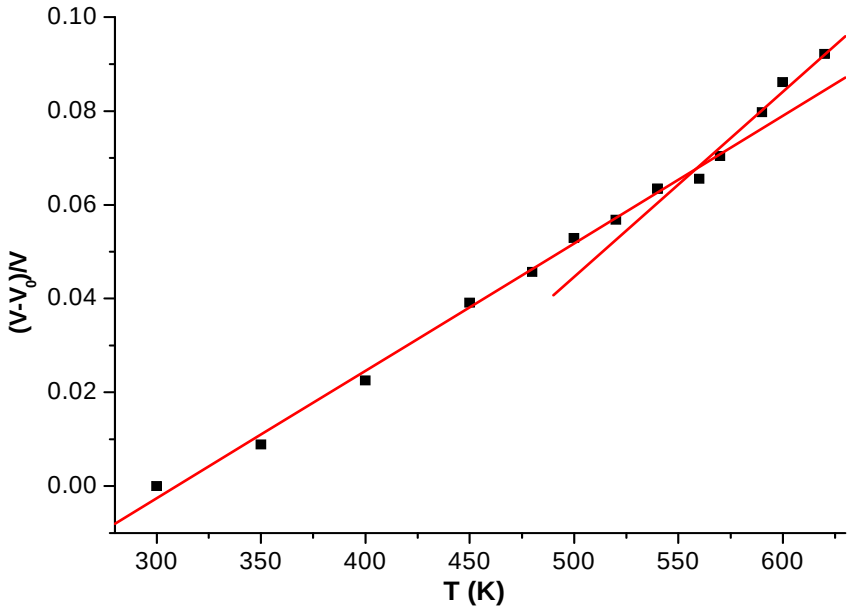

Figure 2-16. Volume change versus temperate of TGDDM/DDS system. ●: simulation data; red lines are linear fitting to the simulation data points.

Bulk epoxies can be seen as isotropic materials, which means polymer segments have no orientation along any direction in a microscopic view and materials have same modulus along all three directions for a bulk. To study isotropy of simulation box, orientation of covalent bonds was characterized with three angles shown in Figure 2-17. The angles between one bond and x, y and z axes are denoted as α, β and γ respectively. Here a special case is used as an example to illustrate how to relate these three angles to orientation of systems. If one bond is parallel to x axis, then α is 0, β and γ are 90 degrees. If the red bond in Figure 2-17 goes through the body center of the cube, then α, β and γ are all 45 degrees. It suggests that if α, β and γ are the same, then the bond has no orientation. When any of α, β and γ is close to zero, it means the bond

has an orientation along the corresponding direction. When dealing with a model system with a number of bonds, the same rule still applies.

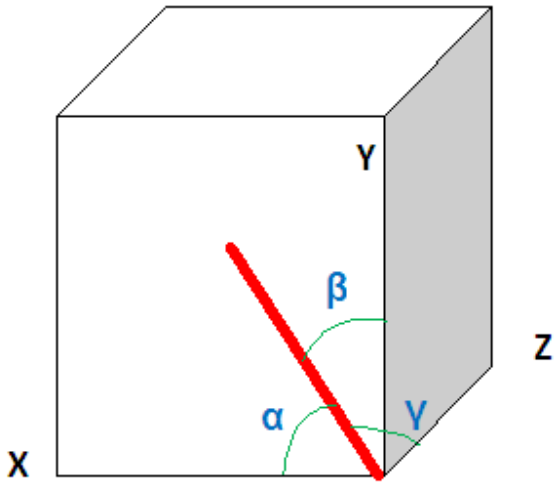

Figure 2-17. Angles between one bond and three axes.

Orientation of bonds along each direction were calculated and shown in Figure 2-18. Since the angles between every bond and three axes were calculated using cosine function, an angle distribution from 0 to 180 degrees was obtained. It is possible that angle distributions of α, β and γ are almost concurrent. Peaks at 90 degrees correspond to 45 degrees in one bond case. Based on previous discussion, one can tell that cured and equilibrated epoxy system is isotropic and close to real epoxy materials.

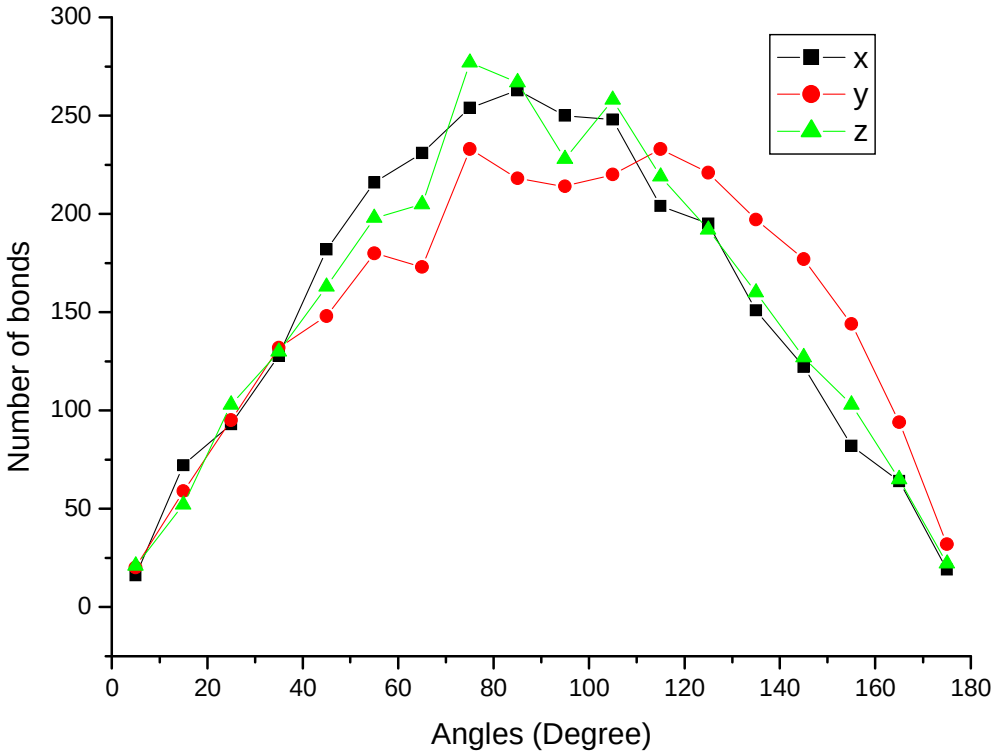

Figure 2-18. Distribution of angles between covalent bonds and X, Y, Z axes.

2.3.2 Mechanical properties

Besides chemical composition and physical properties, we can compute mechanical properties of materials using MD. In literatures, two classes of methods are found for calculating modulus: the static method and dynamics method. In the static method, a small strain is applied to the system followed by an energy minimization at that fixed strain. The energy difference before and after the small strain is derived to obtain stiffness matrix. In dynamic method, system is deformed continuously at a chosen strain rate within the elastic region (<5%). Therefore, modulus can be calculated from the resulting stress-strain curve. Both methods have advantages and drawbacks. In this

work, the dynamic method was adopted to compute mechanical modulus in the small strain region and to observe materials' behavior in the large strain region.

In LAMMPS, tensile or compressive tests were realized using “deform” command under NPT ensemble. Strain rate can be in terms of true strain or engineering strain. To optimize model parameters, system size, strain rate and some other coefficients were varied. Figure 2-19 compares stress-strain curves of systems with different sizes at room temperature. Two lines are highly coincident which suggests size of simulation box has no significant effect on stress-strain curves. Both curves increase linearly from zero at first, level off at around a strain of 0.1 and go up again with increasing strain. This curve of epoxy agrees well with a typical stress-strain curve of a glassy polymer. The initial linearly increasing region of stress corresponds to the elastic region. The atomistic level origin for the behavior in this region is the non-bonded attractive van de Waals forces try to prevent the tensile deformation. At about a strain of 0.1, epoxies yield and come to the plastic region. Because of the short chain lengths between crosslinking points, the curve of epoxies goes up again in plastic region. Since covalent bonds in classical MD are not breakable, the ultimate strength at materials breaking cannot be detected. The shape of stress-strain curves is also related to strain rate.

Figure 2-20 shows the effect of strain rate on stress-strain curves of systems. A larger strain rate increases yield stress and yield strain and stresses in the plastic region. A stronger and harder materials behavior is contributed to a delayed response of polymer chains to a quick deformation. A similar phenomenon can be observed in an actual stretch test. The strain rate in Figure 2-20 ranges from 0.01/fs to 0.006/fs. Either of them is much higher than an experimental strain rate. Due to the limitation of time scale associated with MD, a higher-than-usual strain rate is necessary to achieve an observable deformation. Previous studies already verified that even the strain rate in MD

is extremely high, modulus and strengths of materials are still comparable to experimental values [41, 69].

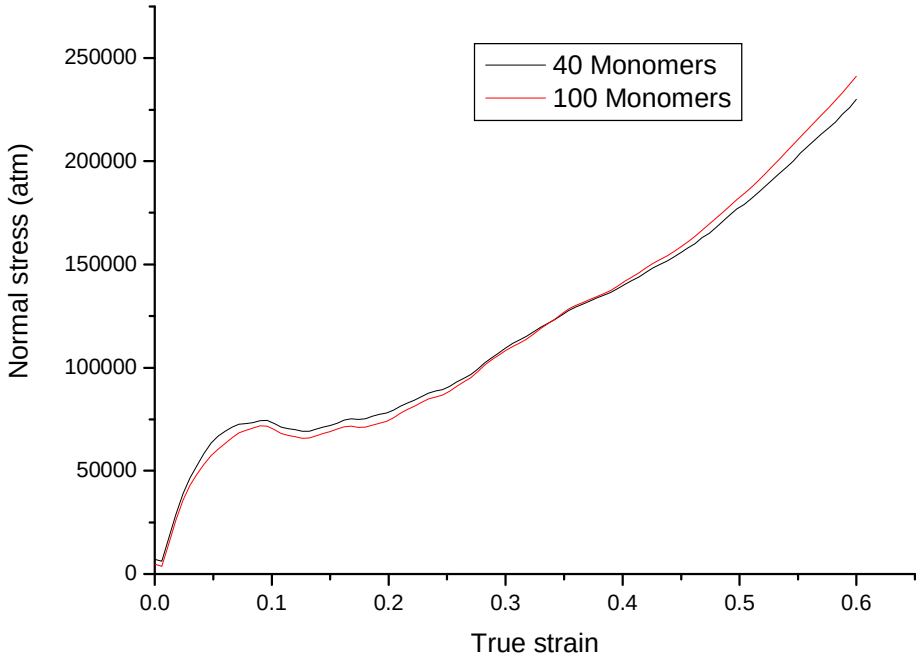

Figure 2-19. Stress-strain curves of systems with different sizes.

Figure 2-21 illustrates modulus of TGDDM systems at varied strain rates. Moduli of TGDDM systems were computed by fitting the elastic region in stress-strain curves with a linear line. Slopes of the fitting lines give elastic moduli. The modulus of the material increases with strain rate. From the curve, we can optimize strain rate to achieve both reasonable mechanical properties and computational time. It turns out that a rate of $1e^{-6}$/fs (engineering strain) is suitable for most mechanical tests in MD. This conclusion was also reached by other reports in the literature [70, 71].

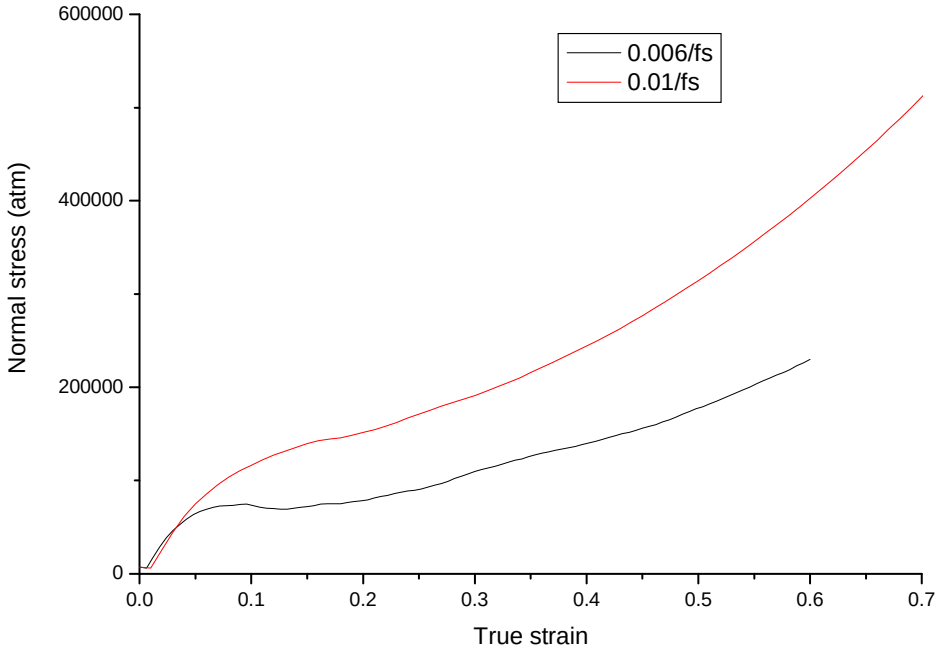

Figure 2-20. Stress-strain curves of systems at different strain rates.

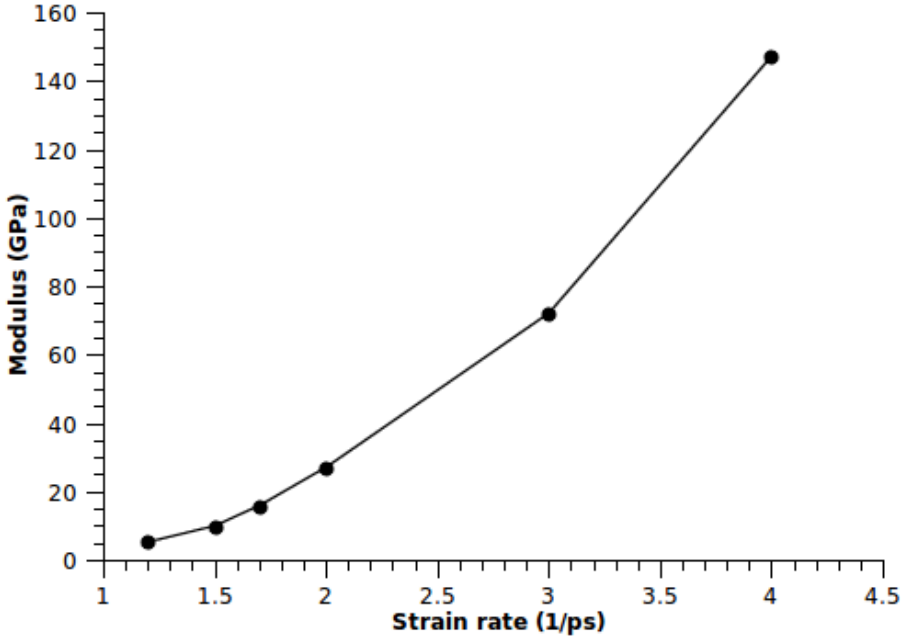

Figure 2-21. Effect of strain rate on modulus of systems.

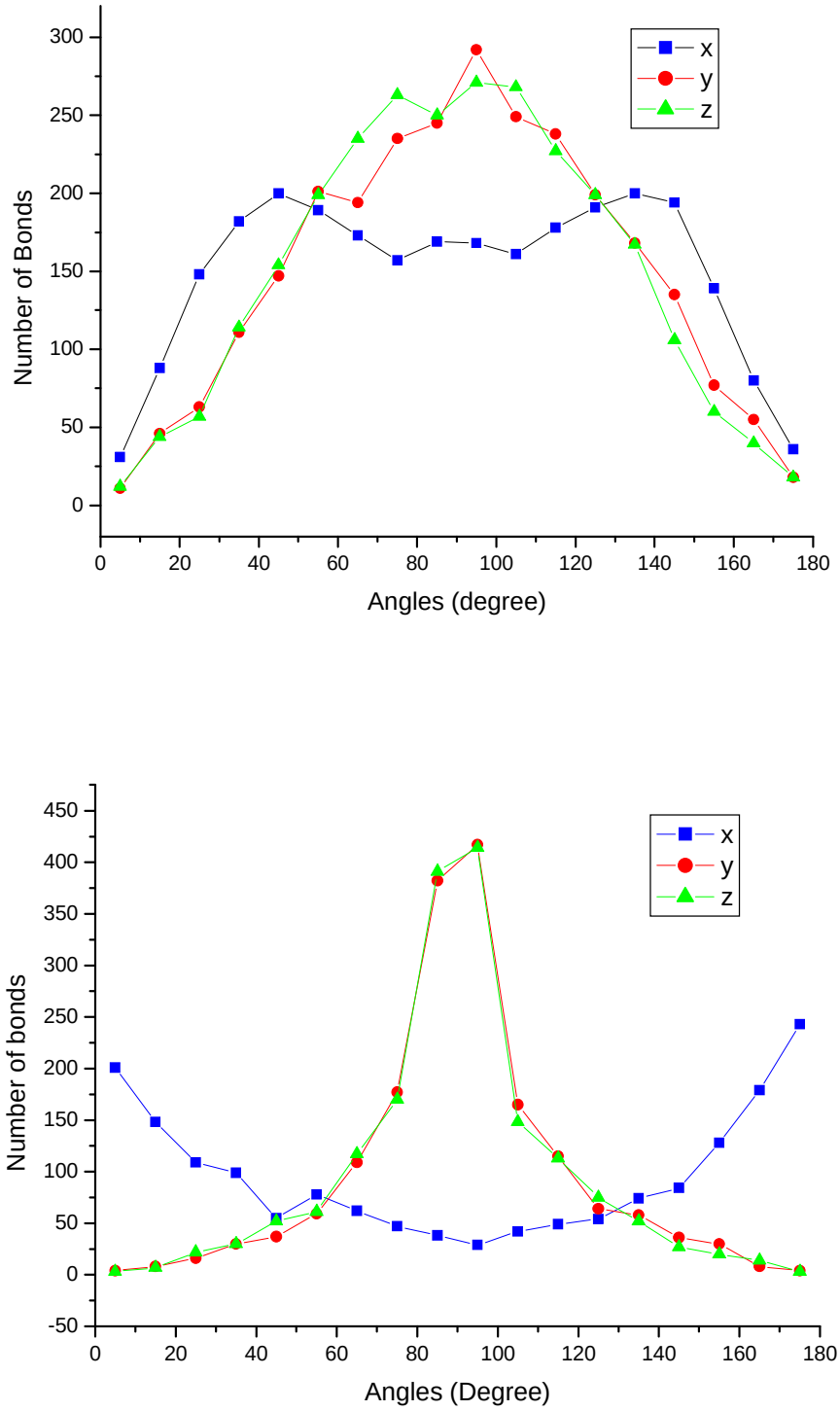

Figure 2-22. Orientation of bonds at varied tensile strain: (a) 20% ; (b) 50%.

Orientation development of polymer chains under deformation is an important aspect and has been studied for a long time. For linear polymer systems, high order arrangement of chains along the tensile direction was observed, which is the fundamental basis for making fibers. It was contributed to a high mobility of linear segments and a low level of energy barrier of chain rotation. The situation of polymer networks is believed to be different from the linear polymers due to the existence of network crosslinking points. Previously, we have demonstrated the isotropy of cured TGDDM box by calculating three angles between bonds and axes. To examine orientation of epoxies after deformation, the material in the simulation box was stretched to different strain and angles between bonds and axes were calculated. In Figure 2-22, distributions of α, β and γ angles at strains of 20% and 50% were shown. An obvious change of angle distributions from the un-deformed box can be observed. The location of α angle peak shifts from 90 degrees gradually to 0 degree and 180 degrees; while peaks of β and γ angles are becoming sharper and sharper at 90 degrees. Recall that in the special case of the one bond, when the bond is parallel to x axis, α equals 0 or 180 degrees and β and γ are 90 degrees. For the entire simulation box, we see that α is getting closer to 0 and 180 degrees; at the same time, β and γ are approaching 90 degrees. It suggests that a majority of bonds in simulation box are prone to be parallel to x axis, which is the direction of tension. Compared to linear polymers, polymer networks have many crosslinking points acting as constraints. These constraints and entanglements try to hold the original structures of networks. However, under a strong external stress, movement of chains will drag crosslinking points to new positions. Besides bond orientation, we can use another parameter for the characterization of structural evolution during deformation.

Pair correlation function *g(r)* calculates distances between certain pairs of particles in simulation box. It gives information about characteristic lengths in model systems. A cured simulation box was stretched uni-axially to varied strain. Pair correlation functions for each system were depicted in Figure 2-23. Only the distances between non-bonded atoms were calculated and graphed. Peaks in Figure 2-23 indicate pairwise distances at highest probabilities, which are also known as characteristic lengths. The comparison between three systems suggests that x values of these peaks did not change during the deformation process despite the change in amplitude of these peaks. This can be interpreted as relative distances between nonbonded atoms are not influenced by external stresses. The characteristic lengths are primarily decided by van de Waals radius of each atom.

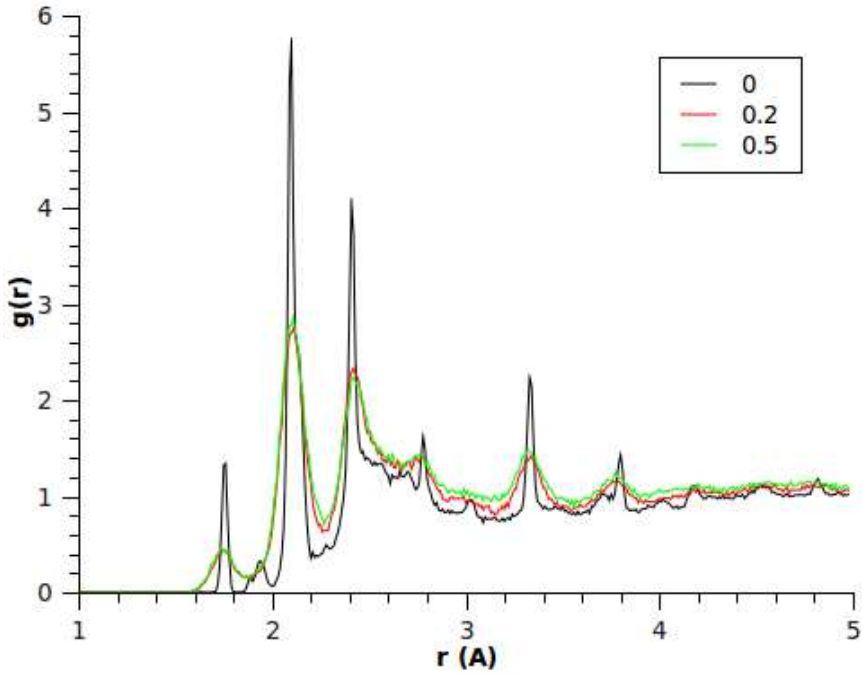

Figure 2-23. Variation of pair correlation functions of systems with different strains.

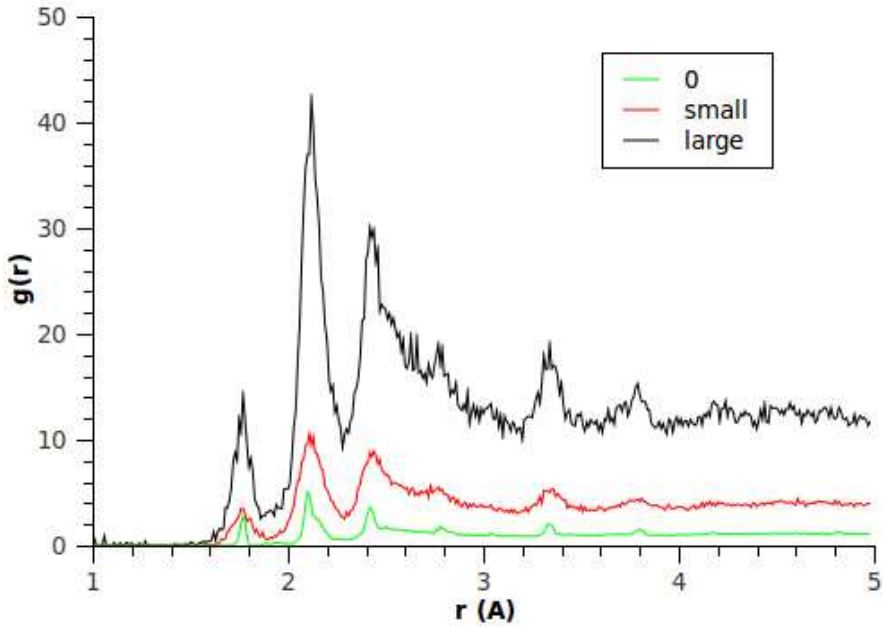

Figure 2-24. Pair correlation functions of epoxy systems at different shear strains.

The same simulation box was also sheared along xy plane instead of uni-axial stretch. Similar conclusions could be drawn from Figure 2-24 with respect to pair correlation function. This further verified that external forces have little effect on g(r).

At last, the effect of temperature on modulus of TGDDM epoxies was studied by conducting tensile tests in MD at varied temperatures. Figure 2-25 shows the variation of modulus in a temperature range from 50K to 300K. A drop of modulus was seen with increasing temperature, which is consistent with experimental results. At a low temperature, mobility of atoms and chains decreases; thus polymer has a slow response to external stress. In macroscopic scale, materials become stronger and more brittle.

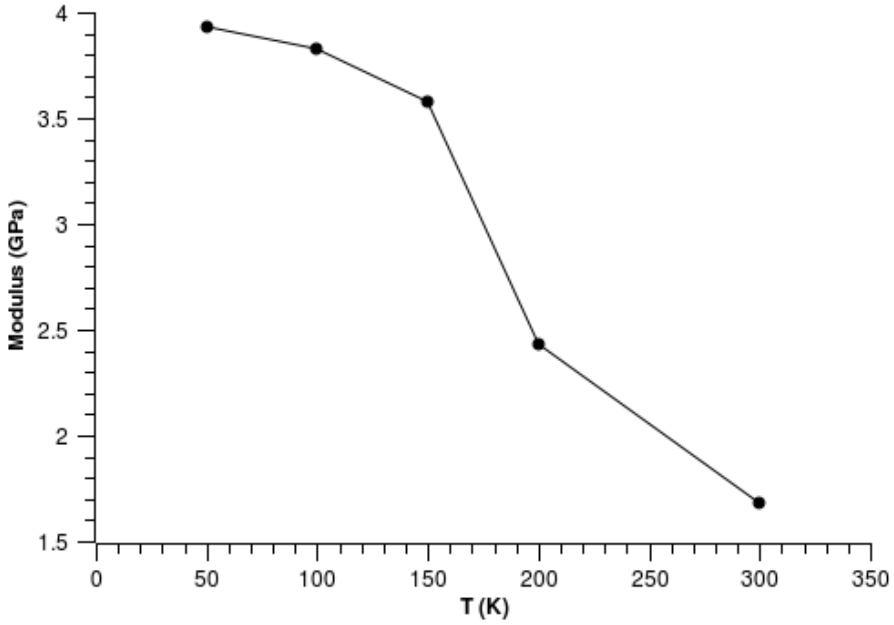

Figure 2-25. Modulus of TGDDM at different temperatures.

Time requirement for the generation of initial structures was analyzed and shown in Figure 2-26. As mentioned before, generating cured epoxy network was consisted of two steps: a step of building monomers in simulation box and a step of crosslinking epoxies and curing agents. Here the total cpu time on a 2.4GHz Intel i5 processor needed to generate initial structures T(t) (following relaxing and checking not included) was broke down into two parts T(s1) and T(s2) indicating time consumed in step one and step two. In a logarithmic coordinate, an approximately linear relationship between total cpu time T(t) and number of atoms generated was discovered and a scale factor of about 1.7 was revealed. When time elapsed in each step was examined, one can find that increasing time is associated with increased number of atoms. However, an intersection of T(s1) and T(s2) curves in Figure 2-25 suggests that when total number of atoms was small, a larger portion of time was consumed to generate monomers. As a

comparison, more time was needed to cure monomers than generating them in a large simulation box. In curing step, distances calculation between atoms has a time complexity of $O(n^2)$. On the other side, generating monomers has a time complexity of O(n). As a result, time consumed in step two increases more rapidly than that of step one.

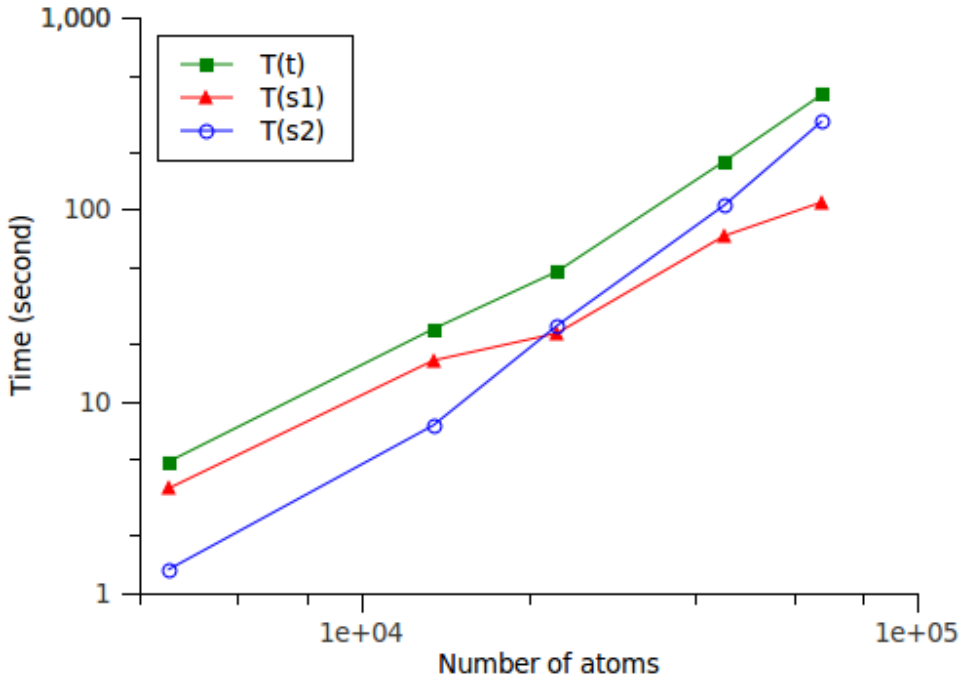

Figure 2-26. Relationship between cpu time and number of atoms generated in simulation box plotted in a log-log coordinates.

2.4 Conclusions

In this chapter, a methodology to simulate crosslinking polymer networks and capture the physical and chemical properties is proposed. A highly crosslinked network with similar physical parameters and chemical connectivity compared to actual epoxy systems can be built via a three-step procedure. First, the monomers were generated in a diamond lattice. Secondly, the monomers were crosslinked based on a cutoff distance,

reaction rate and functional group concentration combined criteria. Third, an energy minimization process was performed to update atom coordinates. A following MD simulation was carried out to obtain final network and thermal parameters. A TGDDM/DDS based epoxy system was taken as an instance to illustrate the algorithm. With a high crosslink density, the epoxy network had a comparable density with experimental values. The conversion and temperature dependence of density were also studied. A higher conversion led to a higher density; while density decreased as temperature went up. A slope change point of density versus temperature defined the T_g of the network. A calculated T_g of 557 K was consistent with experimental results. The volume thermal expansion coefficient above and below T_g were also calculated The two VTEC were found in agreement with other published results. The chemical connectivity of crosslinked network was another important aspect that required special attention. The percentages of moieties of two monomers after crosslinking also validated the reliability of this new method. Overall, the methodology presented here can be transferred to other complex polymer network.

CHAPTER 3

INFLUENCE OF CHAIN SCISSION ON PROPERTIES

3.1 Modeling and simulation details

In this chapter, effect of chemical aging (chain scission) was investigated using MD. Particularly, oxidation and hydrolysis chain scission mechanisms were compared for polymer networks. The structure of TGDDM/DDS cured epoxy is adopted as the model system. Since classical MD cannot model bond breaking, chain scission was conducted manually based on chemical aging algorithms.

TGDDM/DDS epoxy resins were generated using methodology described in Chapter 2. A simulation box containing 100 monomers was generated and crosslinked. The size of simulation box was fixed for this chapter and conversion of monomers was 0.85. The starting point of all chain scission simulations is crosslinked and equilibrated simulation box at room temperature and one atmospheric pressure. The approach of modeling oxidation of TGDDM epoxies is explained below.

A small segment of the crosslinked epoxy resin is shown in Figure 3-1. According to the oxidation mechanism, all possible bond cutting sites were indicated by bold black lines in the chemical structure. These locations were chosen based on several assumptions. First, aromatic rings are very unlikely to be broken. Secondly, only scission of backbones will have an effect on the property of the resin network, so the breaking of short side chains was not studied here. After all possible bond cutting sites were found,

a percentage of sites with respect to the total bond number of the system were cut randomly. After chain scission, the two atoms linked by the broken bond were saturated by hydrogen atoms. Varied percentages of bonds were broken to study the effect of chain scission on performances of epoxy resins. Three independent structures were generated for each cutting percentage to reduce systemic randomness induced by initial structures and cutting. Hereafter, the simulation box, where one percent bonds were broken, is referred as the 1% box. Other boxes are also referred as 2% box, 3% box and so on using the same notation.

After chain scission, compression-decompression and annealing processes were carried out using the same procedures described in Chapter 2. Densities at varied temperatures were calculated in the annealing process. Epoxies in the simulation boxes were stretched or sheared at constant engineering strain rate of 10^{-6}/fs to a small strain of 5%.

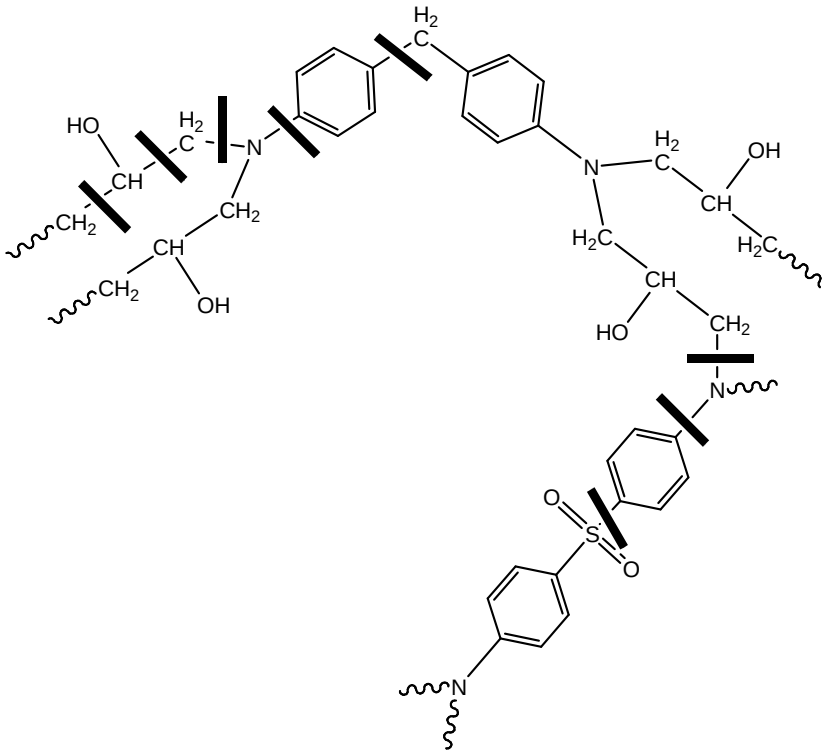

Figure 3-1. Possible breakable bond types in a fraction of epoxy resin network according to oxidation algorithm. All the sites were indicated with bold black lines.

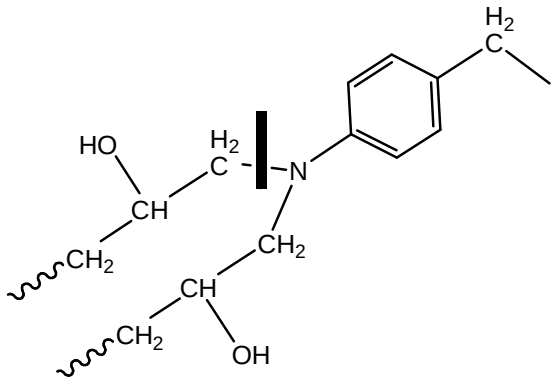

Figure 3-2. Possible breakable bond types in TGDDM according to hydrolysis algorithm.

The algorithm of hydrolysis was shown in Figure 3-2. Only carbon-nitrogen bonds will be broken based on mechanism of hydrolysis. Broken bonds were saturated with water. Since only the effect of chain scission was investigated in this chapter, isolated water molecules were removed from simulation box after hydrolysis. Simulation boxes were equilibrated after hydrolysis as well following the same procedure as used in oxidation.

The fundamental difference between hydrolysis and oxidation can be understood on the basis of the reactions. In modeling, this difference is interpreted by variation of possible breakable bonds. Reaction rate, temperature, reactant concentration and some other factors related to the chemistry of oxidation and hydrolysis were not taken into account. Only the structural change in polymer networks and the impact of such changes on the bulk properties are discussed.

3.2 Oxidation

3.2.1 Analysis of structures

After reaction, the 0% box contains a single network, i.e. no isolated small reactants existed in the box. Figure 3-3 compares the morphologies of the polymer in the 1% box and 5% box. When one percent of bonds were cleaved, the basic network structure remained basically intact. Meanwhile some small fragments, which were cut from the network, were found. In Figure 3-3(b), a significant amount of small molecules were found in 5% box, which suggested that the network has been converted to a blend of small pieces of fractures. To further analyze the results of bond breaking and distinguish large networks and small fractures, the numbers of atoms in each molecule in the simulation box were computed. Figure 3-4 gives an evolution of the number of atoms in the largest molecule in the system (M_{max}). As observed before, the original network was an interconnected structure and has a total 4500 number of atoms. While more and more bonds were broken, M_{max} was becoming smaller and smaller. In the 5% box, M_{max} is only about 400. The rapid drop of M_{max} from 4500 to 400 verified the argument that 5% box is basically a blend of small molecules. The trend of M_{max} suggests that the transition from network structure to small molecules blend takes place when about three percents of bonds are broken.

(a)

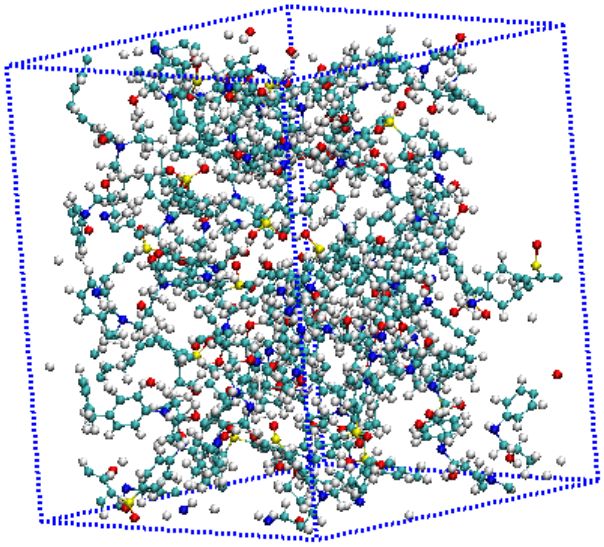

(b)

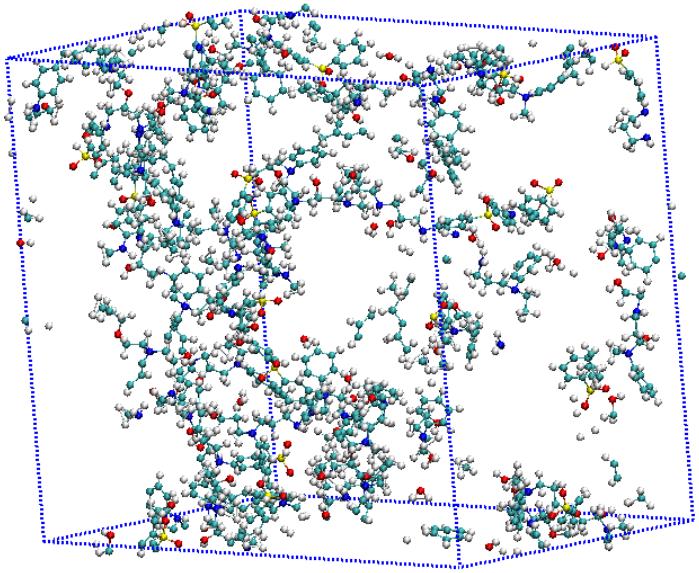

Figure 3-3. Atomic representations of simulation boxes when (a) 1 percent bonds were broken (b) 5 percents bonds were broken.

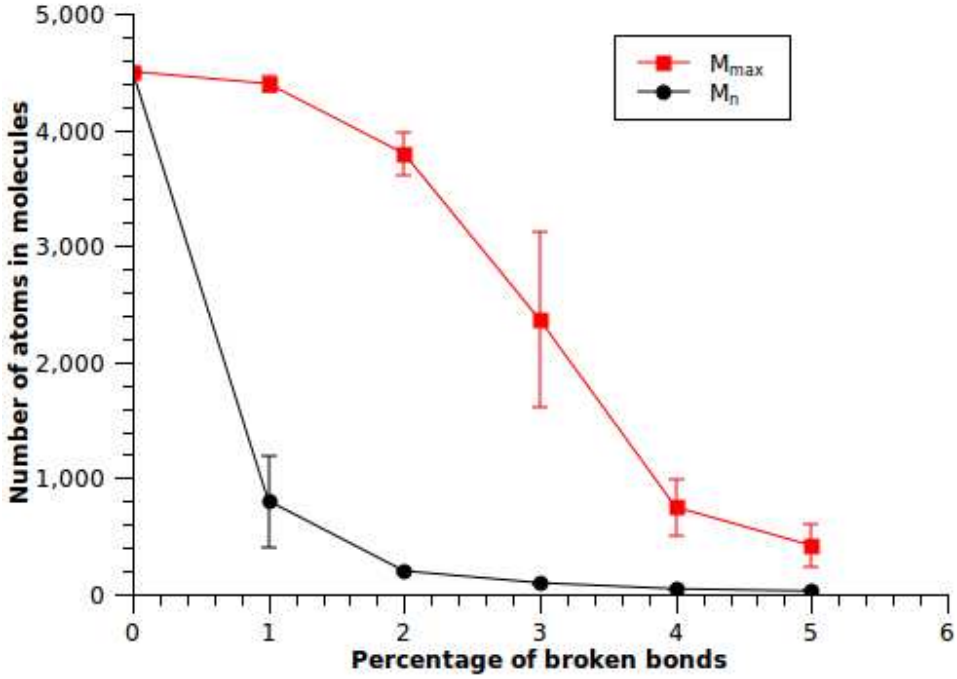

Figure 3-4. Number average number of atoms of molecules (M_n) and number of atoms in the largest molecule (M_{max}) in simulation systems with varied percentages of bond cutting.

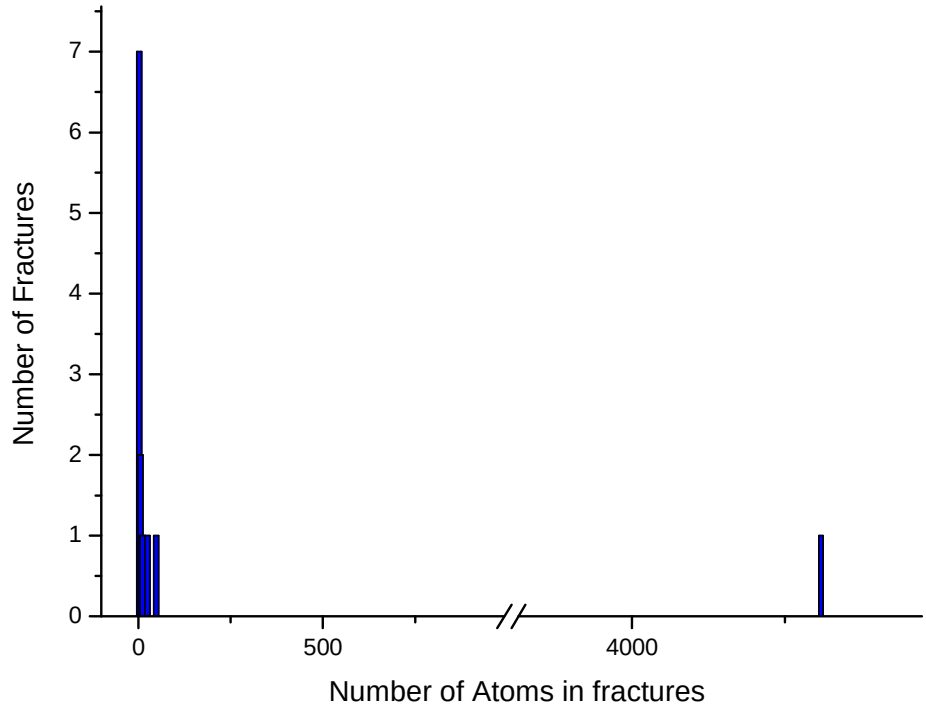

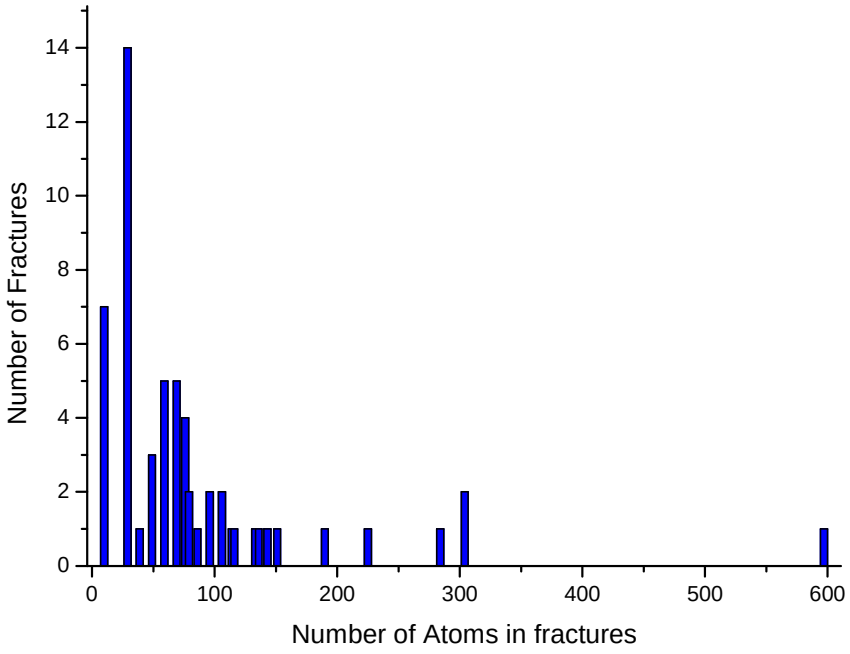

Figure 3-5. Distribution of numbers of atoms in fractures after (a) 1% (b) 5% bonds cut.

M_{max} is one parameter describing structural evolution during chain scission. Besides the largest fracture in the simulation box, a portion of small molecules were also generated as more bonds were cut. Figure 3-5 gives distribution of numbers of atoms in fractures in 1% and 5% boxes. In 1% box (Figure 3-5(a)), the distribution is very diverse as almost all the small molecules have less than ten atoms. If number average molecular weight (M_n) is calculated, we can estimate it to be around 900. The large deviation of M_{max} from M_n is due to the existence of very small molecules. In 5% box, the distribution of numbers of atoms is less broad than that of 1% box. The largest molecule has about 600 atoms while the second largest one has about 300 atoms. The peaks of distribution locate at around 25 and 60 along x axis. It suggests that 5% box is basically a blend of small molecules, which was already verified by the morphology of simulation box in Figure 3-3(b). Number averaged molecular weight also dropped to tens. The variation of M_n was also shown in Figure 3-4.

3.2.2 Degradation of properties

To compare the densities of different simulation boxes at room temperature, densities as a function of cutting percentages are shown in Figure 3-6. As seen in Figure 3-6, the density of epoxy resin increases first and then decreases when cutting percentage is increased. As shown in Figure 3-3, small pieces of molecules will be cut off from the network when bonds were broken. Thus, the compactness of simulation boxes, which decides the density, can be divided into two aspects: the compactness of network matrix and that of small molecules. The change of number average number of atoms of molecules (M_n) in simulation boxes is also shown in Figure 3-4. The dramatic decrease of M_n is observed when one percent of bonds were cut. This can be

contributed to the large difference of molecule sizes in 1% box because the second largest molecule in 1% box only has less than 100 atoms. Since the stiffness of model epoxy backbones is high and side chains are short, the original highly cured epoxy network will have some voids in it, which is often referred as the free volume part, although free volume refers to the unoccupied volume. While some small segments are cut off from the network, they are free to move into the voids region of the network. This process will make the simulation box more compact, and the polymer denser. When more and more bonds were broken, M_n becomes increasingly smaller but more slowly. The reason is that at this stage the sizes of small pieces are increasing while the size of the largest network is decreasing. When the original network is destroyed to some extent, the sizes of small molecules and large ones are comparable. Under this circumstance, diffusion of small fractures into voids of larger molecular segments is difficult. And finally, in the 5% box, the ratio of small molecules to relatively larger ones is so high that small molecules fill the matrix along with some fraction of the original network. The original network is not interconnected anymore, which means the tightly compacted structure is lost. Also it is difficult to organize very small molecules into an ordered structure at room temperature, which leads to the low density of the polymer at a high bond cutting percentages.

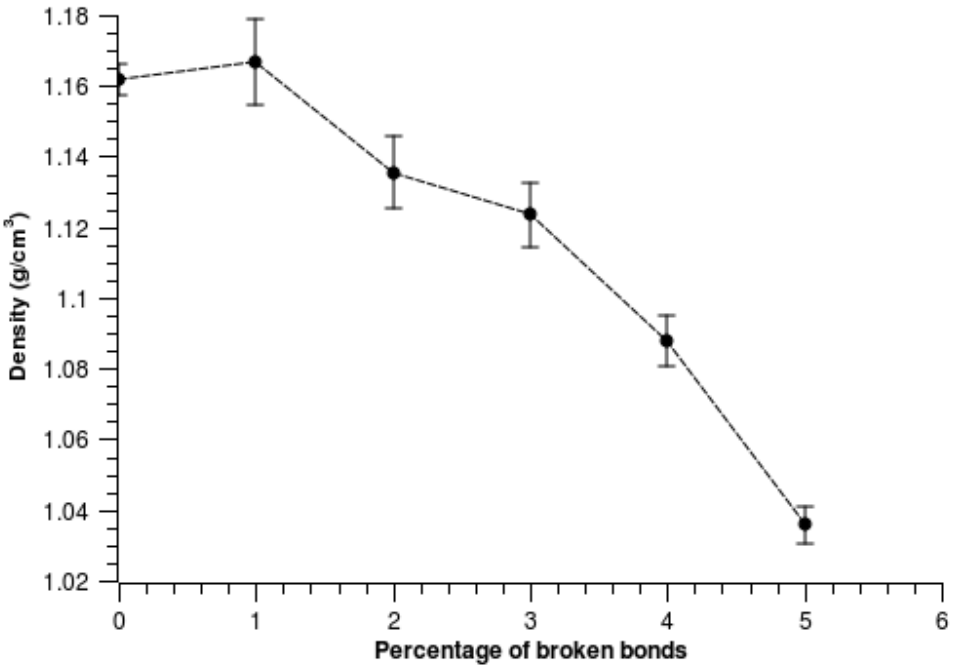

Figure 3-6. Densities of networks with varied cutting percentages at 300 K.

To compute glass transition temperature of different simulation boxes, densities of each box at different temperatures were calculated and plotted as a function of temperature. Figure 3-7 shows the change of densities in the annealing process for different bond cut percentages. To calculate T_g, linear fitting was conducted in high and low temperature regions. The intersections of two fitting lines indicate the occurrence of glass transition. As long as cut percentage is smaller than 4%, T_g were obtained with no difficulties. However, if 4% bonds were cut, something unusual takes place. As seen in Figure 3-7, at high temperatures, a definite density value was not available. As shown before, a 4% box is a blend of small molecules as the interconnected network structure disappears. Small molecules become vapor at high temperatures, so the volume of simulation box fluctuates with high amplitude. A change of slopes does not exist in the

density-temperature plot. As small molecules do not have glass transition, this also agrees well with the structural change from a network to a blend of small molecules.

Figure 3-8 illustrates the dependence of glass transition temperatures on percentages of broken bonds. When the percentage is larger than three percents, the change of thermal expansion coefficient above and below is very small and difficult to detect. As seen in Figure 3-8, T_g is becoming increasingly smaller when more bonds are broken. T_g of polymers are dependent on mobility of polymer segments. So the decrease of T_g is contributed to a better mobility of epoxy segments since some spatial constrains are removed by bond cutting and the resulting molecules are smaller.

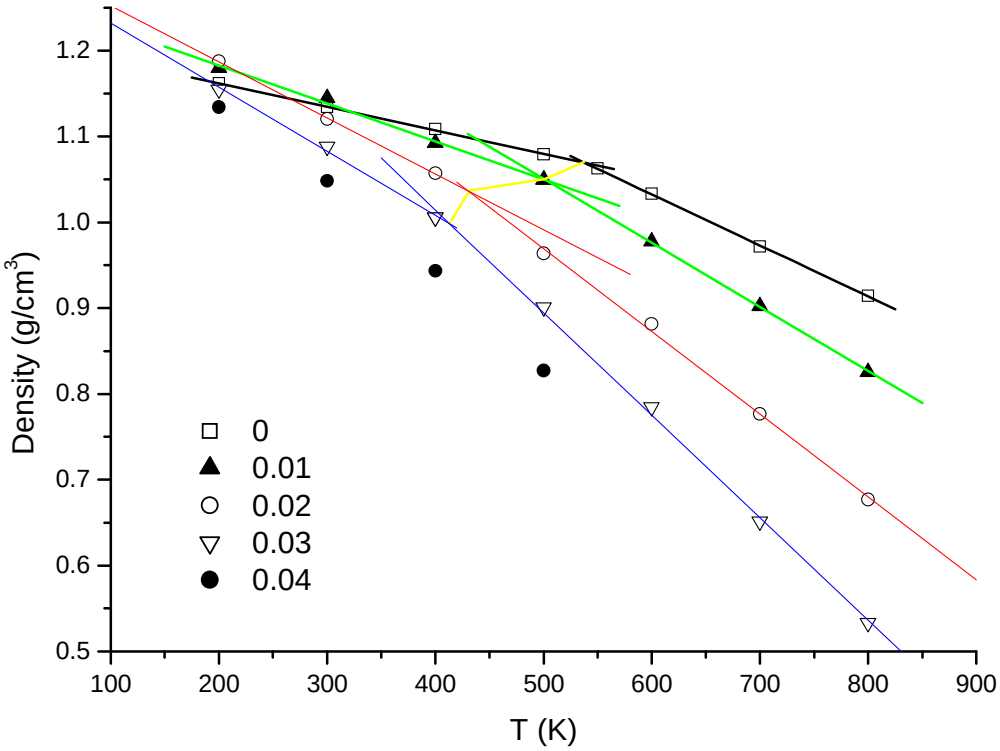

Figure 3-7. Densities of simulation boxes with varied cut percentages at different temperatures.

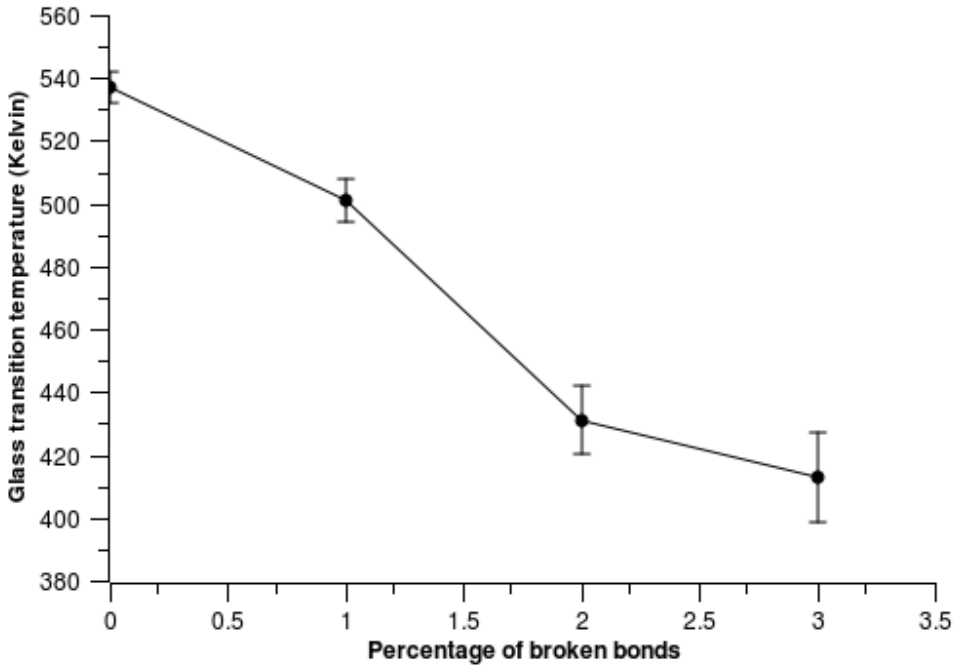

Figure 3-8. Glass transition temperatures of simulation boxes with varied percentages of broken bonds.

As functional materials, epoxy resins are used widely because of their good mechanical strength. How will chemical aging affect the material strength? Network density is the major parameter that governs the mechanical strength of network structures, so it is important to calculate the number of crosslinking points in the simulation. The crosslinking point is defined as an atom having more than two long chain branches. In this model system, tertiary amines are the major part of crosslinking points. Figure 3-9 shows that the number of crosslinking points keeps decreasing when the percentage of bonds being cut is increasing. This almost linear relationship shown in Figure 3-9 is a reasonable result based on the cutting algorithm and an isotropic network structure.

Tensile tests were conducted to calculate moduli of different structures. As shown in Figure 3-10, the modules dropped when more bonds were cut. This can be explained by a loss of network crosslinking density. After comparison of Figure 3-9 and 3-10, the modulus of the epoxies in the simulation boxes mainly depends on crosslinking density when cutting percentage is smaller than 5%. When more bonds are broken, the modulus of epoxy system goes to a steady region since small molecules are the major components of the system. Further cutting will not influence modulus of small molecules significantly.

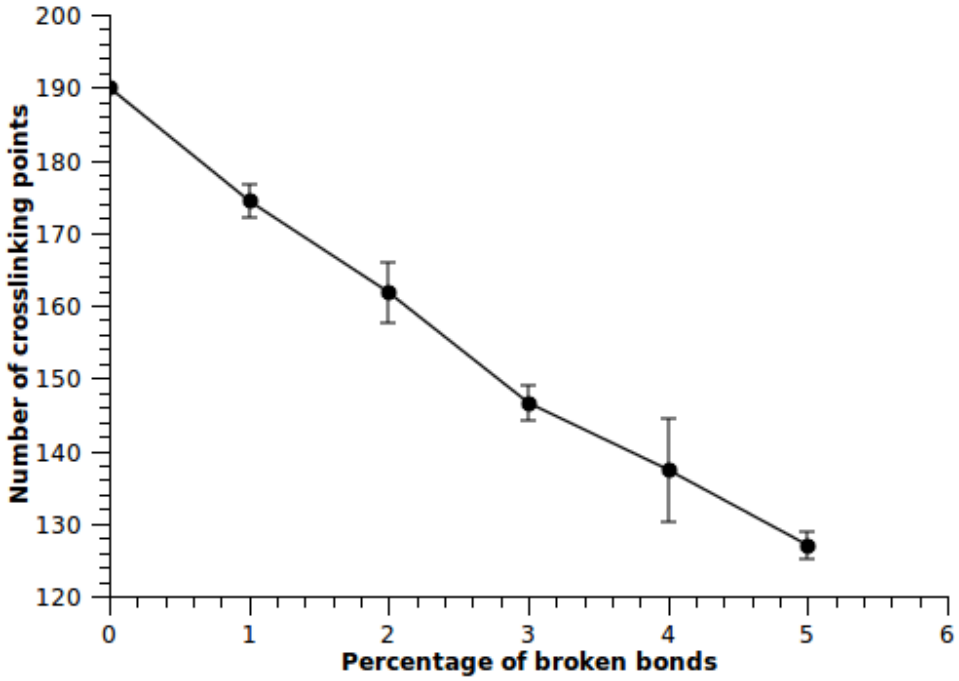

Figure 3-9. Number of crosslinking points as a function of percentages of broken bonds.

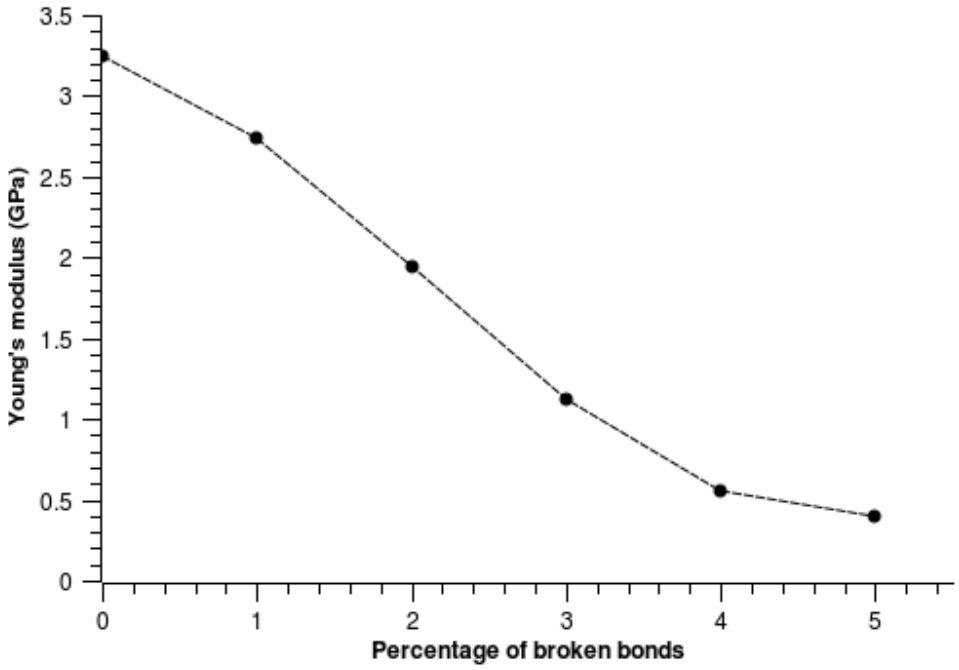

Figure 3-10. Young's moduli of epoxy systems with varied percentages of broken bonds.

3.3 Hydrolysis

3.3.1 Analysis of structures

The difference between hydrolysis and oxidation lies on the types of chemical bonds to be affected. According to the algorithm described in chapter 1, hydrolysis is the reverse reaction of a condensation reaction between amines and alcohols. Given the structure of cured TGDDM/DDS epoxy, the only possible covalent bond that can react with water is nitrogen-carbon bond indicated in Figure 3-2. We are interested in how aging algorithm is related to evolution of network structures. First of all, the same cutting percentages as used in oxidation were employed to compare these two algorithms. In the previous section, a maximum of 5% cutting was achieved while here the maximal

cutting percentage was limited to 4% since the overall number of nitrogen-carbon bonds was small.

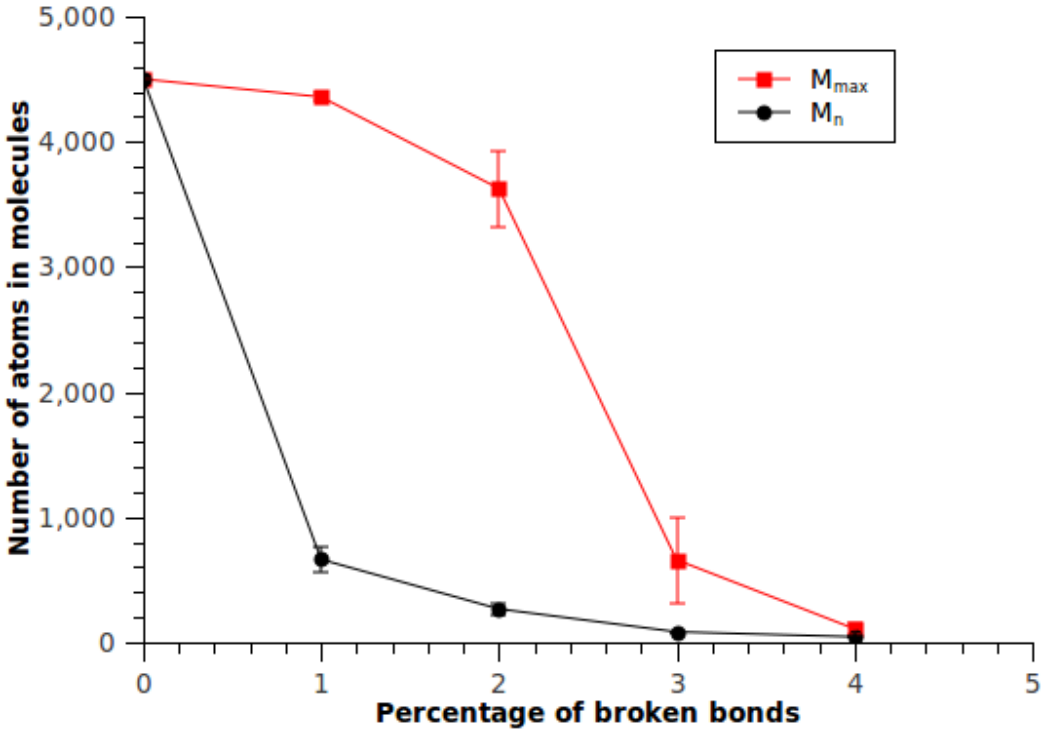

Figure 3-11. Number average number of atoms of molecules (M_n) and number of atoms in the largest molecule (M_{max}) in simulation systems with varied percentages of bond cutting.

Morphologies of simulation boxed after hydrolysis chain scissions were similar to oxidation cases and not shown here. M_n and M_{max} were graphed in Figure 3-11. Comparing this figure with Figure 3-4, we found the shapes of curves to be highly similar. M_n drops sharply ahead of M_{max}. However, there are still two slight differences. Variances of data points in Figure 3-11 are smaller than those of Figure 3-4. This is contributed to only one cutting site compared to multiple possible cutting sites in oxidation. The second variation is critical cutting percentage shifts from 4% in oxidation to 3% in hydrolysis. This may arise from the mechanism of hydrolysis. Hydrolysis takes

place at crosslinking points and therefore leads to a decrease of crosslinking density and demolishment of network structures. To verify this hypothesis, numbers of crosslinking points were calculated for different systems and shown in Figure 3-12.

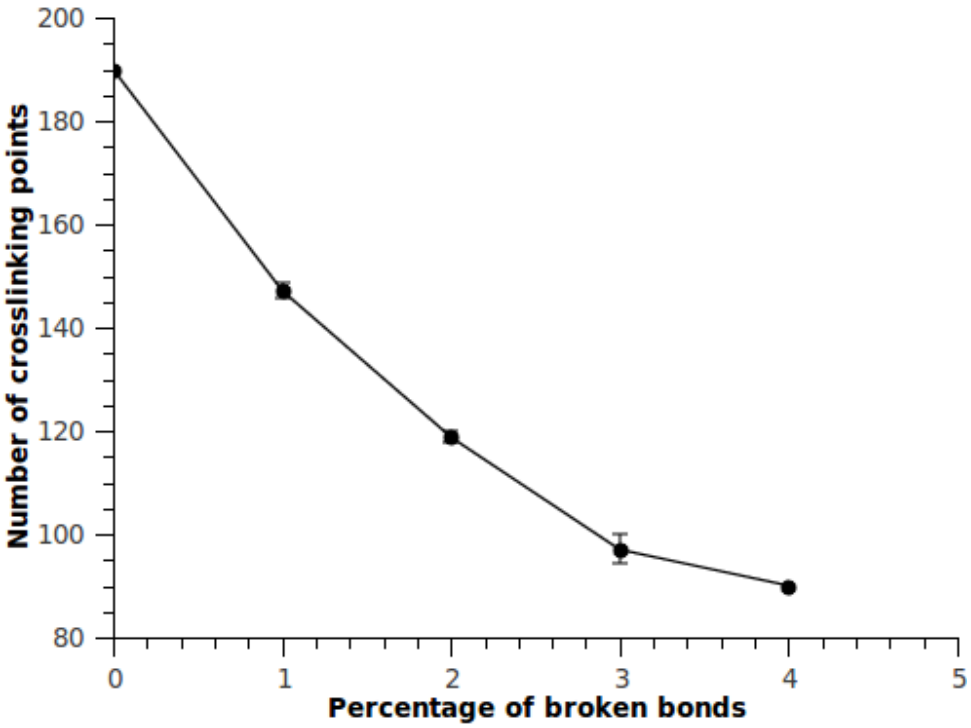

Figure 3-12. Variation of numbers of crosslinking points in systems with varied cutting percentages.

The decrease of crosslinking points in oxidation chain scission was almost linear from 0% to 5%. In Figure 3-12, we see a faster than linear relationship drop in hydrolysis cutting. The reason is obvious: every nitrogen-carbon bond cleavage is associated with one possible disappearance of network node. With the same cutting percentage such as 3%, about 145 nodes were left in oxidation box compared with 100 nodes in hydrolysis box.

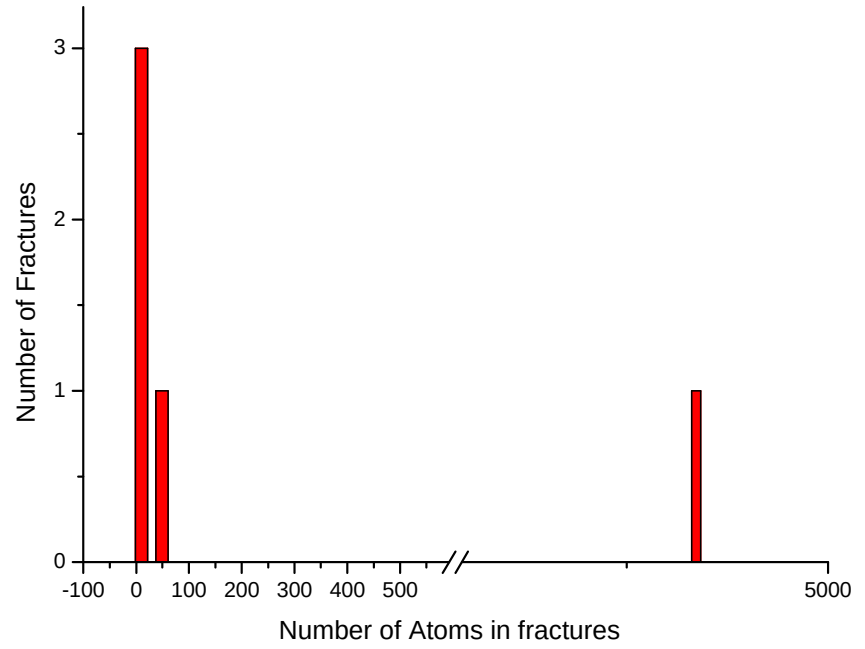

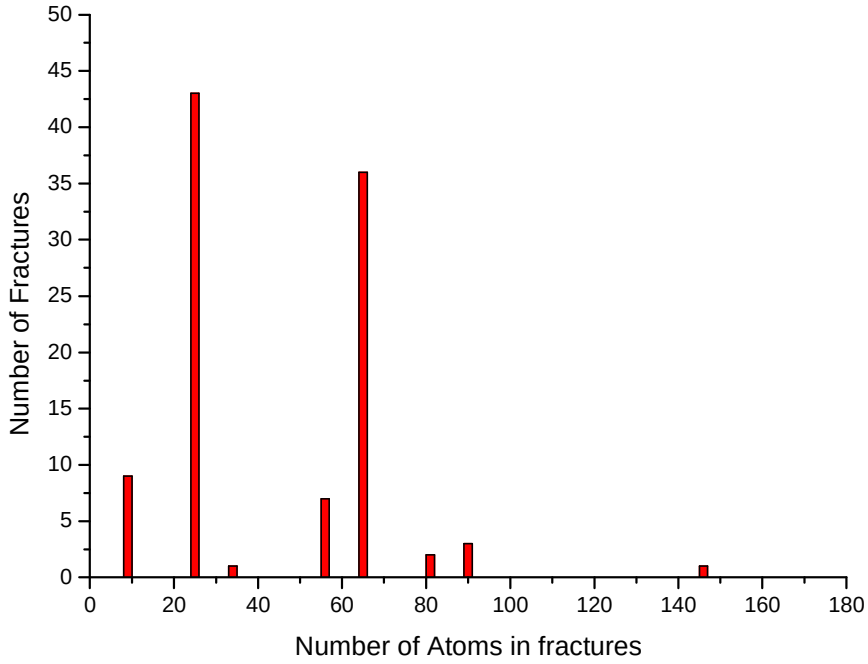

Figure 3-13. Distribution of numbers of atoms in fractures after (a) 1% (b) 4% bonds cut.

To show the effect of different aging algorithms, besides applying at the crosslinking point, distributions of molecular weight in simulation boxes was also studied. Figure 3-13 gives two distributions of numbers of atoms in the network after two percentages bonds broken. The distribution in 1% box shows no obvious difference from Figure 3-5(a). However, in the 4% box, the histogram is different from Figure 3-5(b). A narrow distribution and high peaks suggests that there are a few types of molecules present in the system. Structures of these molecules can be analyzed from backbones of cured TGDDM/DDS resins. As a comparison, types of molecules are more complex in oxidation and more difficult to determine. M_{max} in hydrolysis box is also smaller than that in oxidation box. This demonstrates that hydrolysis can destroy network structures of epoxy resins more overwhelmingly to very small pieces of molecules.

3.3.2 Degradation of properties

Previous sections showed many differences in structures of epoxy degradation products between oxidation and hydrolysis mechanisms. It was demonstrated that hydrolysis mechanism has a more substantial effect of destructing epoxy network structures. Generally, less connection linkages and smaller molecular weights means a material with diminished properties. Same testing procedures used in Section 3.2.2 was conducted again for systems undergoing hydrolysis degradation.

First of all, densities of systems with varied degrees of hydrolysis were calculated and graphed in Figure 3-14. A significant drop takes place at a percentage of 1% followed by continuous but smaller drop at high percentages. The final density at 4% is around 1.02, close to that of oxidation products. The reason for large decrease in the initial stage will be explained with additional results.

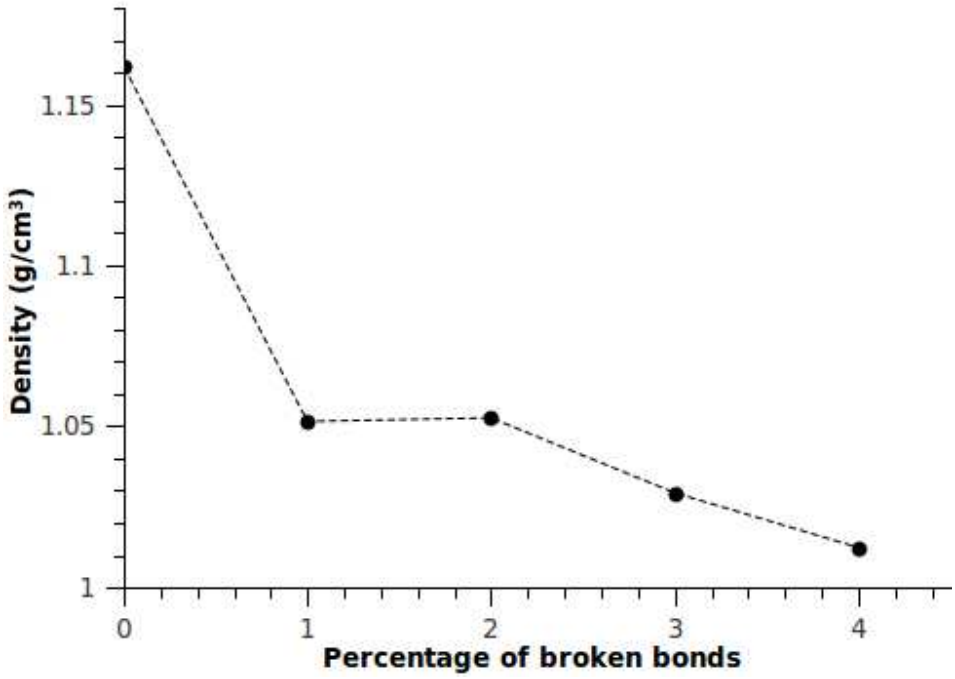

Figure 3-14. Densities of systems with different degrees of hydrolysis.

Figure 3-15 graphs glass transition temperature as a function of degree of hydrolysis. An obvious drop was observed at hydrolysis degree as small as 1%. It implies that resistance of epoxy to high temperature is significantly decreased due to norminal hydrolysis. This can be contributed to a large decrease of number of crosslinking points shown in Figure 3-12 because smaller number of crosslinking points means less constrains, therefore polymer chains and segments can move more freely. As more bonds were cut, T_g continues to drop.

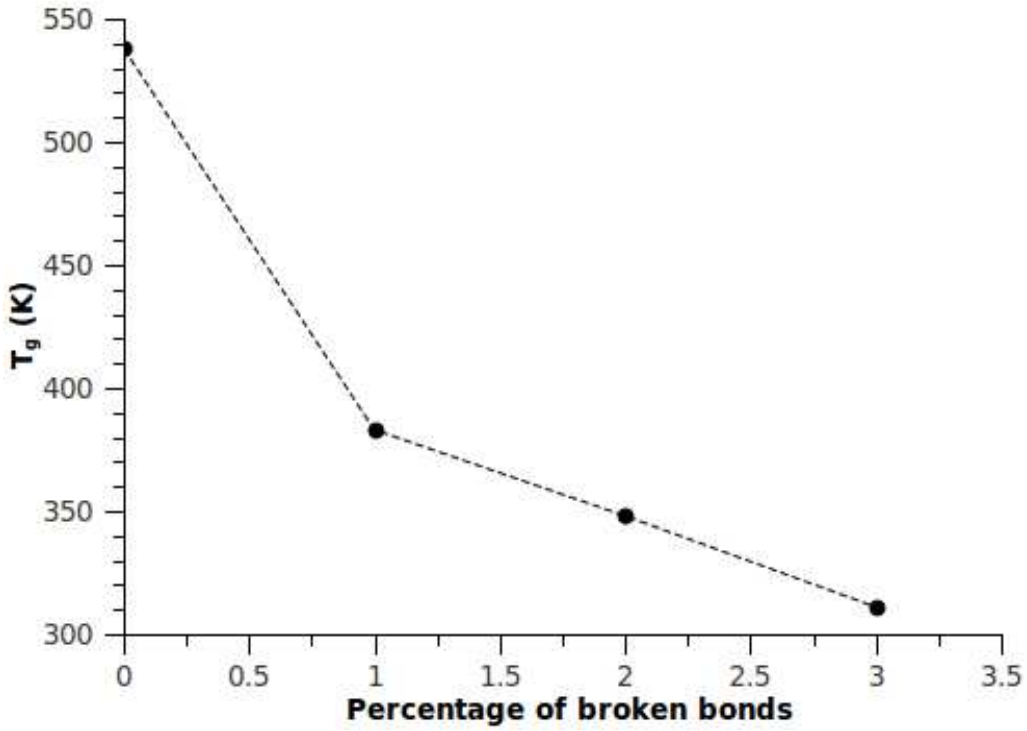

Figure 3-15. Variation of glass transition temperatures of cured epoxy systems at different degrees of hydrolysis.

Besides T_g, modulus of systems at different degrees of hydrolysis was also calculated and plotted in Figure 3-16. It is interesting that Young's modulus decreases in the same way of glass transition temperature. It is obviously not a coincidence. The underlying reason is that similar to T_g, modulus of network structures is also mainly dependent on crosslinking density.

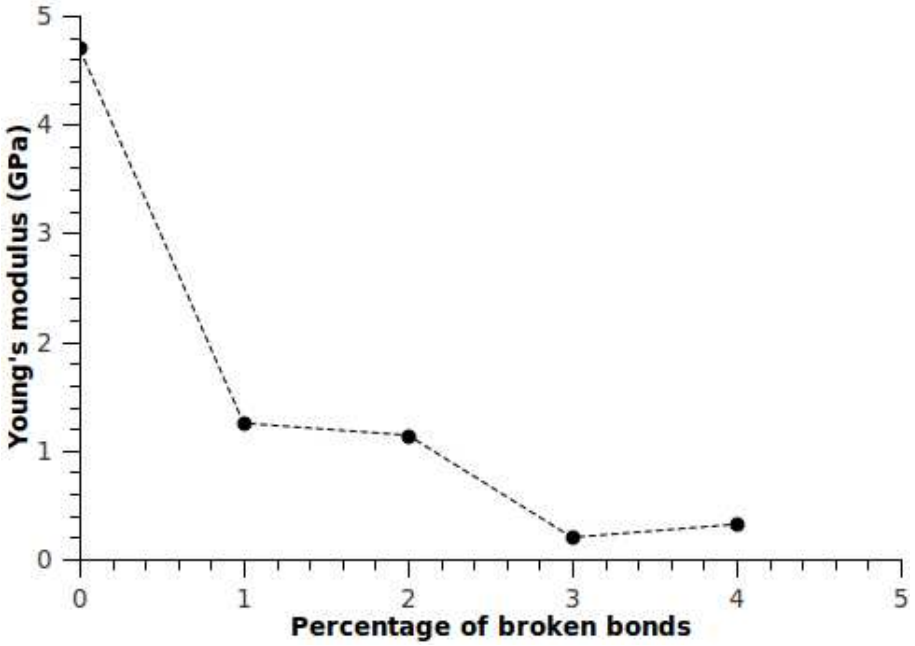

Figure 3-16. Variation of Young's modulus during hydrolysis degradation of an epoxy system.

3.4 Conclusion

Despite the difficulty of modeling bond cleavage with classical MD, chain scission based on chemical mechanisms of oxidation and hydrolysis was studied using an atomistic approach.

Degradation was realized by analyzing all possible chain scission points using two different mechanisms regardless of actual reaction conditions. In other words, particular attention was given to consequences of these degradation rather than possibility or conditions of oxidation or hydrolysis.

Oxidation decomposition can affect many covalent bonds located along backbones of TGDDM. A continuous drop of both thermal and mechanical properties of epoxy networks was observed with chain scission. Structural analysis of degradation

products showed successive decrease of molecular weights and crosslinking points. Visualization of simulation box helped to identify the process of chain scission, which destroyed the initial interconnected network structure to a blend of small molecules. The relationship between the number of crosslinking point and modulus suggested that for network structures properties are mainly dependent on number of crosslinking points.

Hydrolysis degradation targets specific types of bonds compared to oxidation. In the epoxy system, only carbon-nitrogen bonds will be affected. Different from oxidation, every hydrolysis reaction will make number of crosslinking points decrease by one. As a result, hydrolysis brings significantly more damage to network structures than oxidation, which is reflected by a dramatic drop of T_g and modulus of network structures at a degree of hydrolysis as small as 1%.

CHAPTER 4

INTERFACES BETWEEN TWO EPOXY RESIN COMPONENTS

4.1 Introduction

All structural adhesives age gradually in normal conditions in daily use. Extreme environments or strong external stresses can accelerate aging. Cracks and crazes will also initiate and develop in at interfaces as well as in the bulk material. As discussed in the introduction chapter, interfaces are present not only between polymer matrix and fillers but also between two polymer components. There are interesting practical questions regarding crack healing, such as whether it is possible to heal cracks (discontinuities in the material) found in epoxies by using epoxy adhesives, a partially cured epoxy resin, components of which are different from the original adhesive. The healed part should act as well as the original one in the ideal situation. However, a number of factors will affect performances of the part after the cracks are healed. For example, the components of the healing agent should be carefully chosen to leverage strength, toughness, viscosity and curing temperature. Once the crack is removed, one needs to make sure that interfaces between original part and healing agent are strong enough to prevent new crazes or cracks. In this chapter, an account is provided for one actual pair of structural adhesive and healing agent to investigate the relationship between interfacial strength and microscopic structures. The TGDDM/DDS epoxy resin is selected as structural adhesives which contains cracks those need to be fixed. Then,

a new epoxy system is applied on the surface of TGDDM/DDS and interfaces between two epoxies are generated.

4.2 Construction of interface

A difunctional epoxide molecule - diglycidyl ether of bisphenol A (DGEBA) is one component of the healing agent. The curing agent is diethyltoluenediamine (DETDA). Chemical structures of these two molecules are shown in Figure 4-1.

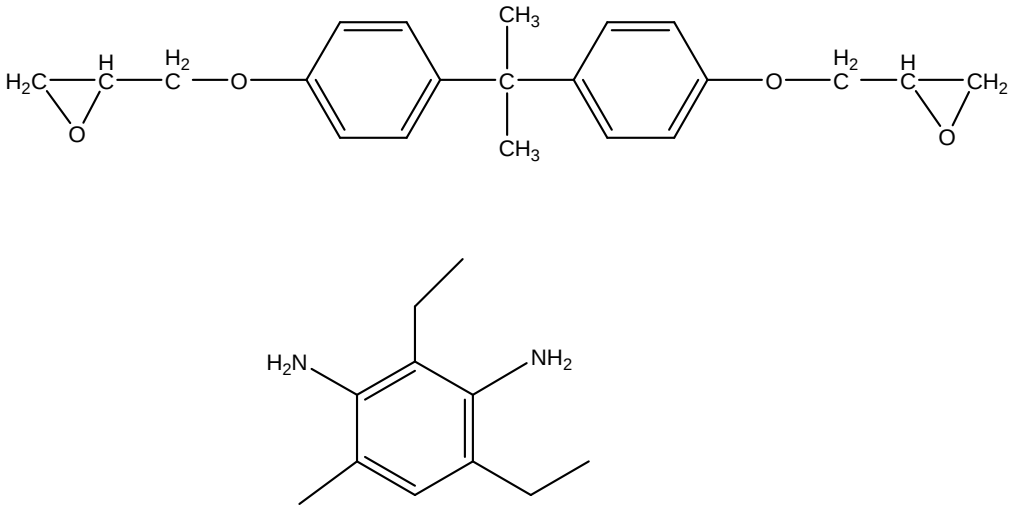

Figure 4-1. Chemical structures of DGEBA and DETDA.

Chemical reactions between DGEBA and DETDA are the same as described in Figure 1-3. Only differences between difunctional epoxy and tetrafunctioal epoxy relates to the backbone structures and number of functional groups in the monomers.

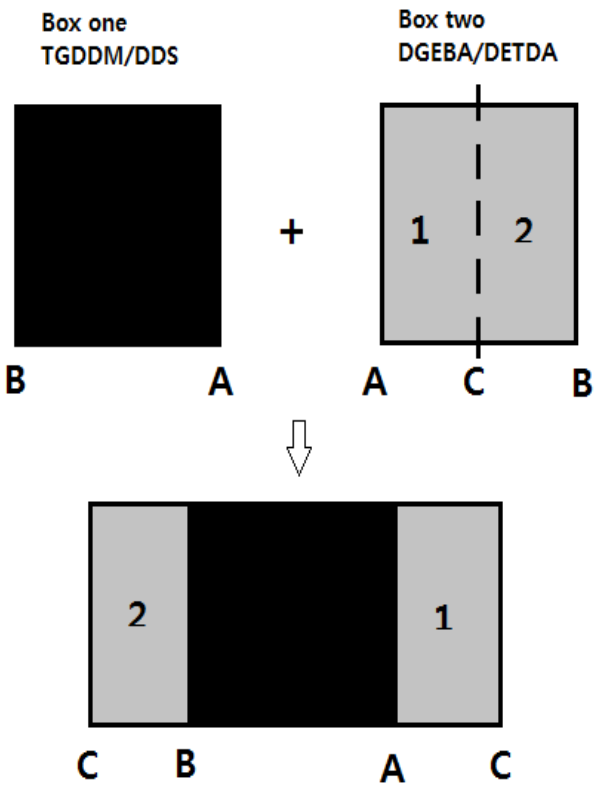

Figure 4-2. A scheme for generating interfaces between two simulation boxes.

Two types of epoxies, with tetra-functional and di-functional components, are used in this investigation as model epoxies. Tetraglycidyl-4,4'-diamino-diphenylmethane (TGDDM) and 4,4'-diaminodiphenylsulphone (DDS) are the epoxy and crosslinking agent modeled in the first system, while diglycidyl ether of bisphenol-A (DGEBA) and diethyltoluenediamine (DETDA) are the other epoxy/crosslinking agent pair modeled in the second system. In this work, it is assumed that TGDDM/DDS resin is the material with cracks to be healed and DGEBA/DETDA is the epoxy/crosslink agent pair used to heal TGDDM/DDS. Commonly, uncured heal agents are applied to the surfaces of materials with crack and cured at an elevated temperature. To mimic this process, simulation boxes containing partially cured TGDDM was generated and placed it together with another box containing uncured DGEBA/DETDA monomers followed by a

final curing process. This entire interfacial system is represented as pT/D. Another type of system is constructed as following. Uncured TGDDM/DDS and DGEBA/DETDA are created in separated boxes, brought together and cured. This system is indicated as uT/D and used as an ideal interface model to compare with pT/D system.

Here are some details about the approach to build all-atom simulation boxes. Each combination of epoxies and crosslink agents were created in separated simulation boxes with exact reaction molar ratios. Hereafter, TGDDM cured with DDS box is referred as box one and DGEBA cured with DETDA is referred as box two. Diamond lattice was used as a template to place atoms in cubic simulation boxes to improve efficiency. A total of 1000 molecules including epoxies and crosslink agents were generated in each box. Periodic boundary conditions were applied to y and z directions but not x direction at this time. As described before, box one was either partially crosslinked or not crosslinked. After completion of generating initial structures, box two was cut in the middle to two halves and two free surfaces were placed toward the two yz free surfaces of box one in the opposite direction to create two interfaces between box one and box two (as shown in Figure 4-2). From this stage, x direction was periodic as well as y and z directions. Dreiding force field [25] was applied to adjust positions of atoms off lattice and run dynamics. An energy minimization process followed by decompression and compression molecular dynamics (MD) steps was performed to approach a realistic state over a simulation period of 100 ps. Molecular dynamics was carried out under NPT ensemble using LAMMPS software package [72]. A time step of 1 fs was used throughout the work.

The crosslink process for partially cured or uncured systems was performed based on an algorithm that was described before. After crosslinking, the simulation box was compressed and decompressed again under NPT ensemble several times.

Customized software package developed within the group was employed to analysis equilibrated structures. Molecular scale mechanical tests were also conducted using LAMMPS. A uniaxial stretch test was modeled in NVT ensemble to calculate elastic constants while the other two directions remained unstretched under 1 atm. A constant positive strain rate of 1×10^{-6} /fs (1×10^{9} s^{-1}) was applied to the simulation box every time step until a 5% strain was achieved. While a large strain (beyond the elastic zone of glassy epoxies) was desired, NPT ensemble was used instead of NVT. The scale of simulation box matters in atomistic level. To obtain better comparison to experimental results, a larger simulation system will yield more reliable outcomes, but that will consume more computational resources. Within the capability of our computing resource, we employed a system containing about 80,000 atoms to decrease the effect of random seeds when generating initial structures. Only one replication is built for both pT/D and uT/D systems. Another concern is the deviation of modeled interface from actual interfaces. Contaminants or air bulbs can always be found in actual interfacial regions even if special effort has been taken to achieve the highest degree of purity. In this work contaminants or air bulbs were not modeled, and to simplify the systems under investigation seamless contact between two components was assumed.

Morphologies of interfaces in uT/D system were visualized using VMD software package [73] and shown in Figure 4-3. It can be seen that reactive sites distribute evenly at the cross-section area, which suggests that monomers were mixed thoroughly. To analyze the location and depth of interfaces, atom concentration profile along the x direction, which is perpendicular to interfaces, is calculated. A small step length of 2 angstroms was adapted to scan along x direction from left to right. The two transition regions along the x direction can be easily identified where specific atomic concentrations in box one increases from zero or decreases from one (Figure 4-4).

These two regions where the lines in Figure 4-4 rise from zero to one or drop from one to zero can be defined as interfaces. The average depth of interfaces in uT/D system is estimated to be 22 angstroms. When using different atom type to scan x direction, no obvious difference was observed. The same method can be applied to pT/D system to calculate interface depth as well; the results are listed in Table 4-1. Compared to uT/D system, the TGDDM part in pT/D system was partially crosslinked, which means that part are not able to move freely as small molecules. As a result, molecules of healing agents in box two (DGEBA and DETDA) cannot diffuse deeply and penetrate into surfaces of box one. Therefore, interfaces in pT/D system were thinner than those in uT/D system.

Either in uT/D or pT/D system, a final curing process will create covalent bonds between atoms from box one and box two. These bonds connected box one and box two and act as the main part of interfaces. In ideally contacted interfaces, a particular reactive amine atom will have the same possibility reacting with an epoxy atom from box one and box two. Here a ratio *p* was used as a criterion to quantify the linkage between box one and box two. In Equation 4-1, N_c is the number of crosslinks formed between box one and box 2; *L* is the length of simulation box in x direction; *N* is total number of crosslinks and D_i is the depth of interfaces. *p* should equal 0.5 for the ideal case. A larger *p* indicates more connections between box one and box two therefore a stronger interface. The *p* values of uT/D and pT/D systems were calculated and listed in Table 4-1.

$$p = \frac{N_c \times L}{N \times D_i} \qquad (4\text{-}1).$$

Both *p* values are smaller than the ideal value, which means an ideal contact interface is difficult to obtain in a small scale simulation. However, as a comparison, the uT/D system has a higher *p* value than pT/D system. The reason is obvious. Box one in pT/D system was partially cured and the concentration of reactive atoms in surface region was low.

(a)

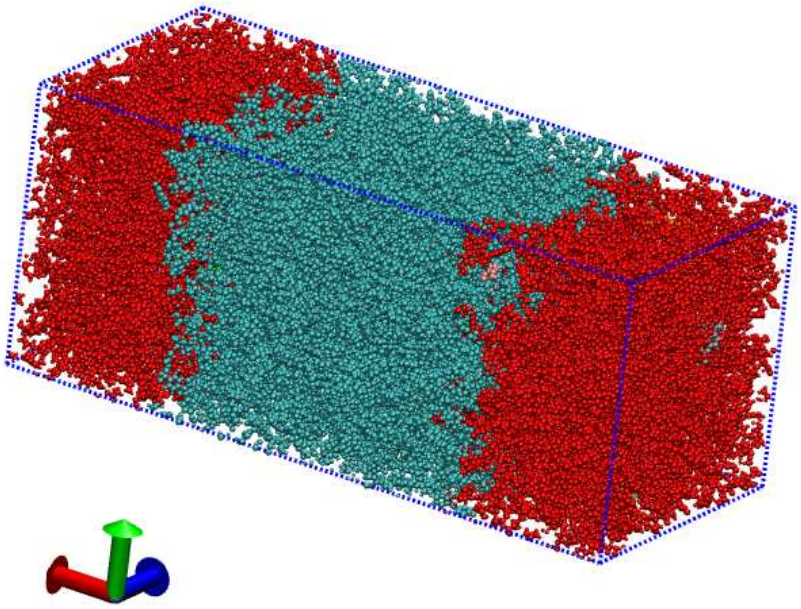

(b)

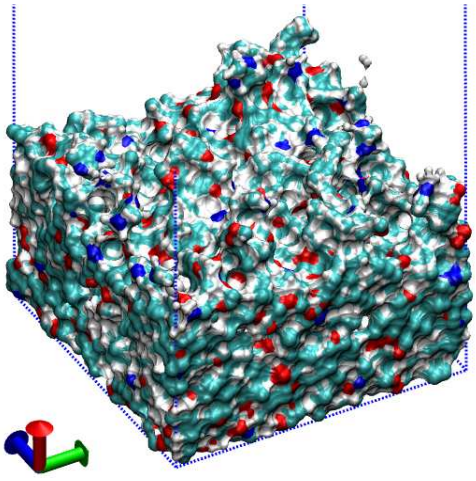

Figure 4-3. Representation of (a) interfacial system including two interfaces: Cyan atoms are from box 1 and red ones are from box 2. (b) cross section of one interface from (a). Atom color legends: cyan: Carbon, red: Oxygen, blue: nitrogen, white: hydrogen.

Table 4-1 Comparison between pT/D and uT/D systems.

System	Depth of interface (Å)	p
pT/D	15	0.19
uT/D	22	0.36

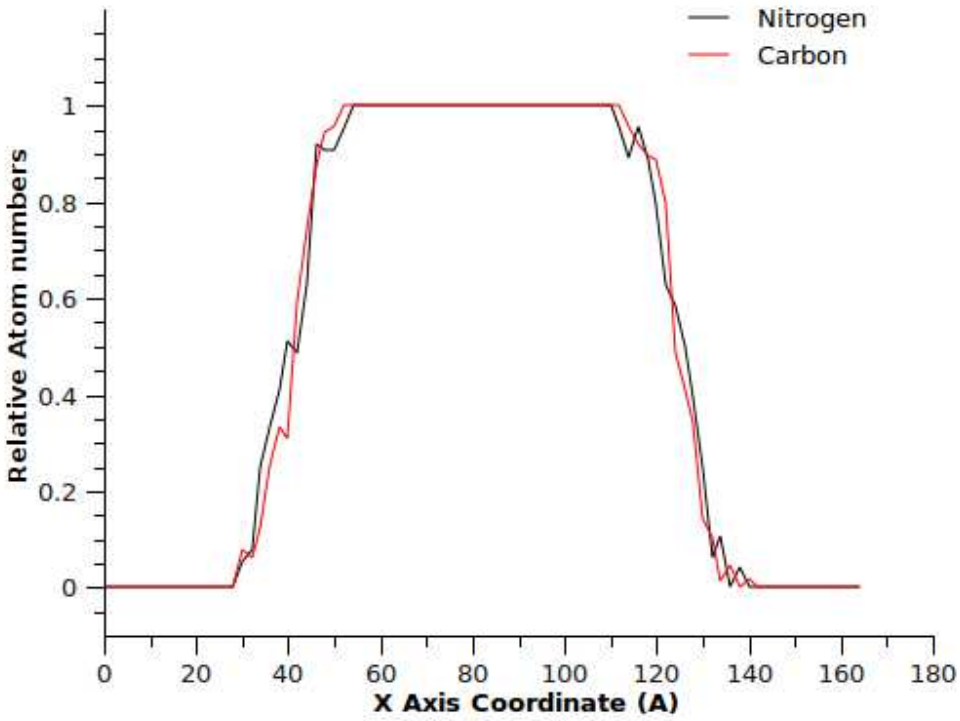

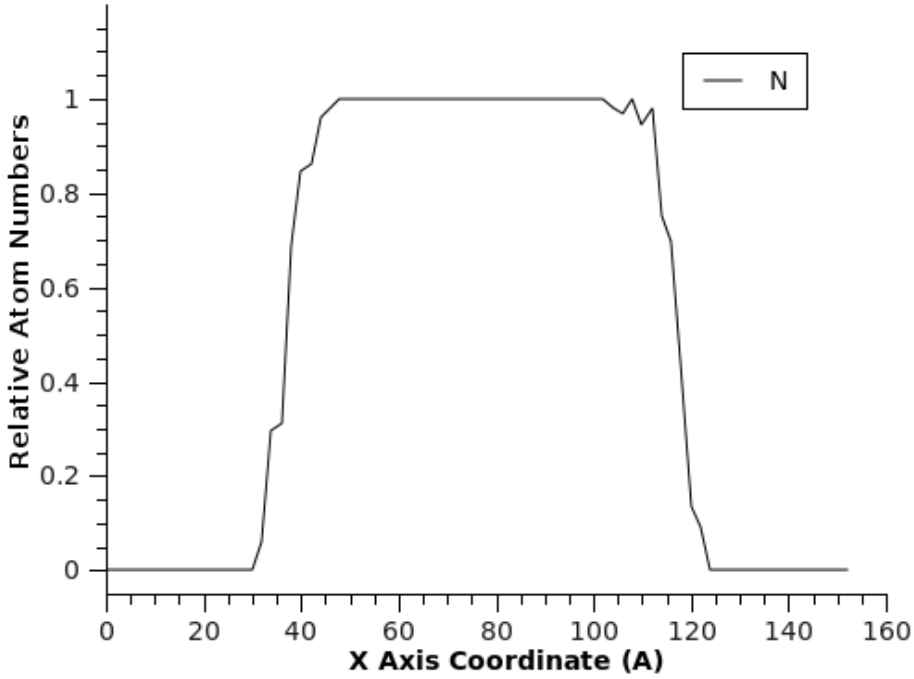

Figure 4-4. Atom concentration profiles of box 1 along the direction normal to interfaces between box 1 and box2. (a) uT/D system ;(b) pT/D system.

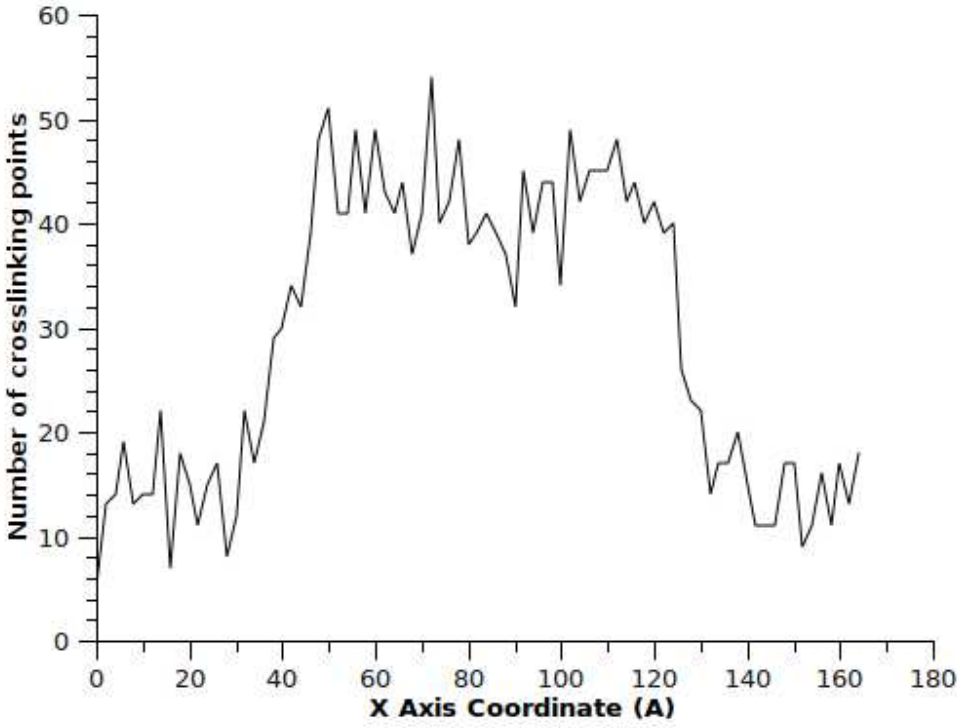

Figure 4-5. Crosslinking point density along the direction normal to interfaces between box 1 and box 2.

Table 4-2 Tensile Strengths along the direction normal to interfaces

System	TGDDM	DGEBA	pT/D	uT/D
Tensile Modulus (GPa)	3.80	1.93	1.66	2.28

The mechanical strength of interface is of most interesting aspect for researchers. Interfaces are believed to be the weakest part of the whole system due to a lack of strong links between two sides of interfaces. Strength of interfaces may be enhanced by introducing more chemical bonds and physical entanglements and minimizing the amount of small molecules and contaminants. Since the case studied here does not include the effect of seams and defects in interfacial region, the tensile strength of

interfaces is mainly dependent on chemical characteristics of local area. As previously mentioned, the density of crosslinking points is used as a criterion to predict difference of modulus in epoxy network system. According to the specific chemical structures in the model system, any nitrogen or carbon atom which has more than one long side chain may be considered as a crosslinking point. Crosslinking points act as main backbones of network and stand external stresses. Density of crosslinking points of the uT/D system along the direction normal to interfaces was calculated and shown in Figure 4-5. Compared to epoxy TGDDM, DGEBA is a linear epoxy monomer. Therefore, cured DGEBA has an average lower crosslinking point density than TGDDM. In Figure 4-5, the density of crosslinking point fluctuates along x direction in DGEBA bulk, increases to a higher value in the interfacial region and fluctuates at a high level in TGDDM bulk. If the tensile modulus has a positive correlation with crosslinking point density, TGDDM bulk will be the strongest part in the system while DGEBA bulk is the weakest part in the whole system. To verify this relationship, tensile test along the x direction was performed using LAMMPS. Calculated tensile strengths along x and y directions as well as Young's modulus of TGDDM and DGEBA bulks are listed in Table 4-2. The overall strength of interfacial system is between Young's modules of TGDDM and DGEBA bulks and more close to that of DGEBA. It suggested that in an ideal connected interfacial system the weaker component will decide the overall performance.

Another small strain test was done with pT/D system. A scan of crosslinking points along x direction (Figure 4-4(b)) gave a similar crosslinking point distribution curve as in Figure 4-4(a). It seems both the uT/D and pT/D system should have the same mechanical behavior. However, the tensile strength of pT/D system obtained from the mechanical test was lower than that of uT/D system.

(a)

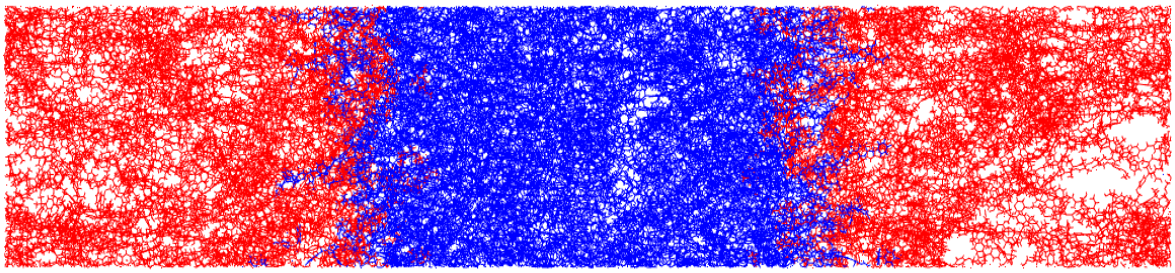

(b)

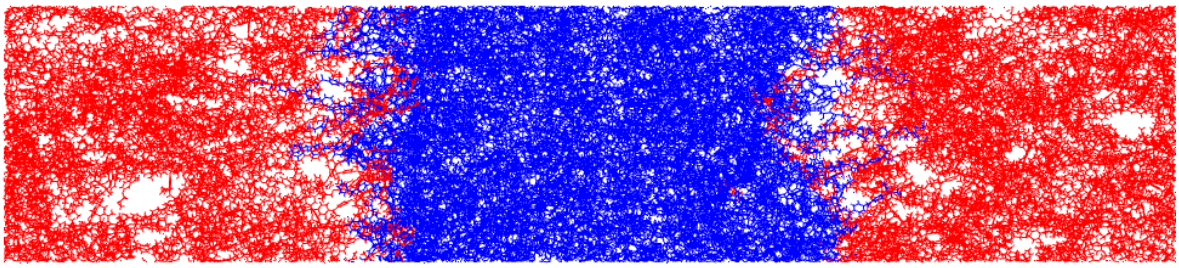

Figure 4-6. Morphologies of deformed simulation box injected on x-y plane. The strain along x direction is 1. Blue part stands for TGDDM and red part stands for DGEBA. (a) uT/D system (b) pT/D system.

Table 4-3. Strains of each component in different interfacial systems while the total strain is 1 (the final length of box along stretched direction is twice of the original length).

System	pT/D			uT/D		
Strain	TGDDM	DGEBA	Interface	TGDDM	DGEBA	Interface
	0.4	1.45	1.87	0.7	1.74	0.45

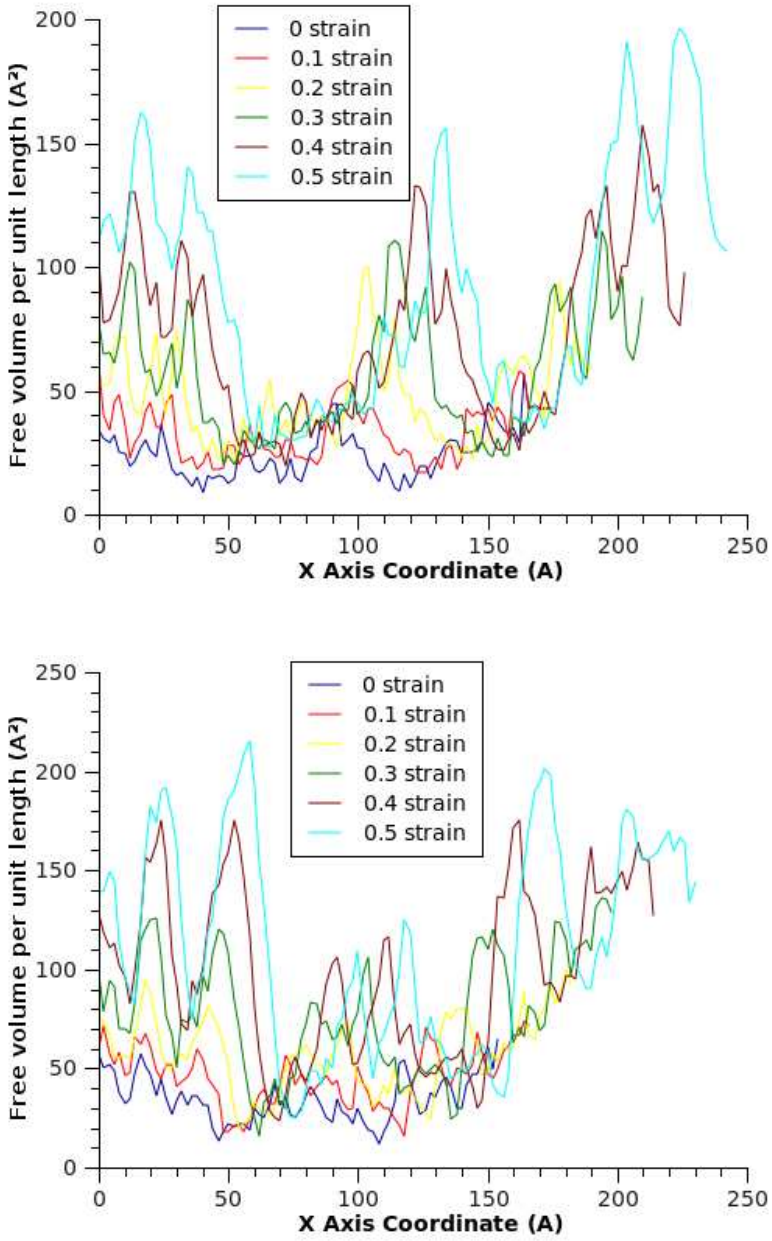

Figure 4-7. Void growth during deformation of uT/D (a) and pT/D (b) system.

To understand what will take place if the total system was stretched to a large strain, a large strain tensile test was conducted in NPT ensemble. An overall engineering strain of 1.0 was achieved after the test. The morphology of deformed box was shown in

Figure 4-6. Atoms of TGDDM and DGEBA were represented by different colors to display actual strain of each part. Specific strains of each component were calculated and listed in Table 4-3. In combination of Figure 4-5 and Table 4-3, one can see that an obvious difference between deformed morphologies of uT/D and pT/D system is the locations of voids. In uT/D system, voids mainly existed in DGEBA bulk, which has the largest strain compared to TGDDM bulk and interfaces. While in pT/D system, delamination of interfaces can be observed and interfaces were stretched the most. The only chemical difference between pT/D and uT/D systems is the number of connecting bonds between TGDDM and DGEBA bulks; in other words, pT/D and a weaker connecting interface than uT/D. In both case a larger strain of DGEBA than that of TGDDM agrees with the modulus difference, which verified that DGEBA is a weaker part than TGDDM. A scan of free volume along x direction is given in Figure 4-6 for each system to find out where the voids or cracks origins from. Compared Figure 4-6(a) with Figure 4-4, it is easy to discover that the voids formed and grew at the locations where the original crosslinking density is low in uT/D system. These regions bear a low density and crosslinking point density, where crazes and cracks may initialize from. It may be out of one's expectation that interfaces are not the most fragile part of composites. However, considering that the interfaces modeled in uT/D system are close to ideal and flawless, the result is not that surprising. In Figure 4-6(b), not only in DGEBA bulk, also in interfacial regions, voids initialization and growth of voids and cavities can be observed. Although the crosslinking point density in interfaces seems higher than that in DGEBA bulk, these crosslinking points mainly belong to one component and cannot connect two components effectively to bear stresses.

4.3 Improvement of weak bonding

4.3.1 Additional compatibilizer layer

To improve the strength of interfacial systems, many methods were employed in experimental work. Among them, one effective way is to add a compatibilizer, which can improve compatibility of two components at interfaces. Compatibilizer molecules always have two ends, one of which can react or have high affinity with one component while the other end has similar attributes as the second component of interfacial systems. So they can link two incompatible components effectively, which can prevent initiation and formation of craze and void at interfaces. Using the same principle, we can design compatibilizer for our system to enhance overall performance.

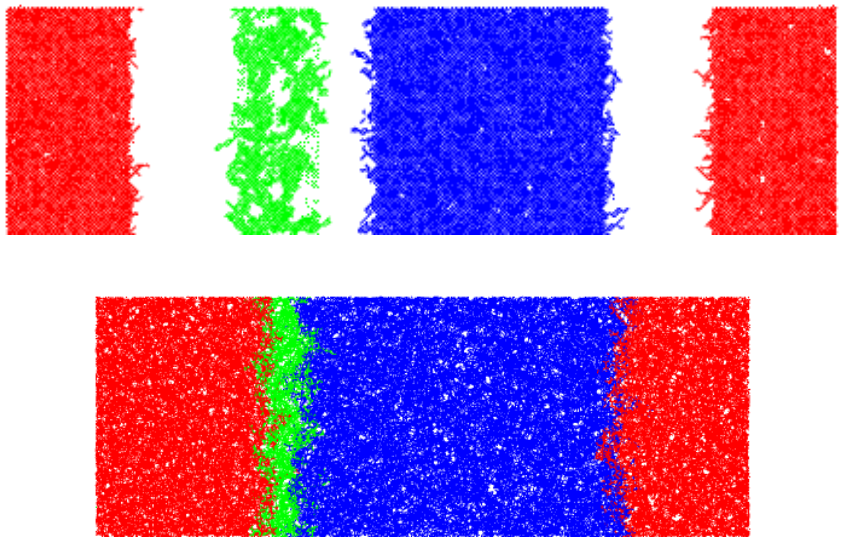

Figure 4-8. Scheme of constructing interfacial system with additional compatibilizer layers.

Since pT/D system has a weak interface and therefore overall low modulus, the pT/D system was selected for additional studies. The compatibilizer added to the interfacial system is the blend of unreacted TGDDM and DDS. On one side, this blend

can react with unreacted blend of DGEBA in box two. On the other side, the compatibilizer has exactly the same chemical composition with box one, which they are fully compatible. The steps involved to apply new layers are shown in Figure 4-8. A green layer, which stands for the compatibilizer, was applied to one or two free surfaces of box one, then box two was added. An equilibration step was carried out before crosslinking. After energy minimization and equilibration, crosslinks were created within the whole box. A final relaxation and equilibration step was conducted before further thermal and mechanical tests. The thickness of compatibilizer layer was estimated to be 7 angstroms.

4.3.2 Improvement of strength

To examine the effect of additional compatibilizer layers, three systems for were generated for comparison. The first one is pT/D, the same box used in previous section. The second simulation box is called pT/T/D, which stands for one layer added on only one side of box one. The last one is referred as pT/2T/D, which stands for two layers of compatibilizer added at each side of box one. Besides number of compatibilizer layers, all other crosslinking and equilibrating steps were carried out using the same procedure.

All three boxes were uni-axially stretched along x direction, which is normal to interface planes, to a strain of 1. Morphologies of all the three deformed boxes were shown in Figure 4-9. Focusing on morphologies at the interface is more interesting than the bulk. As stated before, pT/D system had voids initiated and formed at interfaces. On the left interface side of Figure 4-9(b), one can see that the existence of green compatibilizer layer effectively suppress the formation of voids. Further more in Figure 4-9(c), not only on the left side, but also on the right side, one can see the compatibilizer layer works as expected.

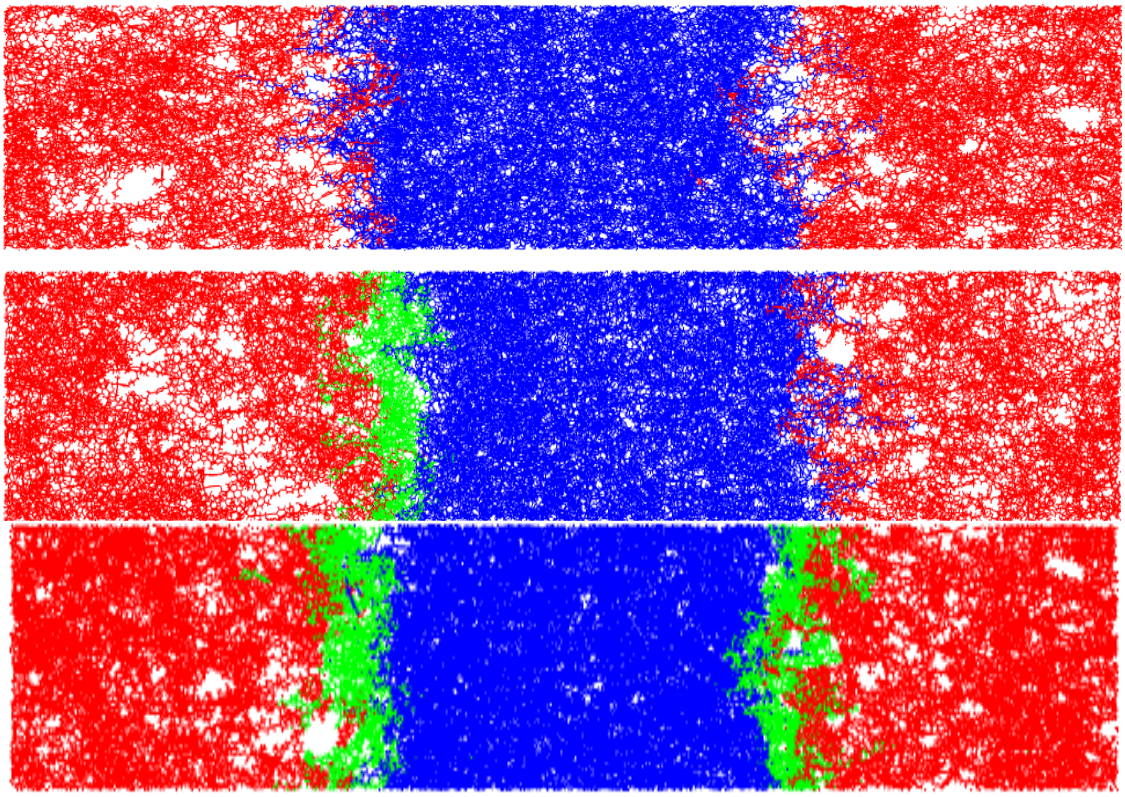

Figure 4-9. Morphologies of simulation boxes at strain of 100%. (a) pT/D,(b) pT/T/D (c) pT/2T/D.

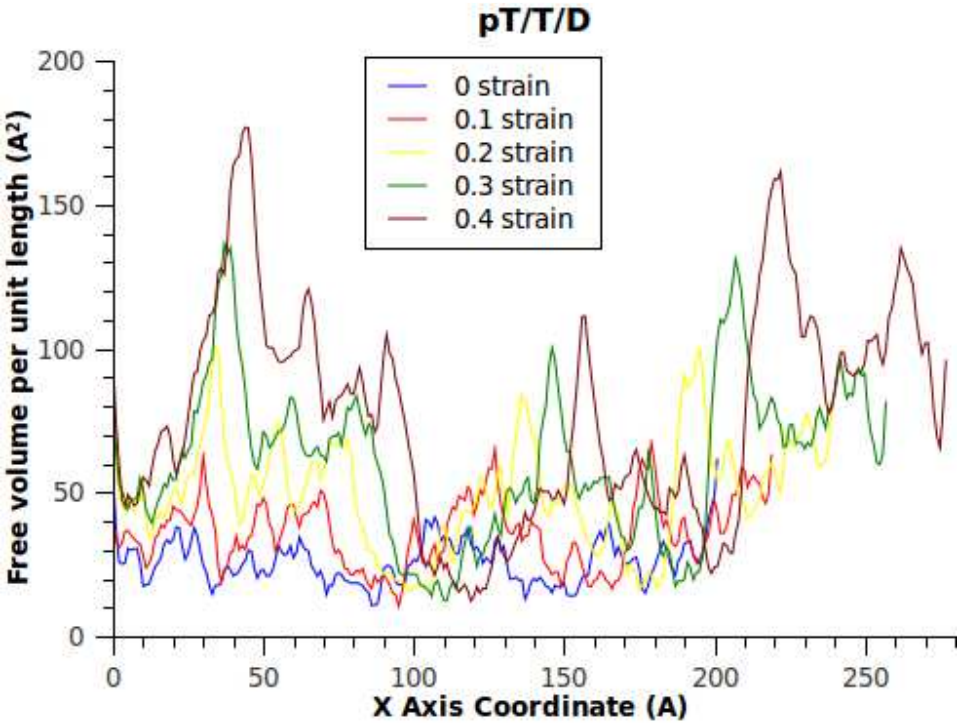

Figure 4-10. Variation of free volume per unit length along x direction of pT/T/D.

Quantitative studies on free volume of different systems can help deeper understanding of the effects of additional compatibilizer layers. Figure 4-10 depicts free volume along x direction for systems with varied strain. Peaks indicate relative high volumes of voids in simulation box. With the aid of Figure 4-10, one can easily identify the location of voids and also monitor the initiation and development process of voids. It is obvious that voids grow in the bulk of DGEBA, not at interfaces compared to Figure 4-7(b). Both the morphologies and quantitative studies lead to the same conclusion that by adding compatibilizer, we can prevent voids formation at interfaces.

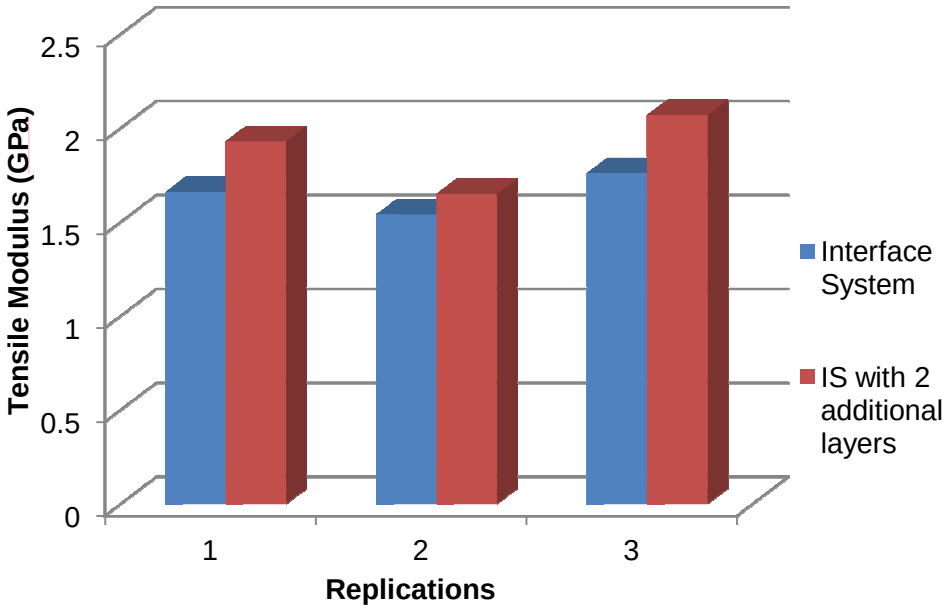

Figure 4-11. Comparison of tensile modulus of two interfacial systems in three replications.

Three replications were built to calculate tensile modulus of systems with or without compatibilizer layers. The results were shown in Figure 4-11. One can see a

consistent increase in all the three replications. The average increase is about 14% when two layers were added.

4.4 Conclusions

In this chapter, model system was changed from bulk epoxy to a system consisted of two epoxy boxes. Degree of reaction in TGDDM bulk was varied to manipulate the number of connecting bonds between TGDDM and DGEBA to create interfaces with different strengths. When one box was partially crosslinked, interfaces between two boxes are weak. This was contributed to a low crosslinking density at interfaces. Tensile moduli of the interfacial systems were lower than bulk moduli of both boxes. Mechanical tests showed that the tensile modulus of the overall interface systems can be improved by increasing connecting bonds between two components. A parameter was utilized to characterize connections between two components to predict interfacial strength.

While a large stress was applied to materials, the present results showed that crazes and voids will first form in a less dense area, which in this study was found to be in the DGEBA bulk. However, if the interfaces were not strong enough between TGDDM and DGEBA, interfaces are very likely to delaminate and fail during a stretch test along the direction normal to interfaces. Free volume calculation provides a convenient way to monitor process of void growth.

To improve strengths of weak interfaces, additional compatibilizer layers were added on free surfaces of box one. Morphologies and mechanical tests verified that

compatibilizer layers can effectively prevent void formation at interfaces. As a result, moduli of interfaces were increased by the addition of compatibilizer layers.

CHAPTER 5

WATER DIFFUSION IN EPOXY MATRIX AND INTERFACES

5.1 Introduction

Water absorption of epoxy matrix is a major concern in semiconductor, aerospace industry etc. Since water absorption usually lead to internal stress, aggregation of water at metal/epoxy interfaces can decrease their strength. At elevated temperatures, water may react with metals or epoxies, which can lead to further unpredictable problems that may lead to failure of materials. If a moisture environment is unavoidable, prevention of water absorption is necessary to enhance durability. To achieve a low water uptake level, one has to understand the basic laws and principles of water diffusion, which was described in Chapter 1. In addition to that, the relationship between water absorption and attributes of materials also play an important role in the study of water diffusion.

A large number of studies, especially experimental investigation, have been published on many areas of water diffusion and absorption. In this work, an attempt is made to understand this problem by means of molecular modeling, which is ideal for addressing molecular level problems. For the model TGDDM system, high temperature moisture environment is a major threat to structural adhesion. So water transport at varied temperatures will be investigated.

5.2 Diffusion Behaviors of water in epoxy bulk

5.2.1 Diffusion pattern

A three dimensional simulation box with periodic boundary conditions was used for the study described in this chapter. A TGDDM epoxy resin is the model polymer network in this study. The ratio of tetra-functional TGDDM epoxy to the di-amine DDS curing agent is 5:5 to keep an equivalent amount of reactive sites. A blend of TGDDM and DDS was generated on a diamond lattice and equilibrated at room temperature. Crosslinks were created in the equilibrated box and relaxed when a conversion rate of 80% or larger was achieved. Water absorption was studied first by inserting water molecules into the simulation box. Both epoxy resin and water molecules are charged. Force field for water is given by the TIP3P model. Bond angle and bond length of hydrogen-oxygen bonds are fixed throughout this work, implemented by the shake command in LAMMPS. In other words, hydrogen-oxygen bonds are not allowed to bend or stretch in simulation. MD simulations were carried out under NPT ensemble using a time step of 1 fs. Since all three boundaries are periodic, water molecules cannot escape from epoxy bulk. Wrapped or unwrapped positions of water molecules were recorded every certain time interval. Simulation time for diffusion was 1 ns at least and elongated sometime.

Using atomic coordinates obtained as output from molecular dynamics, one can track the path of a single water molecule diffusing in a polymer matrix. Figure 5-1 shows positions of a particular water molecule during a 50 fs period. The displacement for each time step (1fs) was also computed from coordinates of the molecule. Generally, water molecules move in steps smaller than one angstrom in one fs. The mechanism of diffusion of small penetrants in polymer matrix has been well studied using molecular

dynamics. A common activated/jumping mechanism was reported for most cases. Small penetrants collide with polymer atoms frequently within a cavity. The ballistic motion within a cavity may be observed at any time. Also, large jumps with displacements larger than the average cavity diameter may be observed sometimes. This is called a jump event. In practice, we averaged out the ballistic motion within a cavity over a time interval and detected sudden changes of positions of small penetrants. Figure 5-2 shows positions of one water molecule in 1 ns. One can see a jump from a cavity to another in this figure. To quantitatively describe the jump behavior of penetrants, the positions of penetrants were averaged over 1 ps and the signs of the slopes of x, y and z components of the trajectory were followed. When a slope sign change was detected and the jump distance was larger than the Lennard-Jones diameter of penetrants, recorded it was treated as a jump event and was recorded. The distances penetrants travelled between two successive jump events were computed. Figure 5-3 shows a typical jump map for water molecules in an epoxy matrix. The jump size is related to size of the cavities in the polymer matrix, size of penetrants as well as some other factors such as phase state of penetrants and interactions between penetrants and polymers. Here one can observe an average jump size of 0.4 angstroms. At an elevated temperature, thanks to a larger diameter of cavities in polymer matrix and a larger diffusion coefficient of penetrants, a larger jump size was observed (Figure 5-4). Here, the jump size of water molecules is smaller than typical jump sizes of other gas molecules. The first reason is that water is in the liquid state at 300K compared to other gases. The second one is due to hydrogen bonds formed between water molecules or water molecules and polymer atoms. Most water molecules exist in the form of clusters instead of single molecule. This will be discussed again later.

If the time intervals between two jump events were computed, we can obtain the distribution of residence time. To average down stochastic deviation of original positions of water molecules, number of penetrants was increased in the polymer matrix from one to fifty. Figure 5-5 gives the distribution of residence time of water molecules in TGDDM matrix at 300K. The smaller residence time, more likely it is that a jump event takes place. Temperate also has an impact in the residence time.

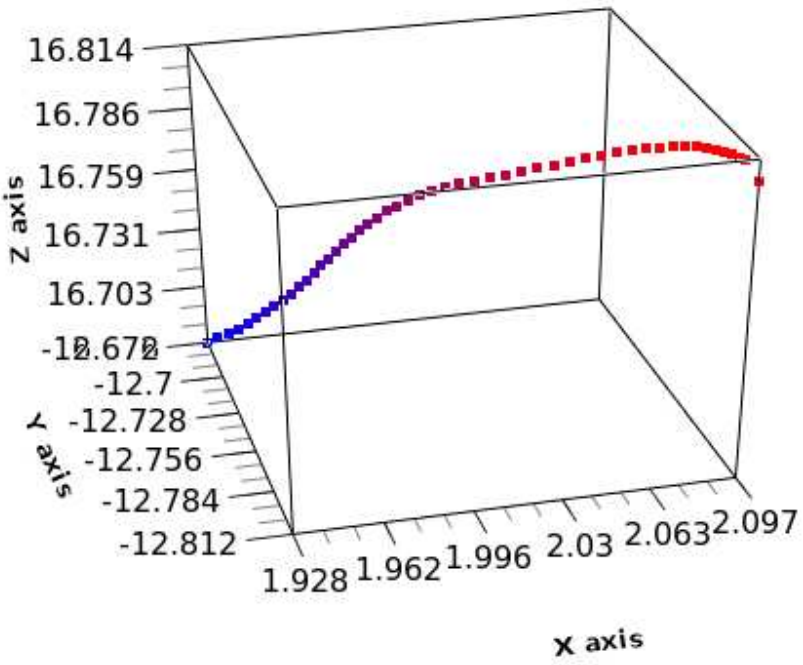

Figure 5-1. Trajectory of one water molecule in epoxy matrix in 50 femtosecond at 300K.

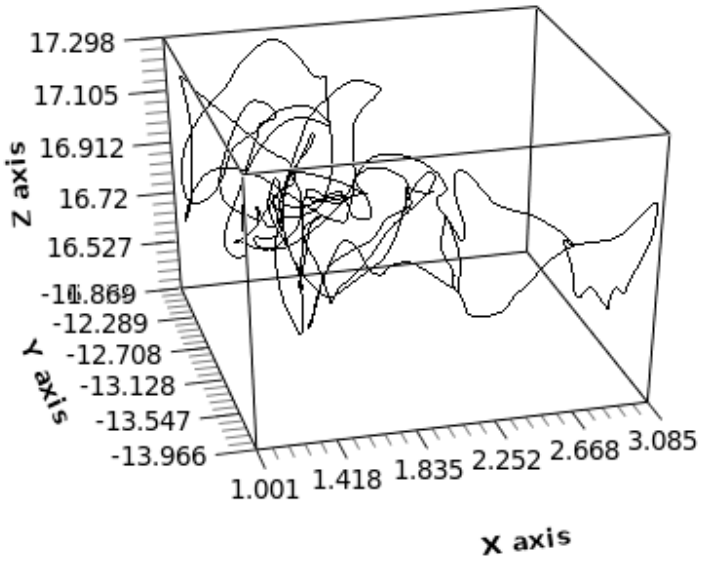

Figure 5-2. Trajectory of one water molecule in epoxy matrix in 1 nanosecond at 300K.

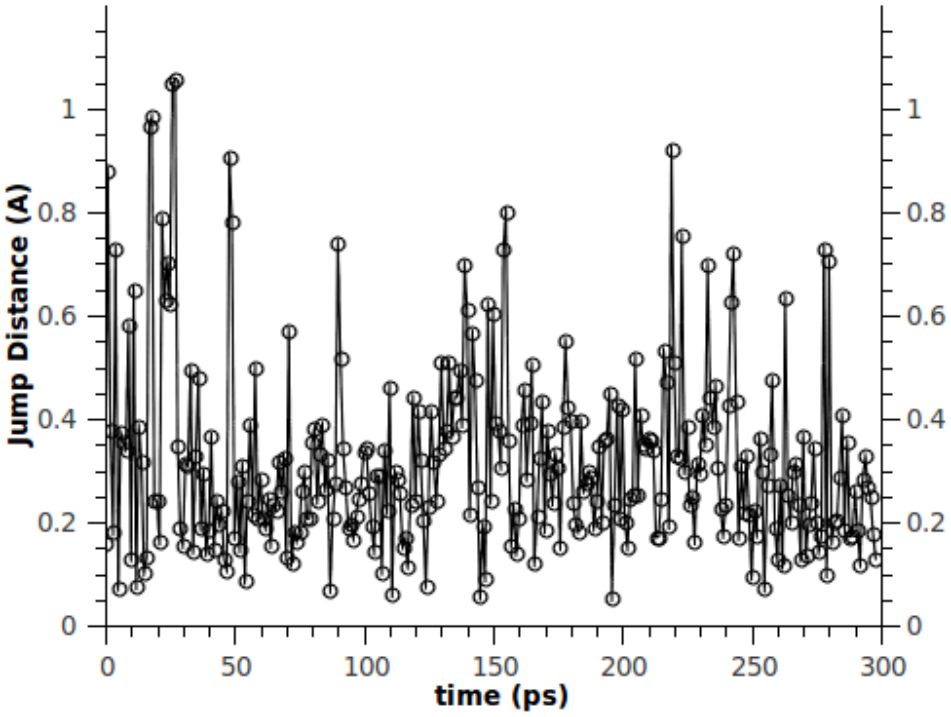

Figure 5-3. Jump map of one water molecule in epoxy matrix in a duration of 300ps.

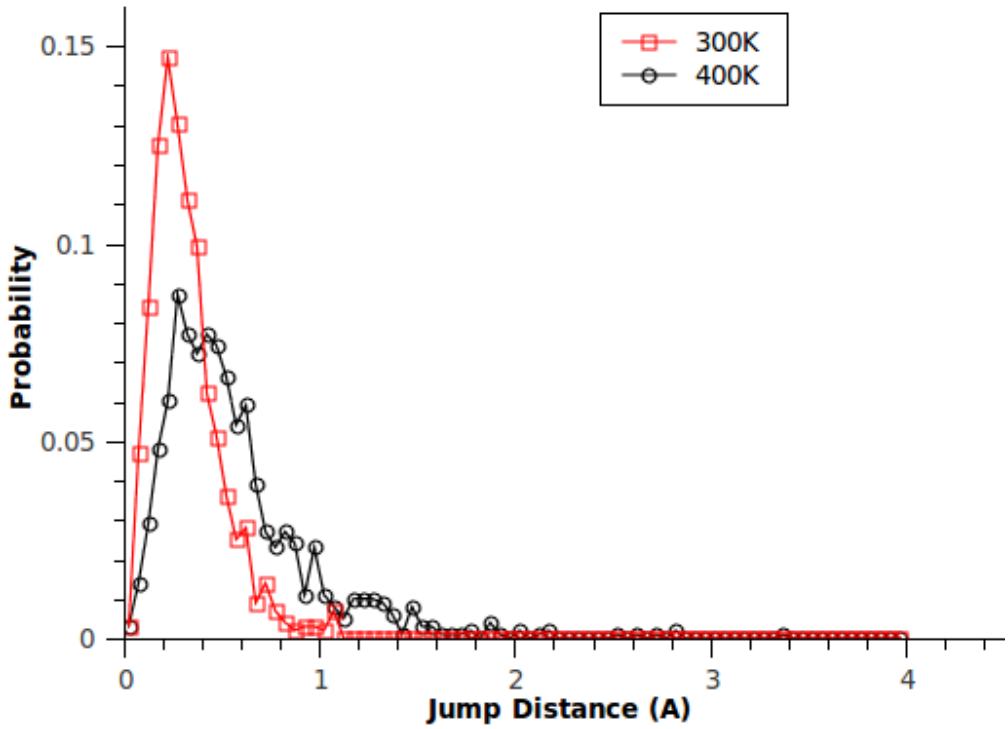

Figure 5-4. Distribution of jump sizes of water molecules in epoxy matrix at varied temperatures.

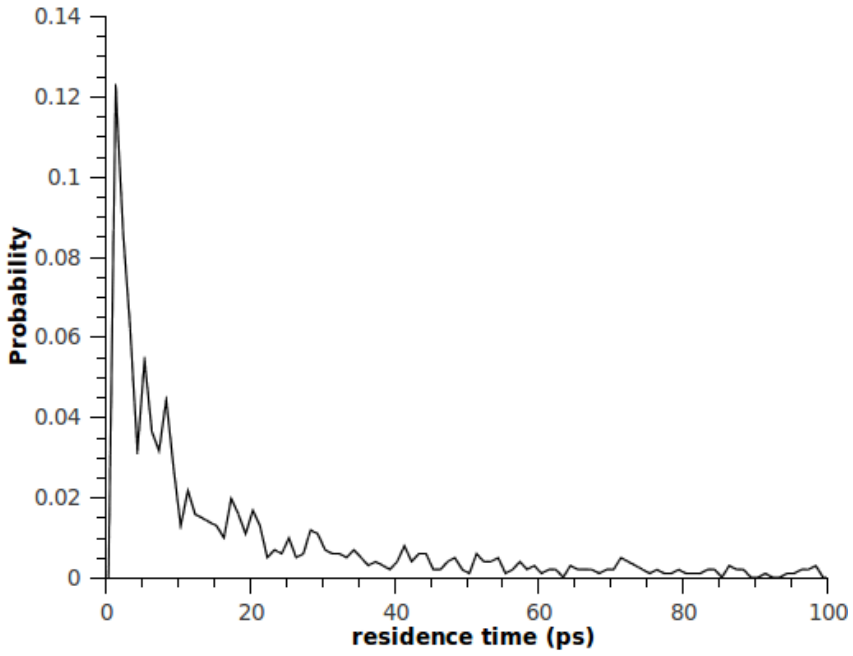

Figure 5-5. Distribution of residence time of water molecules in epoxy matrix.

5.2.2 Diffusion coefficient

In previous section, we discussed short time behavior of penetrants in polymer matrix. Here we focused on the long time behavior to calculate diffusion coefficients of water molecules in TGDDM matrix at different temperatures. According to Equation (1-20), averaged positions of water molecules in TGDDM were tracked and mean square distances (MSD) from the original point were calculated. A plot of MSD as a function of time was shown in Figure 5-6. A linear fitting to data points will yield the diffusion coefficient. At some temperature, the fitting should be conducted in the diffusive regime where the slope of log-log plot equals 1. The time required to reach the diffusive regime depends on penetrant size.

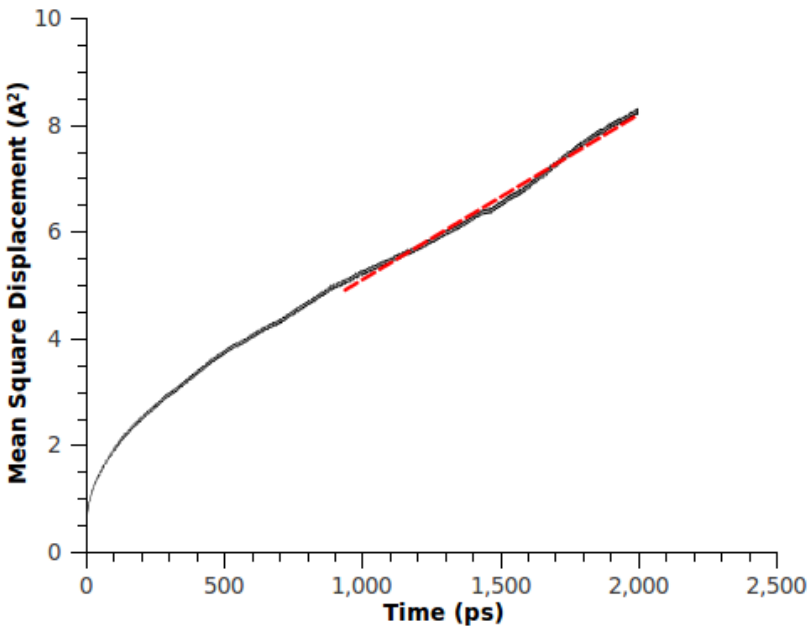

Figure 5-6. Mean square displacement of water molecules as a function of time.

Figure 5-7 gives diffusion coefficients of water molecules in TGDDM bulk at different temperatures. It is usually assumed that the relationship between diffusion

coefficient *D* and temperature *T* obeys the Arrhenius equation, which means that a linear fitting of ln(*D*) and 1/*T* will lead to diffusion activation energy. The temperature range studied here spanned from 100K to 800K. Three different slopes were obtained in Figure 5-7. If no phase transition of penetrants or polymer were taking place, only one slope should be expected. However, in a temperature range from 100K to 800K, water will go through solid phase, liquid phase and gas phase while polymer will transit from glassy state to molten state. In this course, both mobility of water and polymer are increased, which means a decrease of activation energy of diffusion. From the intersection of fitting lines in Figure 5-7, one can obtain an estimate of the phase transition temperature. The first temperature from Figure 5-7 is about 300 K, this corresponds to the melting temperature of water. The second transition temperature is about 500K, which is close to the glass transition temperature of TGDDM. So, from this plot, one can also estimate T_g of polymers as well as T_m of penetrants and polymers depending on whether the polymer is crystalline or semi-crystalline.

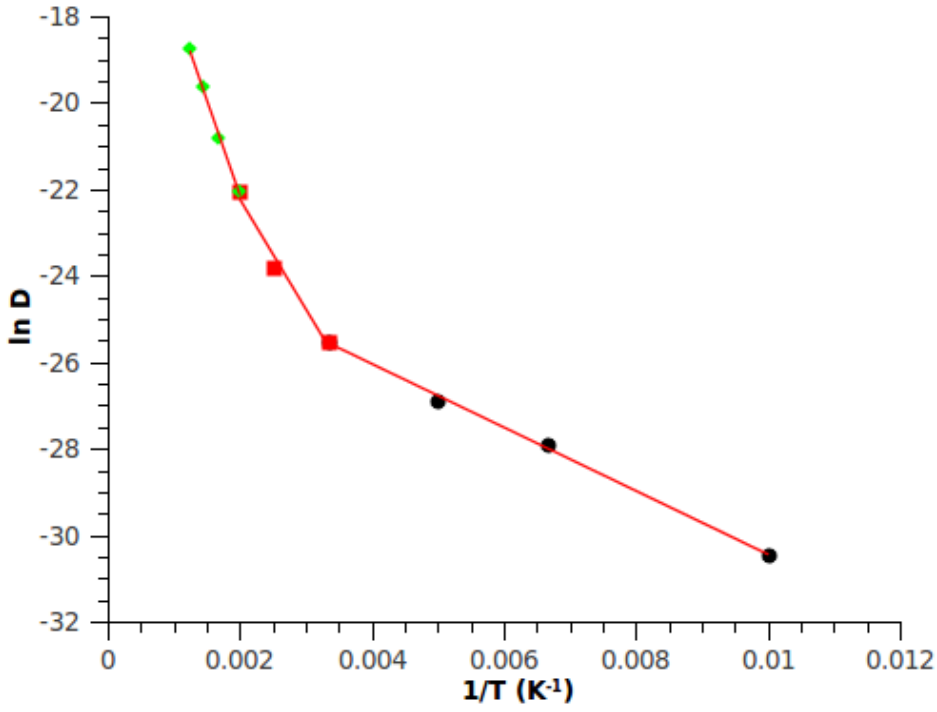

Figure 5-7. A plot of diffusion coefficient of water molecules as function of temperature.

The diffusion coefficient of water molecules in TGDDM bulk was calculated to be 8.35×10^{-12} m^2/s, while experiments gave a D of 1×10^{-13} m^2/s. The difference between two values arises from the simplified model of epoxy resins. In actual resins, small additives, toughenners or remaining monomers will effectively reduce size of cavities. In modeling, to simply chemical structures, these small molecules are always ignored, which make a larger portion of free volume compared to actual resins.

As a common phenomenon, small molecules, such as water, can swell polymers. Experiments showed that TGDDM epoxy can bear a water uptake amount as high as 7% after a long time exposure in a moisture environment. It is interesting to find out the extent of polymer swelling if 5.5% water absorption takes place. Figure 5-8 shows volume of simulation box as a function of water uptake amount. Basically, volume increases linearly with weight ratio of water. The curves flattened at high water uptake level, which corresponds to saturated stage of water absorption. A 5.5% water absorption can enlarge the total volume of epoxy resin by 3.5%.

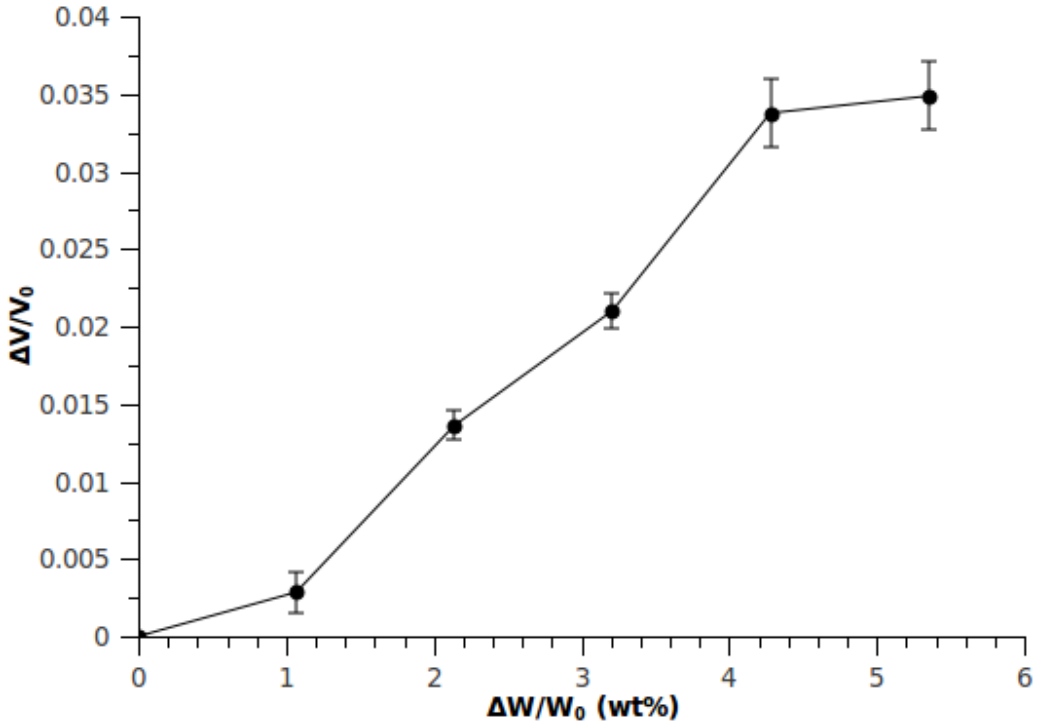

Figure 5-8. Volume change as a function of weight increase of epoxy resins.

5.2.3 Free volume

To relate free volume in polymer to *D*, the free volume and its distribution in the model system was investigated. In order to calculate the free volume, a spherical probe was employed, which was moved such that it covered every region within the cell. This was achieved by meshing the simulation box to a large number of cubes. The side length of cubes can be varied. A spherical probe of pre-determined size then is moved from one cubic mesh to another, one by one to cover the whole volume. If the distance between the center of the sphere and any atom in the neighborhood is larger than the radius of probe sphere, the cube is labeled as not occupied. The total volume of all not-occupied cubes is a measure of the free volume of the polymer bulk system. The radius of the probe sphere is a parameter which can affect total free volume. This method of

calculating the free volume is known as the hard probe method. A probe sphere with a rigid radius is often called a hard sphere. Here, the radius is changed from 0 to 1.5 angstroms. Figure 5-9 shows a plot of free volume fraction as a function of radius of the probe. A small sphere will yield a larger free volume. The radius of probe sphere was fixed at 1 angstrom hereafter, to match with the experimental probe size in PALS. Side length of cubes is another parameter associated with free volume calculation. The side length was varied from 0.2 to 3 angstroms. Figure 5-10 indicates the trend of free volume fraction as a function of cube side length. Smaller side length gives more accurate solution. However, a small mesh will lead to a high computational cost. When side the length is smaller than 0.5 A, the free volume fraction did not show any significant difference. As a result, the side length of cube was fixed at 0.5 angstroms.

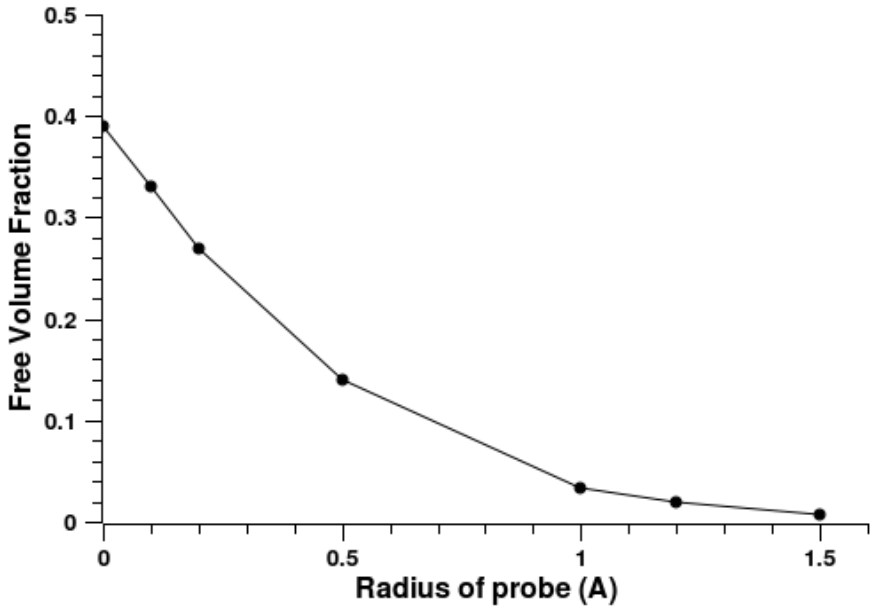

Figure 5-9. Variation of free volume fraction as a function of radius of probe.

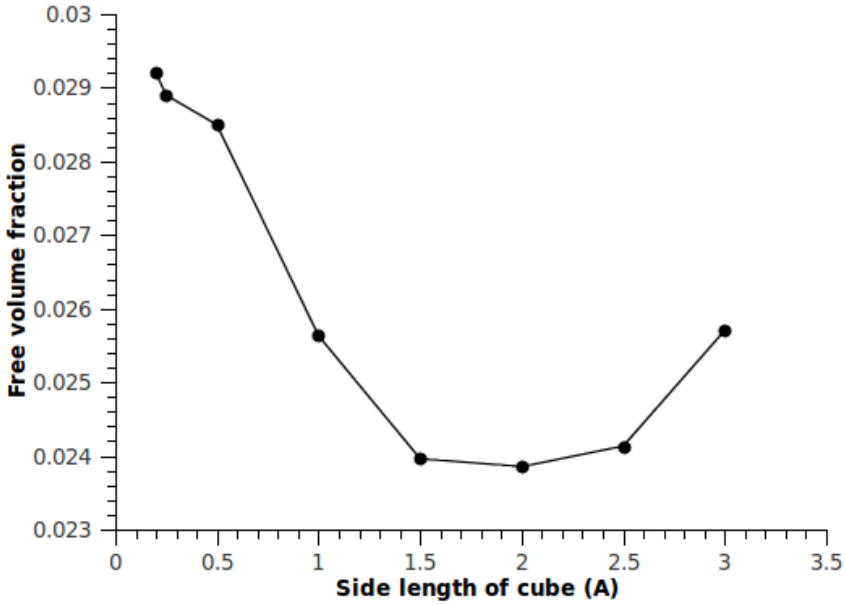

Figure 5-10. Free volume fraction as a function of side length of cube.

When water molecules are added into the simulation box, the question is where water molecules prefer to stay. Two approaches adding water into box were considered. The first one inserts water randomly, while the second one inserts water in cavities and voids based on a free volume calculation. Figure 5-11 compares the equilibrated position of water molecules in a simulation box with water inserted using two approaches. Figure 11(a) shows a line scanning along the x axis to locate cavities and voids. Figure 5-11(b) gives atom concentration of water molecules along x axis. If water was inserted into voids, they would like to stay in voids (the peak of black curve). If water was inserted randomly into simulation box, water molecules would move to free volume cavities of polymer matrix after a long time dynamics equilibration, although the transport is relatively slow. In the red curve, the broad peak emerges at the same position as the sharp peak in the black curve. As a conclusion, water needs more room in polymer bulk, so they prefer free volume.

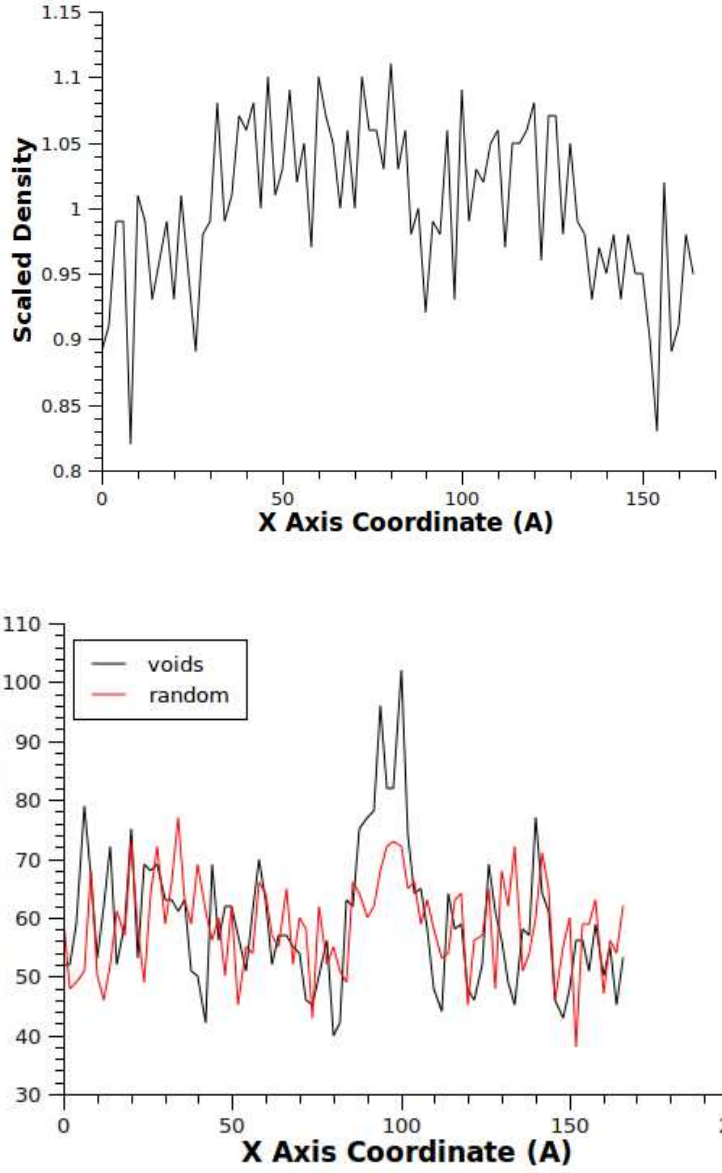

Figure 5-11. (a) Plane density along x direction of epoxy system; (b) positions of water molecules in epoxy system.

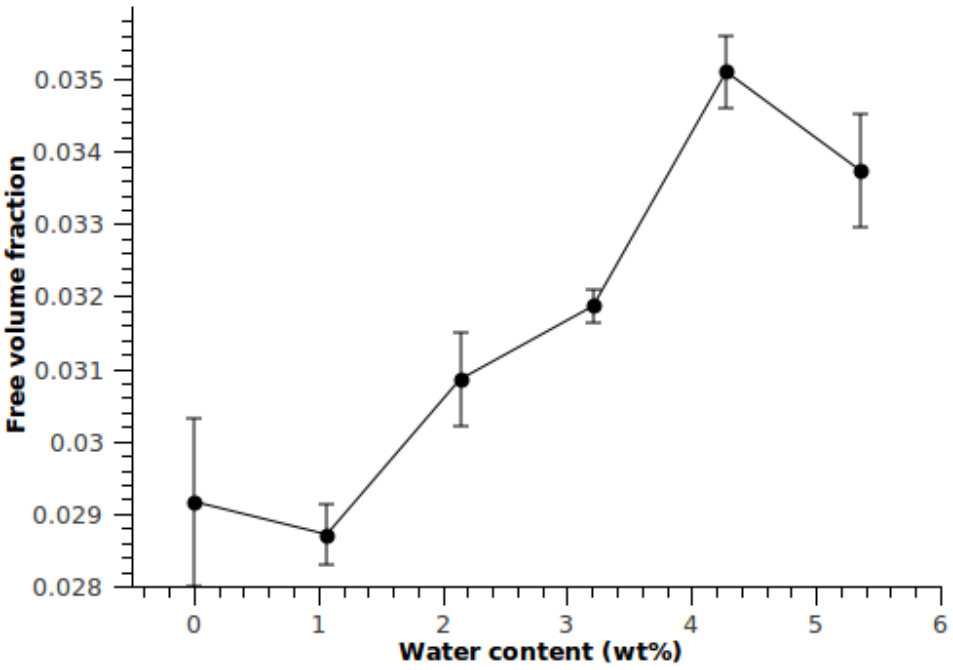

Figure 5-12. Variation of free volume fraction of systems with different water uptake amount.

For epoxy bulk system, because of a positive thermal volume expansion coefficient, the total volume of simulation box is increasing as temperature increased. It would be interesting to find how the free volume responds to temperature. Figure 5-12 is the plot of free volume as function of water uptake amount. Trend of the plot in Figure 5-12 is similar to that observed in Figure 5-8. As discussed before, water molecules prefer to stay in voids. When water uptake amount was 1%, we see a drop in free volume fraction because voids are filled by water. As more water absorbed, free volume fraction increases along with total volume of simulation box.

Figure 5-13 shows free volumes of wet epoxy systems at a temperature range from 100K to 700K. Data points were fitted using a linear relationship in two temperature ranges. Slope of lines changed at around 500K, which is the same as the kink point in

Figure 5-7. This can be contributed to the difference of thermal expansion coefficient of epoxy resins above and below T_g.

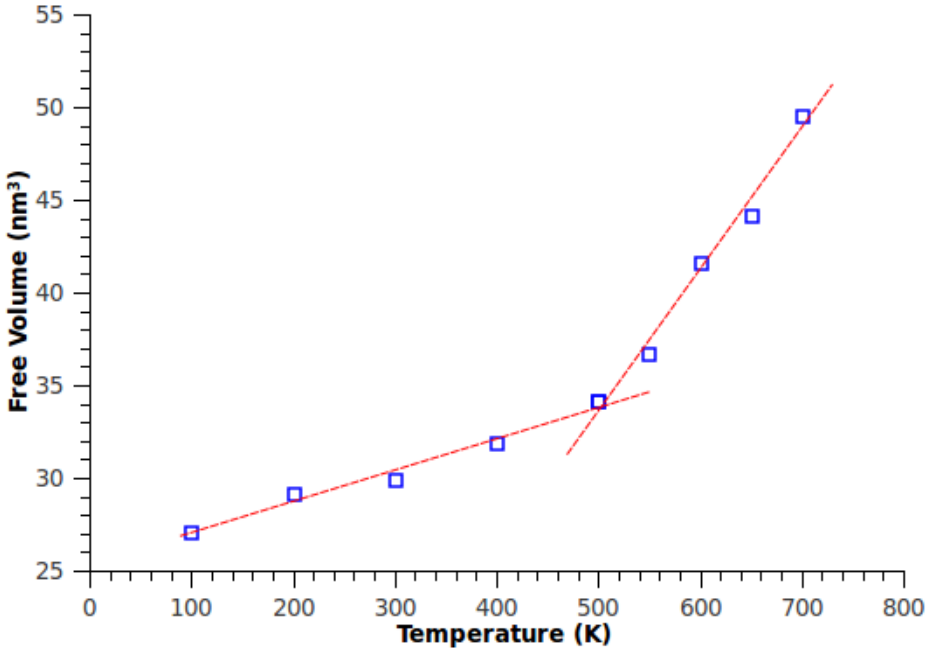

Figure 5-13. Free volume of wet epoxy resins as a function of temperature.

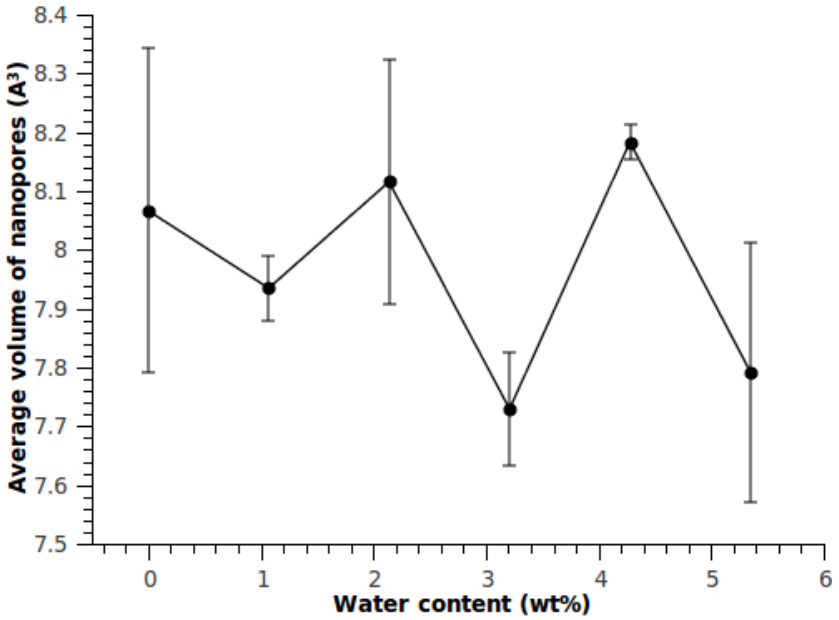

Figure 5-14. Average volume of nanopores in epoxy systems with different water content.

Size of nanopores in epoxy resins is another parameter we can obtain from free volume calculation. Volume of pores has a distribution; here one can use averaged volume as an indicator of sizes of voids. Figure 5-14 depicts variation of average nanopores volume when water absorption content was changed. The average size of pores in epoxy was about half of pores in other polymer systems obtained using PALS measurement. No obvious trend was observed because of the presentence of large variance. If most water molecules are constrained in small pores, average free of voids should increase since small voids are occupied. In an opposite way, if water prefers large room, oner should see a decrease in Figure 5-14. For epoxies, neither is the case. Possible reason could be water molecules are confined in local areas and have limited mobility.

5.3 Hydrogen bonds and water clusters

The results from section 5.2 show that water molecules take jumps with small jump distance. As pointed out before, diffusive behavior of penetrants are associated with Lennerd-Jones diameter of penetrants, temperature, free volume of polymer as well as interactions between penetrant and polymer bulk. Among these factors, the one factor significantly distinguishes water from other gas penetrant is the interactions between water molecules and polymers in the epoxy system. This interaction, due to partial charges, is known as hydrogen bond (HB).

A hydrogen bond is an attractive interaction of a hydrogen atom with an electronegative atom, such as nitrogen, oxygen or fluorine that comes from another molecule or chemical group (Figure 5-15). Hydrogen atom is always called the electron

donor and electronegative atom is called electron acceptor. In the epoxy model system, acceptor can be nitrogen, oxygen. Donor can be any hydrogen atom linked to an electronegative atom such as nitrogen or oxygen but not carbon and sulfur. Hydrogen bonds are commonly found in water and between water and polar polymers with oxygen and nitrogen atoms.

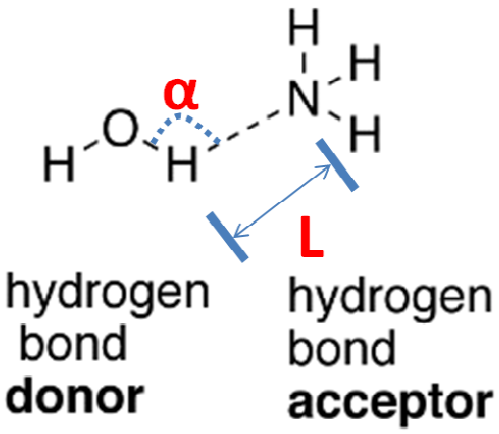

Figure 5-15. A scheme of hydrogen bonds between water and amine.

Modeling makes identification of the contribution of hydrogen bonds much easier than experiments. After checking all possible donor hydrogen, one has to look for the acceptor meeting two criteria (Figure 5-15). The angle between donor and acceptor α should be larger than 145 degree and the distance between donor and acceptor must be smaller than 2.45 angstroms. As long as these two prerequisite are meet, the interaction can be identified as a hydrogen bond. It should be pointed out that one hydrogen atom can form hydrogen bonds with more than one acceptor as long as the two criteria are met. Another underlying condition embedded in the definition of hydrogen bond is that acceptor and donor should come from two molecules or chemical groups. In other words, they should not be linked via covalent bonds. So hydrogen bond can only form between two or more water molecules. Experimental results already confirmed the existence of

hydrogen bonds between water molecules, that keeps the water as a liquid at room temperature. Actually, water exists mainly in the form of clusters. Water clusters can be made up of two, three, or more single water molecules. Hydrogen bond is relatively stable at room temperature and will become unstable at a high temperature, since due to thermal vibrations these partial bonds will continuously form and break. Compared to single water molecule, water clusters possess a much large diameter, which makes the movement of clusters much more difficult compared to single gas molecules. The movement of a water cluster needs enough space for atom rotation and rearrangement of configuration. This is believed to be the first reason of a small jump size and lower diffusion coefficient. Dimers, trimers and water clusters consist of more than three molecules are found in model system. Numbers of all the clusters at different temperature were computed and shown in Figure 5-16. Clusters made of two to six molecules were found in simulation box. At high temperature, large clusters were broken into smaller clusters mainly dimers. Above 300K, we can see an obvious decease of number of clusters. This can be contributed to the phase transition from liquid to gas at 373K. Water molecules move faster in a gaseous state. However, in pure gaseous state of water stable hydrogen bonds cannot exist. Here one can still find some dimers above 373K. Since some water molecules are trapped in some small voids of polymer bulk, the confinement made formation of HBs possible. Until now, using modeling the existence of hydrogen bonds was shown between water molecules, which leads to the formation of water clusters and explains the diffusive behavior of water molecules in an epoxy bulk.

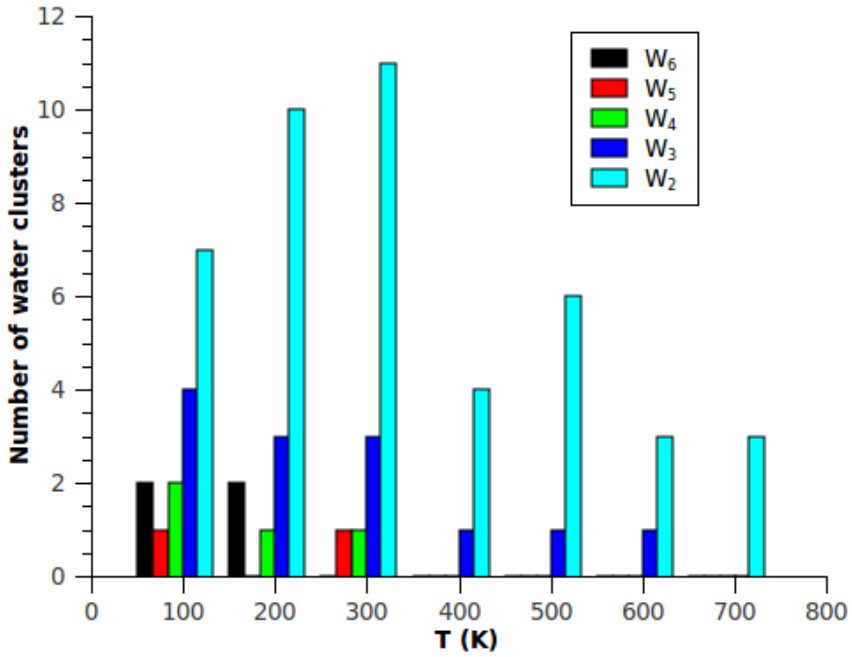

Figure 5-16. Number of water clusters in wet epoxy system at varied temperatures.

Besides hydrogen bonds between water molecules, HB can also be found between epoxy and water molecules. The interaction between polymer bulk and penetrants is likely confine the moving of penetrants. Here all these HBs between epoxy and epoxy, epoxy and water, water and water are taken into account. Figure 5-17 shows numbers of all type of HBs at different water uptake level. Total number of HB increases as more donor and acceptor are introduced. Both the number of water-water and epoxy-water HBs increases as well, but the number of epoxy-epoxy HBs decrease. In Figure 5-18 we see the number of clusters is decreasing as temperature is increased. This suggests that HBs between water molecules were broken at high temperature. Figure 5-18 shows the total number of all HBs at different temperatures. The same declining curves in Figure 5-18 verify that number of HBs has a negative correlation with temperature. A sudden drop in number of water-water HBs above 273K was also seen in this figure, which indicates a phase transition of penetrants.

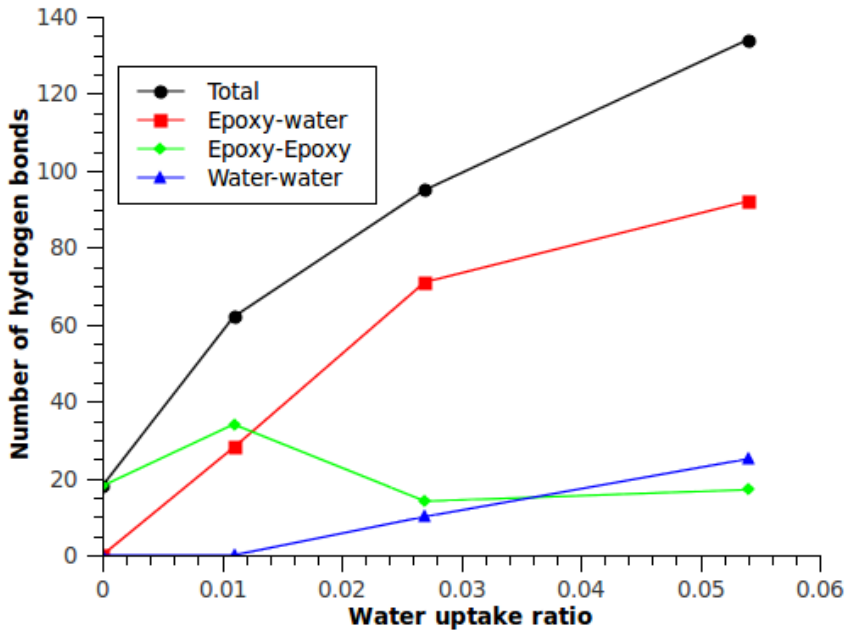

Figure 5-17. Numbers of different types of hydrogen bonds at different water uptake level.

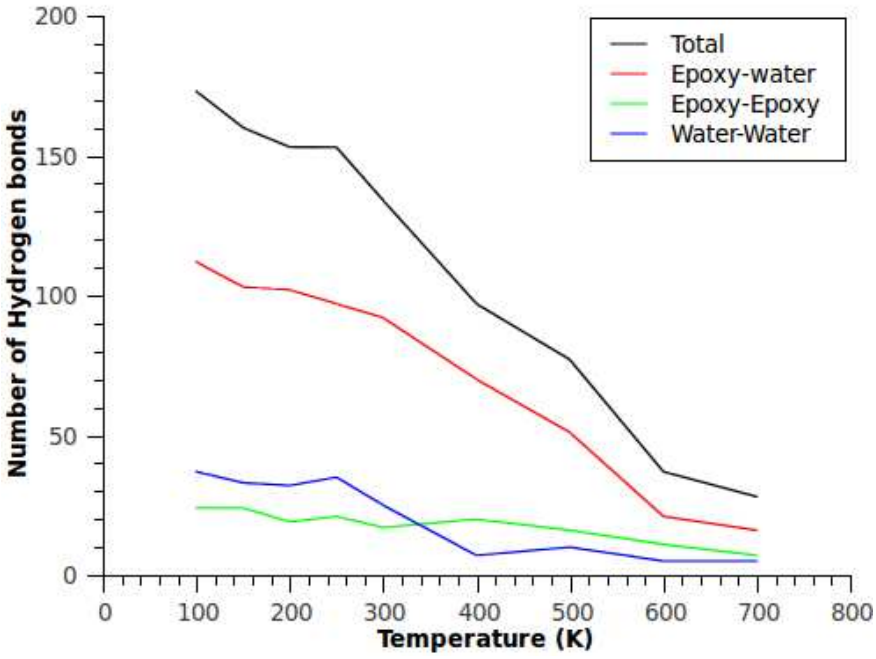

Figure 5-18. Number of different types of hydrogen bonds in epoxy resins at varied temperatures.

Other than water, the diffusion behavior of oxygen in epoxy resins was also studied. As discussed previously, the main difference between oxygen and water is the capability of forming hydrogen bonds. The LJ diameters of oxygen and single water molecule are comparable so one can use oxygen as a control penetrant to probe the effect of HBs. Figure 5-19 compares *ln*(D) at a temperature range from 50K to 600K. It is clear that within the temperature range that was investigated, oxygen molecules move faster than water molecules. The kink at 100K of the red curve corresponds to the liquefaction temperature of oxygen at around 57K. Numbers of HBs in water absorbed epoxy system and oxygen absorbed epoxy are listed in Table 5-1. As expected, addition of oxygen molecules only induces a small increase of number of HBs. No HBs exists between oxygen molecules. With this information one can conclude that HBs between epoxy and water limit mobility of water molecules and HBs between water molecules make penetrants larger. These two reasons can explain the difference in the diffusion behavior of water compared to oxygen.

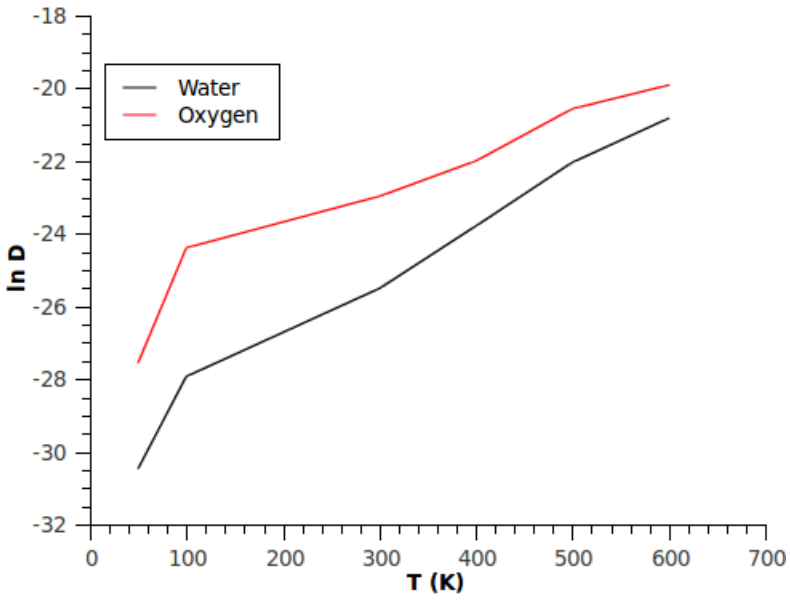

Figure 5-19. Dependence of diffusion coefficients of oxygen and water molecules in epoxy matrix on temperatures.

Table 5-1. Numbers of different types of hydrogen bonds in varied epoxy systems.

System	Total H bonds	W-E H bonds	E-E H bonds	W-W H bonds	Modulus (GPa)
0	18	0	18	0	4.71
50 Water	95	71	14	10	6.82
50 Oxygen	23	0	23	0	3.89

To relate HB to possible property changes of epoxy resins, mechanical modeling of simulation box with and without water was performed. In detail, simulation box was pulled along x direction at a fixed rate. Based on the previous study, a strain rate of $1e^{-6}$ /fs was chosen, which was relatively slow in mechanical modeling. All other settings are the same as in the diffusion study. Epoxy samples with oxygen molecules were also stretched using the same condition for comparison.

5.4 Effect of water on properties

All three modulus of epoxy system and epoxy with 50 water molecules or oxygen molecules are listed in Table 5-1. If no interactions between penetrants and matrix exist, penetrants will decrease mechanical strength of polymer systems. Modulus of epoxy with oxygen is smaller than that of pure epoxy. The root reason is that swollen polymers have weak intermolecular interactions. However, if epoxy was swollen by water, more HBs make the system even stronger than pure epoxy. In real life, water absorption always degrades mechanical strength of epoxy resins. The deviation of modeling results

from actual experimental observation origins from a simplified model. Some other researchers also reported an increase of modulus in modeling study [74].

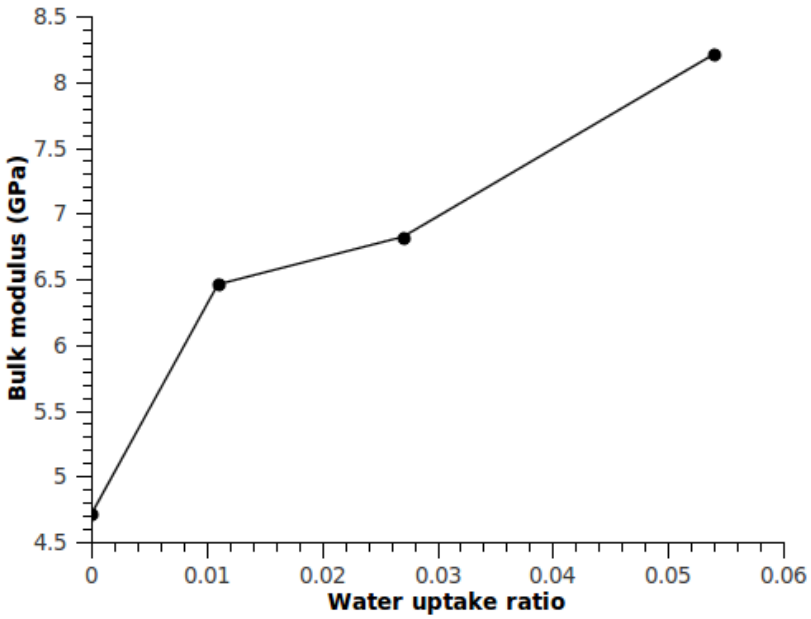

Figure 5-20. Dependence of bulk modulus on water uptake level.

Given the hypothesis that hydrogen bonds can strengthen epoxy matrix, water uptake level was changed by varying the number of water molecules in the simulation box. Bulk modulus of wet epoxy resins kept increasing in Figure 5-20. As more water molecules were added, more hydrogen bonds were formed between water and epoxy, which leads to a stronger matrix.

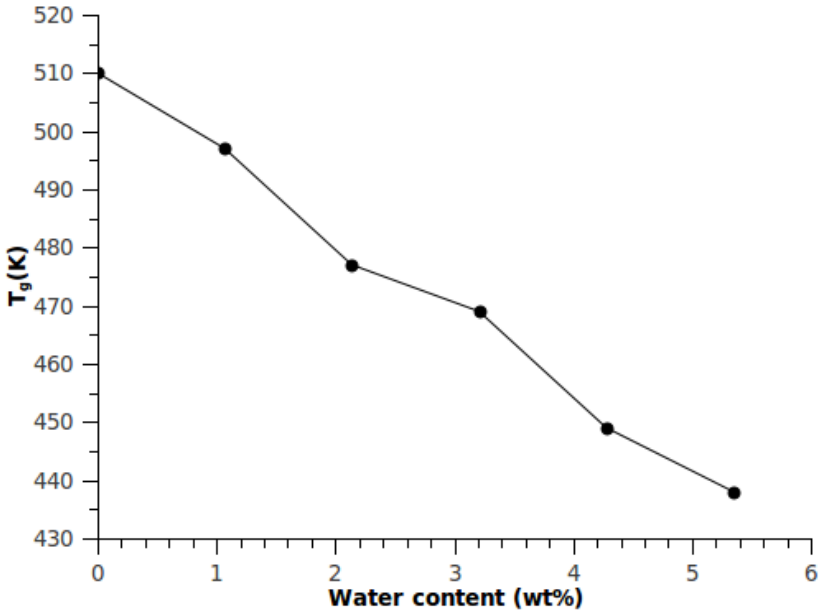

Figure 5-21. Glass transition temperatures of epoxy resins with varied water uptake amount.

Finally the glass transition temperatures of epoxy resins with varied water uptake amount were computed from plots of densities vs. temperatures. A linear decrease of T_g implies water has a destructive effect on thermal stability of epoxy resins. Experimental studies also showed a drop of T_g of epoxy resins with absorbed water [75, 76].

5.5 Conclusions

Importance of water absorption motivates one to investigate water diffusion and transport in epoxy resin. Water absorption was studied by adding varied amount of water molecules into simulation box. A dynamic process of surface absorption and diffusion into epoxy was not modeled since it is very time consuming.

Diffusion of water molecules in epoxy resins follows the classic jump-diffuse pattern. Jump sizes and residence time of water molecules were calculated and

compared with other systems. Water in epoxy was found to move faster than in linear polymers, but the jump size was smaller than other small gas molecules.

Free volume calculation was performed to explain diffusion pattern of water molecules in epoxy resins. It was found that volume of nanovoids in epoxy matrix has a broad distribution. Most water molecules are confined in local small voids and have limited mobility. The rest the molecules diffuse fast in large pores in epoxy matrix, which contributed to a large diffusion coefficient of water in epoxy.

The other factor which makes water different from common gas molecules is the existence of hydrogen bonds. Hydrogen bonds were found to exist between water molecules, water and epoxy as well as epoxies. Interactions between water and epoxy further restrain movement of water molecules. Hydrogen bonds between water molecules lead to the formation of water clusters. Increased size of water clusters makes them fixed to small pores.

Lastly the effect of water absorption on properties of epoxy matrix was studied. On one side, hydrogen bonds strengthened interconnecting network structures of epoxy, which gives rise to a higher bulk modulus. If penetrates were changed from water to oxygen, we observed a drop of modulus because of the absence of hydrogen bonds. On the other hand, absorption of water reduced the glass transition temperature of epoxy resins.

CHAPTER 6

MODELING OF CHEMICAL REACTIONS

6.1 Introduction

Chemical reactions are quite common phenomenon observed with polymers at elevated temperature. Since the weight loss of polymer samples and emission of small gas molecules are always associated with chemical reaction of polymer samples at high temperature, these reactions are generally referred in terms of chemical degradation or decomposition. A loss of mechanical strength and other properties generally accompany the chemical degradation reactions in polymers. From a molecular point of view, degradation stems from chain scission and cleavage of covalent bonds in polymers. The onset of temperature of degradation depends on strength of covalent bonds in materials.

In Chapter 3, the effect of chain scission on the properties of epoxy resins was investigated. However, the chain scission mechanism was based on empirical and experimental observations of chemical reactions. On the basis of IR results, one can mimic bond cleavage at certain sites depending on the reaction mechanism. The reason for using an empirical cleavage algorithm earlier is that classical molecular dynamics is not able to simulate chemical reactions as addressed in Chapter 1. To overcome the shortness of classical MD in modeling reactions, researchers have put significant efforts in developing new algorithms or force fields for reaction modeling.

Until now, three main categories of methodology are developed to simulate reactions of polymers. The first one is called reactive molecular dynamics (RMD). RMD

typically made modification to the bond length term in classical MD to allow bonds break if some conditions are met. One example of such condition is bond length. If the length of a bond exceeds a critical value due to physical stretch or thermal stretch, then that bond will be removed from the list of covalent bonds, which means the bond is broken. The idea is always implemented by changing the common harmonic bond potential to more complex equations. The other terms such as bond angle, dihedral angle will be modified accordingly depending on models of systems. The second category of methodology is called ab initio molecular dynamics (ab initio MD). It unified quantum mechanics and MD to achieve a first principle real modeling of materials including reactions. The basic idea underlying ab initio MD method is to compute the forces acting on the nuclei from electronic structure calculations that are related to the molecular dynamics trajectory. Instead of selecting the model potential, ab initio MD chooses a particular approximation to solve the Schrodinger equation. The advantage of ab initio MD is the well established assumptions of modeling on a fundamental level of electronic structures. In other words, it is a first principle method with least usage of empirical equations and parameters. The drawback is that only small systems can be studied with ab initio MD since the computational cost is very high. The last category of methodology is reactive force field (ReaxFF) developed by Goddard and his coworkers. It uses distance-dependent bond-order functions to represent the contributions of chemical bonding to the potential energy. One type of chemical element is dealt as one atom type, i.e. sp3 carbon and sp2 carbon are the same atom type in simulation. Equations and details descriptions of energy terms can be found later in this chapter. ReaxFF has been successfully applied in many research areas. In this chapter, ReaxFF is utilized to study the thermal decomposition mechanisms of epoxy resins in different environments.

6.2 Modeling and simulation details

Two sets of epoxy resins were studied in this work. A tetrafunctional epoxy tetraglycidyl-4,4'-diamino-diphenylmethane (TGDDM) and a difunctional epoxy diglycidyl ether of bisphenol A (DGEBA) was cured separately with the same hardener diethylmethylbenzenediamine (DETDA). Chemical structures of epoxies and hardener were shown in Scheme 1. A periodic box containing stoichiometric amount of epoxy and hardener molecules was created as model system. After crosslinking epoxy with curing agents, a classical force field Dreiding was applied to perform a molecular mechanics minimization, followed by dynamics runs. Molecular dynamics (MD) simulation was performed using LAMMPS under a constant temperature and constant pressure condition (NPT). Time step was 1 femtosecond. After a 100 ps run at room temperature and one atmosphere pressure, an equilibrated state was achieved. Coordinates of all atoms and boundaries were then recorded to be used as the starting stage for degradation studies.

In the thermal degradation part, ReaxFF, a general bond-order-dependent force field, was adopted to describe bond formation and breaking. ReaxFF was used to calculate distances between atoms to determine bond connectivity in simulation box. Bond order information were updated every MD step. ReaxFF also distributes atomistic charges based on geometry of models and includes non-bonded van der Waals interactions.

ReaxFF implementation in LAMMPS together with a force field was employed to perform the degradation simulations. Different from classical MD, a time step of 0.1 femtosecond was used here and a constant volume condition (NVT) was assumed instead of NPT. After importing coordinates from equilibrated structures, another

minimization and equilibration step at room temperature was conducted using ReaxFF force field. Bond information was recorded every certain time steps. To study thermal degradation, system temperature was increased gradually from 300 K to 1800 K at varied speeds.

One problem of ReaxFF is the system dependency and complexity of force field parameters. In this study, a general ReaxFF force field for organics was employed without validation by quantum mechanics calculation since chemical elements in the model systems used here have already undergone substantial investigations.

Before the thermal degradation study, one issue that should be addressed is to ensure that the model system has exact the same structure as the one produced by Dreiding force field. Bond information in the model system after equilibration in ReaxFF was recorded and compared with the one from Dreiding. For all the model systems, ReaxFF recognized all bonds between atoms correctly. The typical crosslinking degree was 80% before the degradation reactions.

The pure DGEBA/DETDA system was used at first, which was heated to study possible thermal decompositions. Heating was realized by Nose-Hoover thermosetting algorithm from a starting temperature of 300K to a final temperature of 1800K almost lineally. Simulation time over the fixed temperature range was varied to examine the effect of heating rate on thermal decomposition. A system which contains 14 DGEBA and seven DETDA reagents was generated as a model system. Figure 6-1 shows the number of molecules in the simulation box during the heating process at different heating rates. All the three heating process started from the same configuration of epoxy resin and the shapes of three curves in Figure 6-1 are similar. Basically, the number of molecules remains unchanged until the onset temperature of decomposition, which is

around 800K. When temperature was increased beyond the onset point, epoxy resin was cleaved to more-than-one small pieces until the end of decomposition, which depends on the heating rate. The final number of molecules in simulation box was oscillated around six for all three curves. Another increase observed in 15K/ps curve starting from 1700K may have resulted from a second stage of decomposition, which was not focused in this work. It can be seen from Figure 6-1 that a faster heating rate increases the onset temperature of decomposition. Although the heating rate used in modeling is not comparable to experimental setting in a thermal test, the same effect of heating rate in TGA measurements were also reported. In practice, low heating rate is necessary to obtain good resolution thus increasing time required for experiments. However, in our work, a higher rate of 50K/ps was adopted to save computational cost.

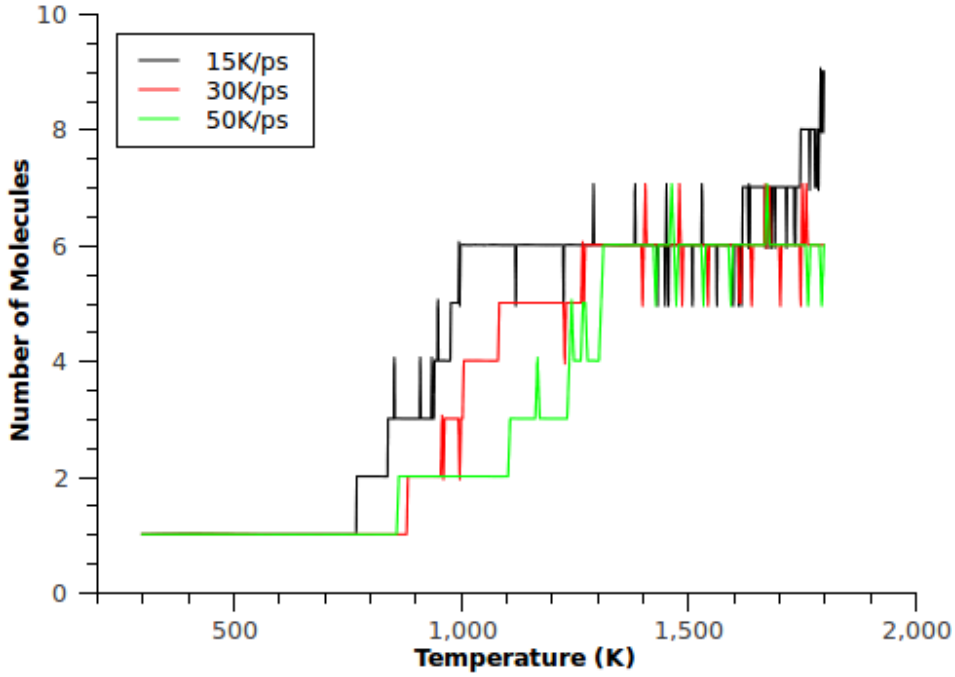

Figure 6-1. Evolution of number of molecules in simulation box at varied heating rates.

In a molecular modeling study, the size of simulation box is a parameter which always has an effect on results. Figure 6-2 compares two systems with different number of molecules included. The first system contains 14 DGEBA and seven DETDA reagents which the second one doubles the numbers of DGEBA and DETDA. As a result, the total number of original molecules in simulation box before curing was 21 and 42 respectively and became one after curing. Each system was heated at a heating rate of 50K/ps from 300K to 1800K and evolution of number of molecules was examined. Figure 6-2 clearly shows increase of number of molecules in both systems, which indicate thermal decomposition did take place. The similar shape of both curves suggests bond breaking in both systems may obey the same mechanism. It is believed that larger simulation box leads to more reliable result. However, for the sake of simulation time, number of original reactants in simulation box was fixed at 42 hereafter and not increased to larger values.

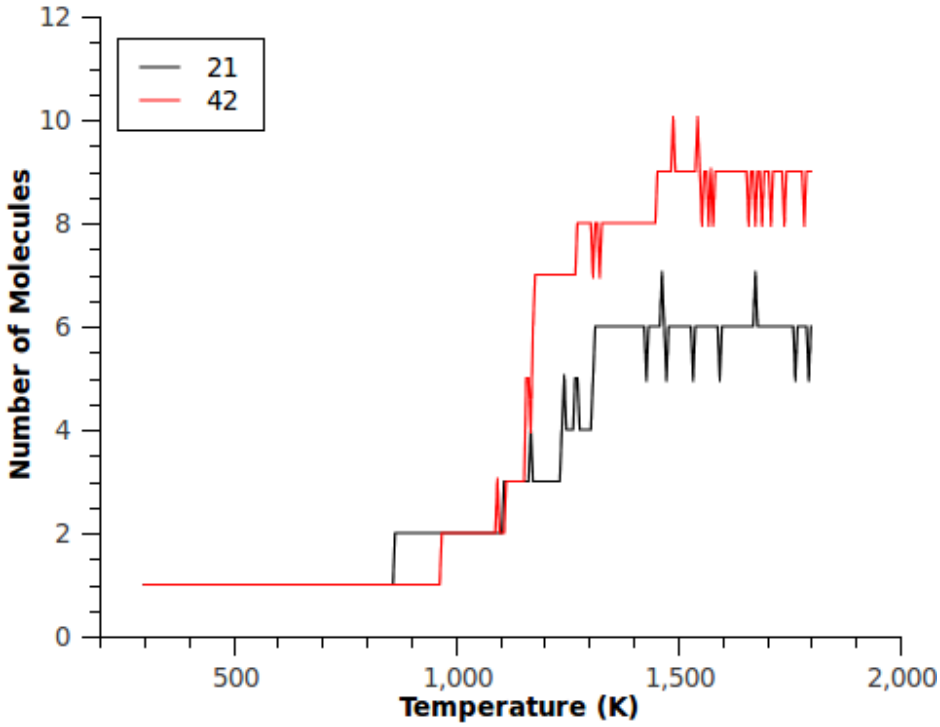

Figure 6-2. Evolution of number of molecules in simulation boxes with different sizes.

Two independent structures of DGEBA/DETDA systems were built and the same annealing procedure was performed to look for any bias introduced by initial configuration of epoxy resins. Figure 6-3 compares the decomposition curves of two trials. It is obvious that the evolutions of number of molecules in two systems are essentially equivalent, which suggests that the system settings are fairly good and appropriate to study thermal degradation in order to obtain meaningful results.

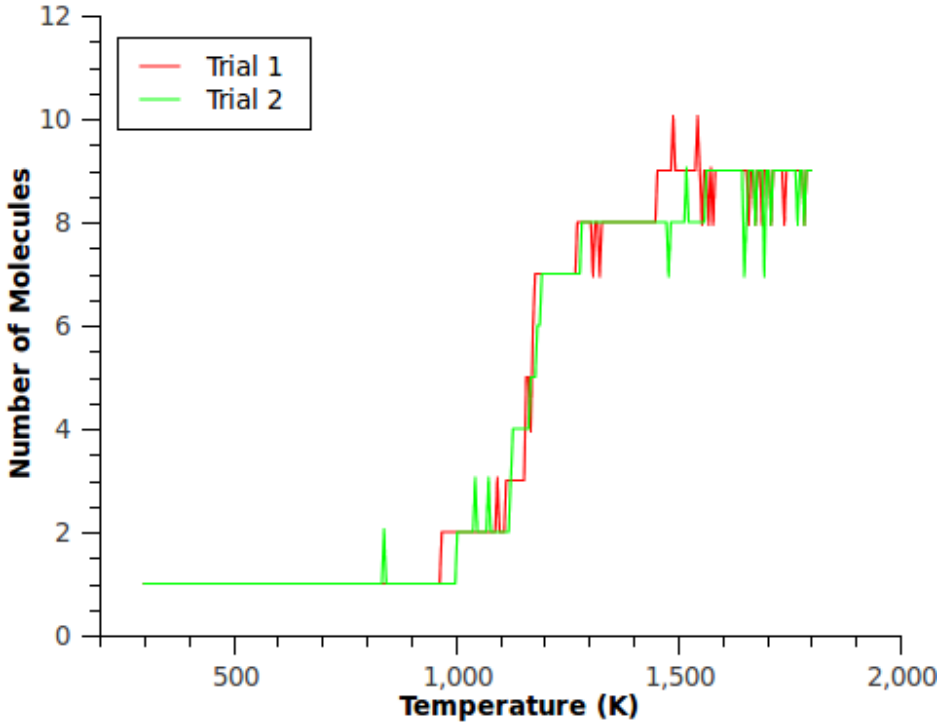

Figure 6-3. Evolution of number of molecules in two trials.

6.3 Decomposition mechanism

6.3.1 Difunctional system

After identifying the system settings, one can look deeper into the bond information to extract decomposition mechanisms. All possible types of covalent bonds between two atoms involved in DGEBA/DETDA system were tracked and analyzed. The number of all combinations of connections between four types of atoms in the system is ten. However, not all possible bonds may form or break in thermal degradation. In the temperature range of interest, changes in the numbers of C-C and C-O bonds were observed. Figure 6-4 gives the time evolution of C-C and C-O bonds in the simulation box. As seen in Figure 6-4, number of C-C bonds decreased by one at about 660K which indicates occurrence of reactions. A continuous drop in numbers of C-C and C-O bonds started almost at the same time at an onset temperature of about 1000K. This onset temperature of bond cleavage is consistent with the onset temperature of network scission from Figure 6-2 and Figure 6-3. Here we take 1000K as the onset temperature of thermal decomposition (T_d) of DGEBA/DETDA. Experimental measurement of thermal degradation temperature of DGEBA based epoxy resins is 600-630K. The deviation of simulation result from experimental value is mainly contributed to a high heating rate. If a relatively low heating rate was used, Figure 6-1 showed that a lower T_d was obtained. However, the higher priority of decomposition mechanism over a realistic T_d is the reason for choosing a faster heating rate for the sake of simulation time. Also, using the same modeling parameters, one can still compare T_d of different systems.

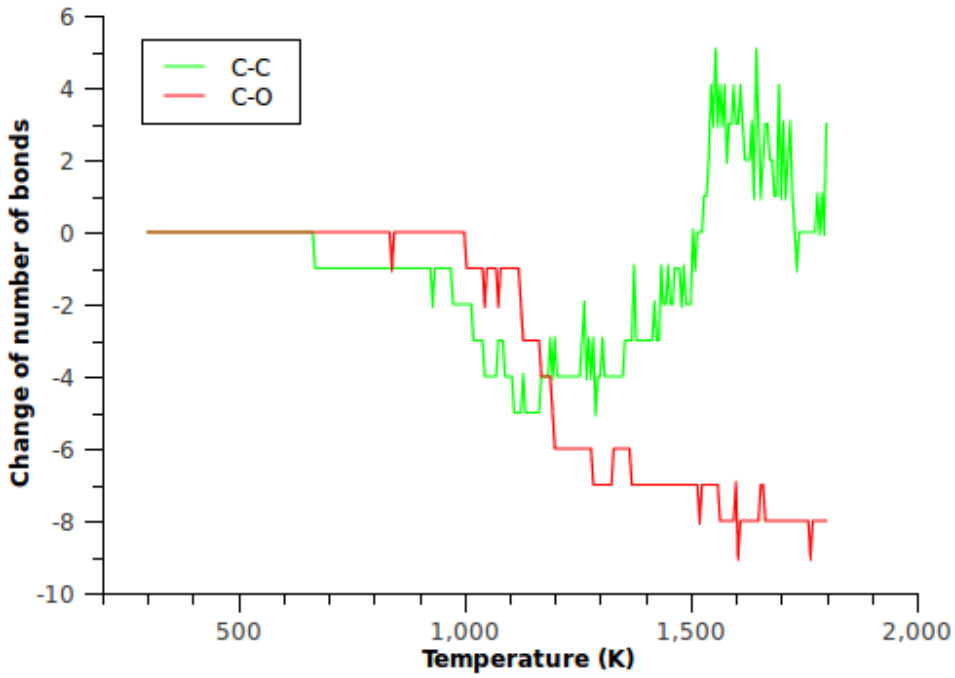

Figure 6-4. Variation of numbers of C-C and C-O covalent bonds during a thermal degradation modeling progress.

It is obvious that in Figure 6-4 numbers of C-C and C-O bonds follow different trends. Number of C-O bonds started to decrease at T_d and was stabilized at around 1500K. As a contrast, number of C-C bonds decreased first and went through an increase stage after that. To find out whether network scission is due to bond cleavage of C-C bonds or C-O bonds, positions of all the broken bonds were located in the network structure. It turned out that all the broken C-O bonds were ether bonds located along the backbones of DGEBA. More specifically, ether bonds formed between O and sp^3 C atoms not the aromatic carbon are the first bonds to be cleaved. At the same time of ether bonds being cleaved, C-C bonds from benzene rings were also affected by heating in the form of bonds rearrangement which leaded to damage of aromatic rings. As pointed out before, break of network structure and cleavage of ether bonds took place at almost the same time. This suggests that scission of ether bonds located at

backbones is the reason of network being destroyed at the initial stage of thermal degradation of epoxy resins.

Thermal decomposition mechanism of DGEBA epoxy resins uncovered in this work was supported by many experimental studies [77, 78]. FTIR showed scission of C-O bonds and some other C-N, C-H bonds followed by rearrangement of aromatic carbon atoms. Figure 6-5 gives evolution of more types of bonds in thermal degradation. Besides C-C and C-O bonds, C-N, C-H and O-H bonds are also affected.

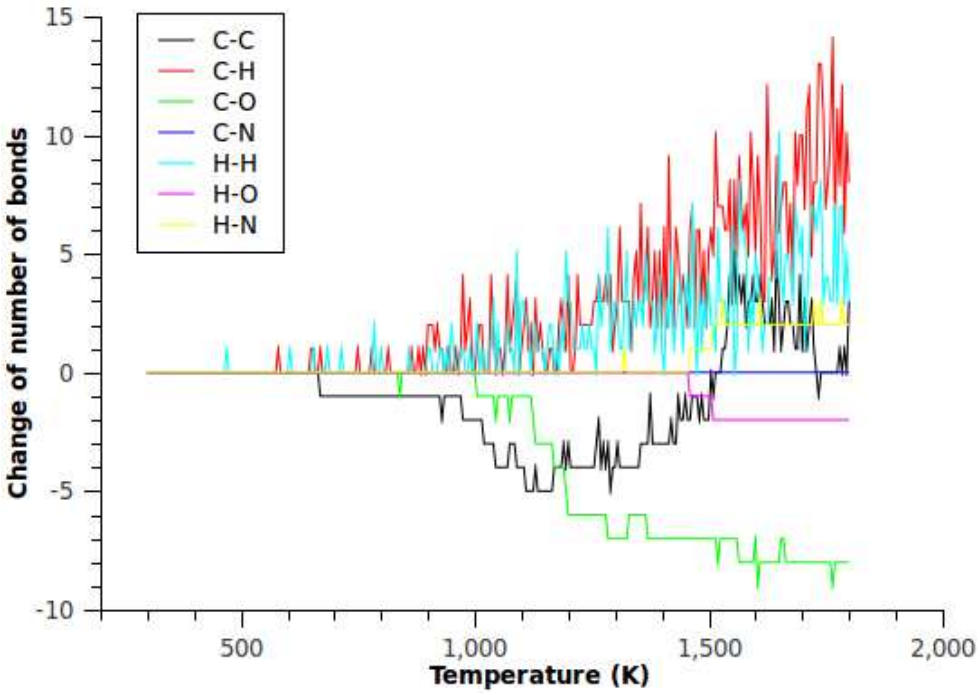

Figure 6-5. Evolution of all types of bonds in difunctional epoxy during heating.

6.3.2 Tetrafunctional system

To compare degradation mechanism of tetrafunctional epoxy with difunctional epoxy, DGEBA was changed to TGDDM. All other modeling procedures and parameters remained unchanged. DGEBA and TGDDM have similar backbones structures despite

the difference of functionality. Instead of ether bonds, secondary amines were found in chemical structure of TGDDM in Scheme 1. Using the same heating rate from 300K to 1800K, evolution of the number of molecules in the simulation box was compared in Figure 6-6 for DGEBA and TGDDM. It can be seen that TGDDM is more durable than DGEBA in terms of onset temperature T_d and final number of molecules. Network scission took place at around 1300K, 300K higher than of that of DGEBA. After the heating process, about 5 molecules existed in system instead of 9 in DGEBA case. TGA analysis of TGDDM also proved that TGDDM is more stable than DGEBA. To uncover the underneath reason of these difference, a bond information analysis was performed for TGDDM system.

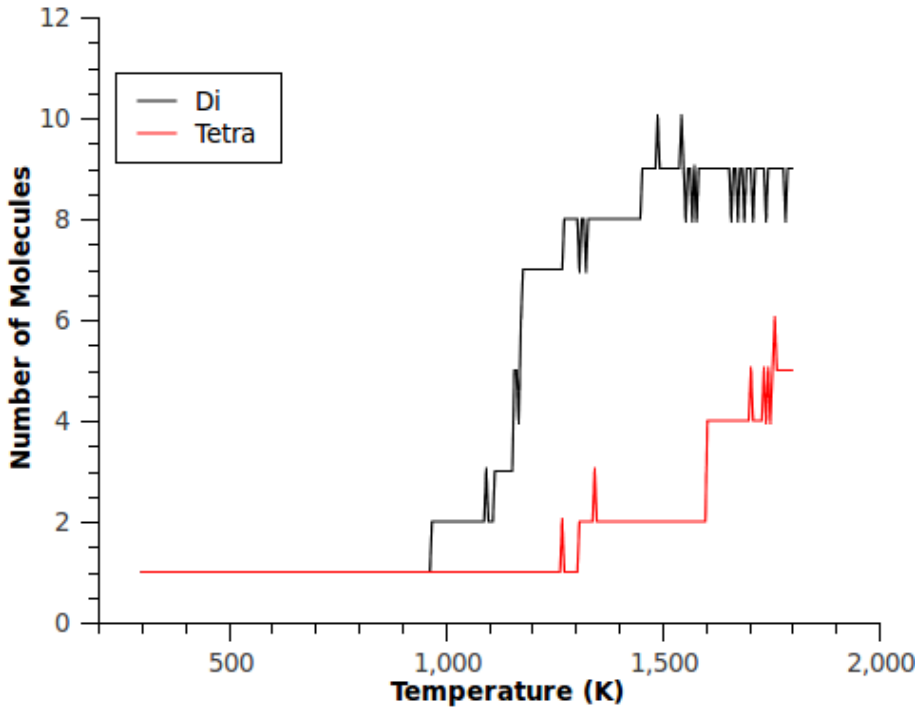

Figure 6-6. Variation of number of molecules in difunctional and tetrafunctional epoxy resins.

Figure 6-7 gives information about C-C and C-O bonds in TGDDM system. The curve of C-C bond evolution was similar to that of DGEBA system. However, a very small fluctuation of number of C-O bonds was observed when temperature was above 1500K. If one examines the structure of cured TGDDM, it can be seen that C-O bonds are formed between carbon atoms and oxygen atoms that are bound to hydrogen atoms as well as in some unreacted epoxide groups. In other words, C-O bonds exist in the form of alcohol and epoxide. There are no linear ether groups, which are weaker than alcohol groups, in TGDDM. As a result, TGDDM can stand heating better than DGEBA with ether groups and therefore have a higher T_d. It is worth mentioning that C-C arrangement began at nearly the same temperature in Figure 6-7 as in Figure 6-4. However, this arrangement did not destroy the network linkage in epoxy resins and there was no weight loss. Therefore, change of aromatic structures did not necessarily lead to a degradation of epoxy resins.

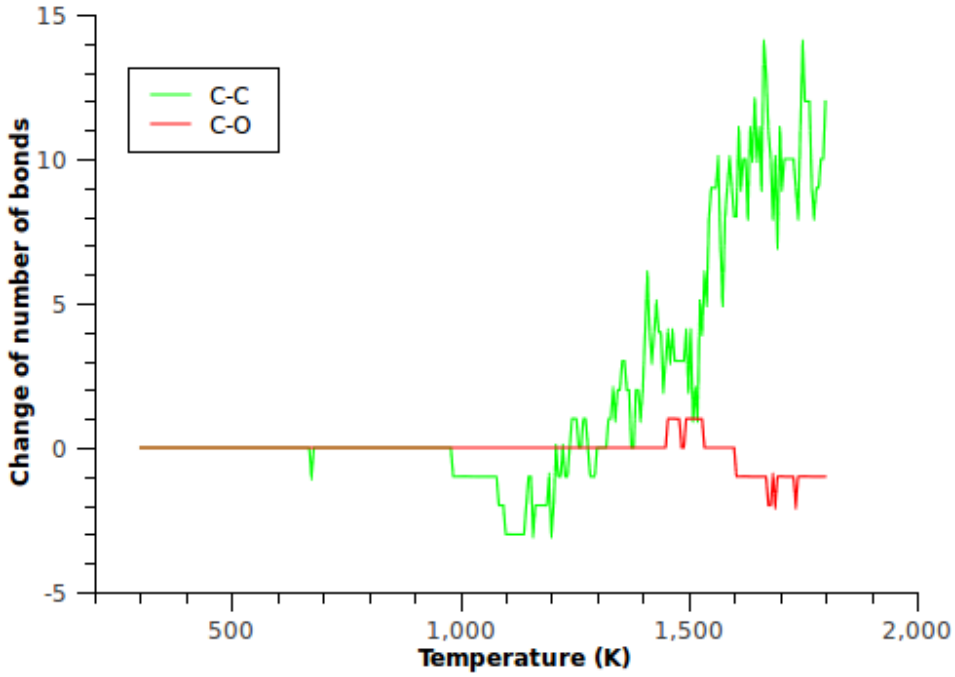

Figure 6-7. Variation of numbers of C-C and C-O covalent bonds in tetrafunctional TGDDM epoxy system during a thermal degradation modeling progress.

6.4 Effect of environment

Probability of thermal decomposition depends not only on materials themselves but also on the environment. Environment is more specifically referred as the chemical environment. Small gas molecules and moisture may have some effect on the degradation behavior of epoxies in the way of diffusion and/or reaction. In chapter 3, consequences of possible chemical reactions were studied; in chapter 5, the effects of water absorption were investigated. Here these two topics were combined to identify any interferences or relationship between chemical reaction and water diffusion.

Oxygen and water are two types of penetrants used for this part since oxygen may initiate oxidation degradation and water may lead to hydrolysis.

40 water and oxygen molecules were added into modeling system, respectively. Simulation box was equilibrated three times under NPT ensemble and transferred to reactive molecular dynamics run. The total number of molecules is 41 at room temperature. From room temperature to 1800K, heating rate is the same as the one used in Section 6.3. Variation of number of molecules in the simulation box for each system was tracked and compared in Figure 6-8.

If we choose the onset temperature where the number of molecules increases in Figure 6-8, we could gain some information on the change in T_d. When oxygen was added, one can see an oscillation in the curve starting from the beginning. The number of molecules in box with epoxy and oxygen fluctuates in a range from 38 to 41. Until 1000K, a continuous increase was observed. For the epoxy with water system, a similar curve was generated. However, T_d of epoxy and water system was lower compared to the epoxy oxygen system.

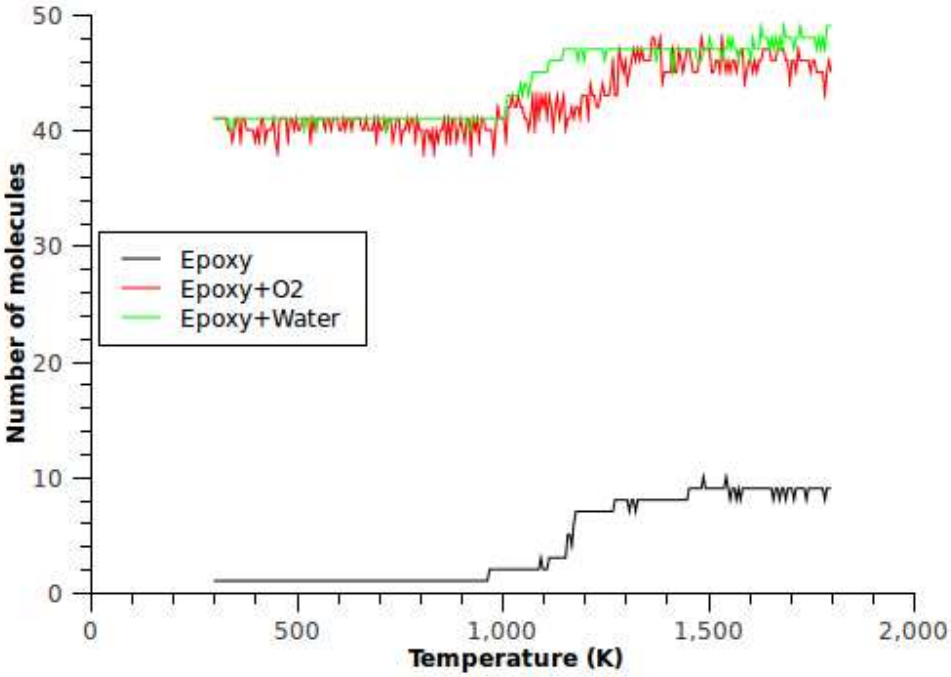

Figure 6-8. Variation of number of molecules in different system during a thermal degradation process.

To explain the change for number of molecules, the variation of C-O bonds was also tracked during the heating process. As pointed out before, ether bonds located at backbones of DGEBA epoxy are the very first bonds to be affected. From Figure 6-9, one can see all the three curves begin to go down at about 1000K. For the epoxy and water system, the number of bonds goes down faster than pure epoxy system. While in epoxy and oxygen system, the curve changes its direction at around 1500K; however, that change did not necessarily mean a formation of ether bonds. If the changes of all types of bonds were considered, one can obtain further information about this trend.

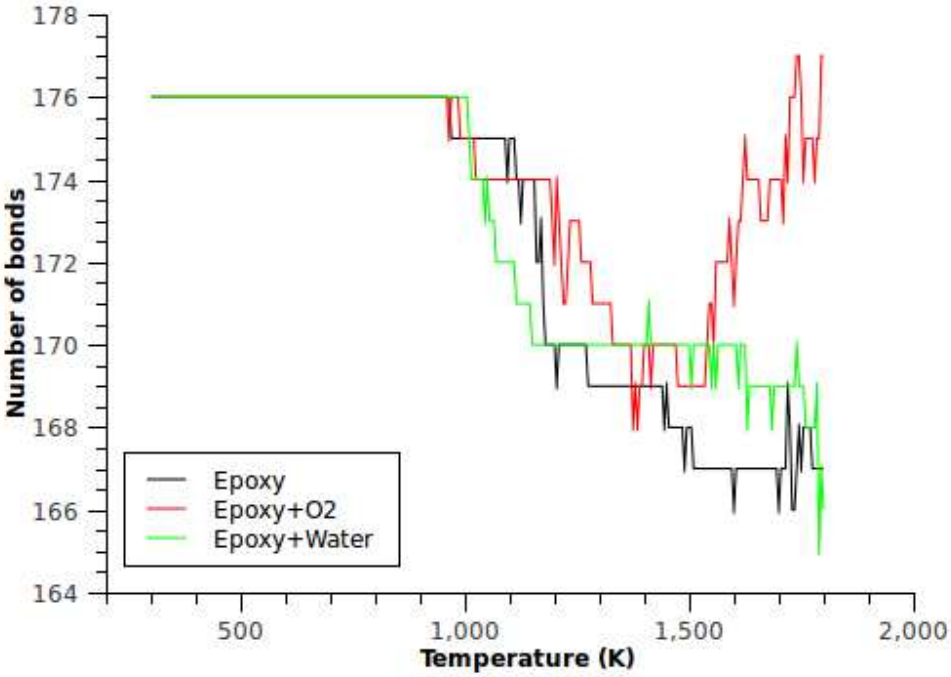

Figure 6-9. Variation of number of C-O bonds in different systems during heating.

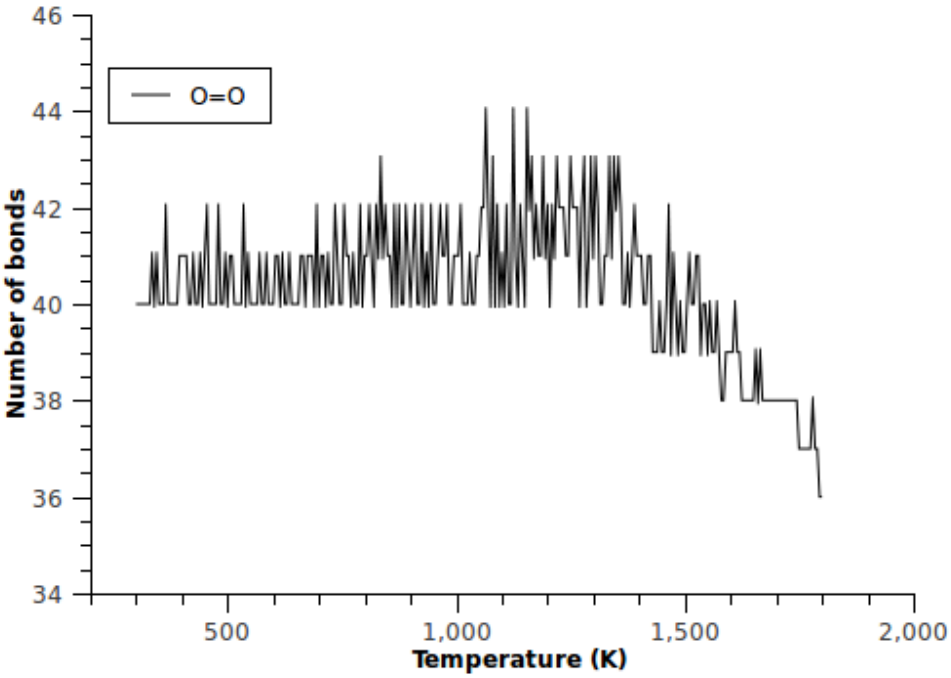

Figure 6-10. Change of O=O bonds during heating.

Figure 6-10 gives the variation of O=O bonds between two atoms in oxygen molecules. A clear oscillation pattern was recognized from 300K to about 1500K. It we recall the change of molecules in the same box shown in Figure 6-8, a similarity was discovered. Considering the high reactivity of oxygen molecules, this oscillation can be attributed to successive reactions talking place between oxygen molecules. But strangely, these reactions seem to be reversible until 1500K. In addition to that, these reactions did not destroy network structures of epoxy resins. It can be verified by the graph showing the number of total molecules.

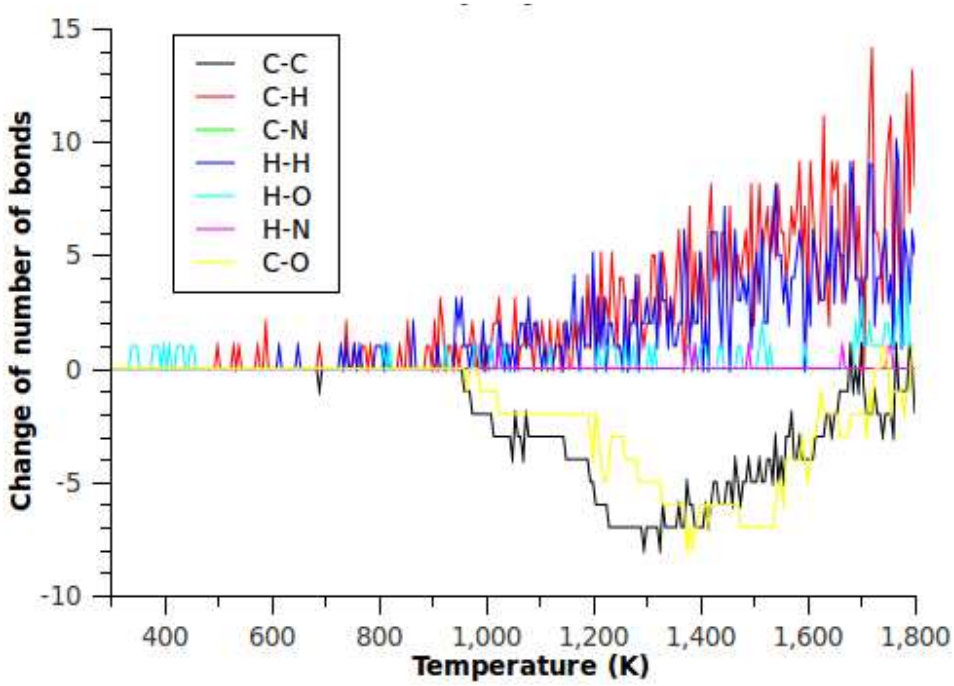

Figure 6-11. Trends of different types of bonds during a heating process.

Further analysis is made possible by displaying trends of more bond types in Figure 6-11. Among all these bonds involving oxygen atoms, we see only C-O bonds have some fluctuation under 1000K. The high reactivity of oxygen molecules initiates bonds formation and breaking mostly between oxygen molecules. Above 1500K, oxygen

started to react with carbon atoms from epoxy resins, which consumed oxygen quickly. It is worth mentioning that all the reactivity and reaction projections are based on empirical reactive force field. It may seem unreasonable that epoxy did not burn down at such a temperature as high as 1500K. The unusual behavior of epoxy and oxygen system stems from the basis of molecular dynamics. Only the force field takes account in the possibility of combustion can mimic the reaction correctly. This is a limitation of reactive force field, which may be overcome by other approaches.

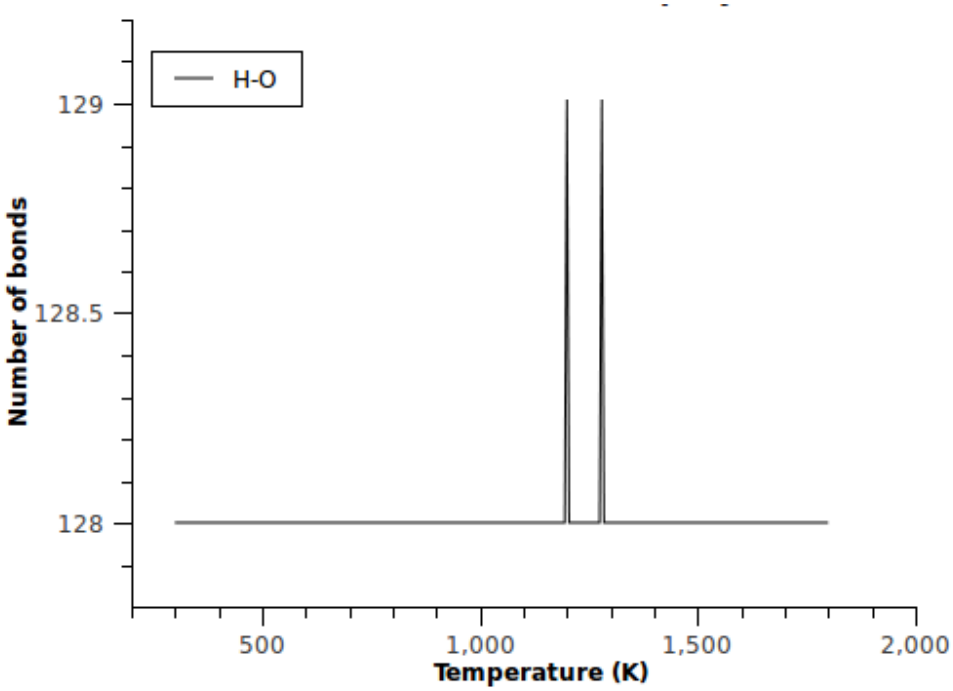

Figure 6-12. Variation of number of O-H bonds with water during thermal decomposition.

Now for system contains epoxy and water, evolution of the number of hydrogen-oxygen bonds in water molecules was shown in Figure 6-12. If the two isolated peaks were discarded, number of hydrogen-oxygen bonds remains almost unchanged. It implies that there is no reaction involving water molecules. All types of bonds were

tracked and the evolutions of their numbers are shown in Figure 6-13. One can observe a slight lowering of T_d for epoxy and water system compared to pure epoxy. This is contributed to the swelling of epoxy matrix by water, which may introduce some internal stresses to the system and make bonds vulnerable.

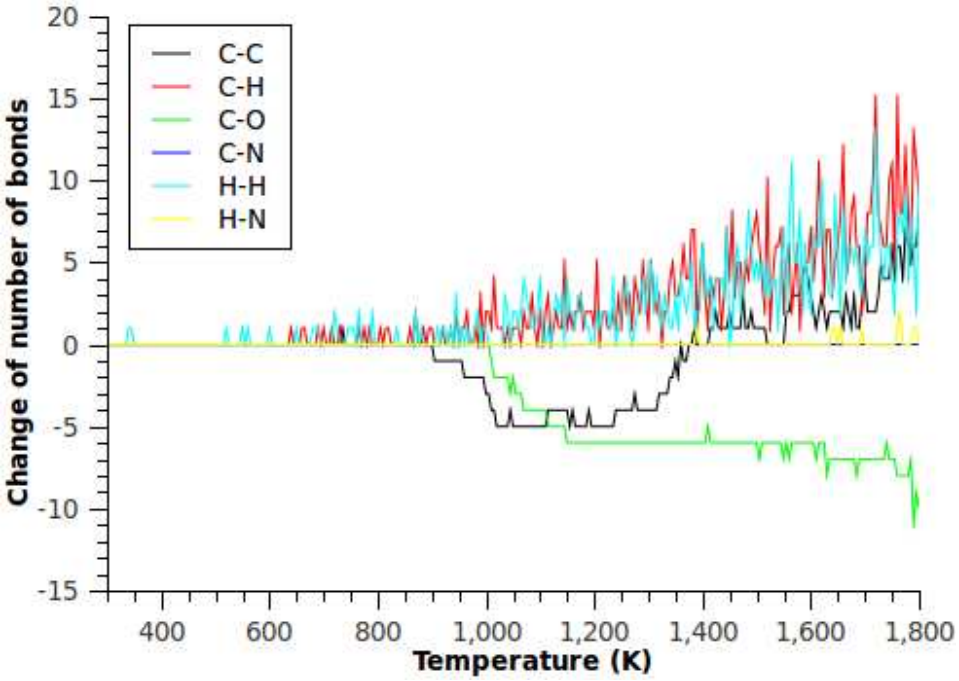

Figure 6-13. Variation of all bond types in epoxy resins during heating with the presence of water.

6.5 Conclusions

In conclusion, a reactive force field ReaxFF was used for full-atom models of difunctional and tetrafunctional epoxy resins. After carefully choosing modeling parameters, model systems were heated up from room temperature to 1800K. A higher onset temperature for thermal decomposition was observed in modeling compared to experimental measurement due to a higher heating rate. Analysis of variation of bond numbers suggested that C-O bonds were the first bonds to be cleaved during the

thermal degradation process. At the same time, rearrangement of aromatic carbon atoms took place which has little influence in network structures of epoxy resins. A comparison study of tetrafunctional epoxy resins validated that ether bonds are the key factor dominating decomposition behavior of epoxy resins.

CHAPTER 7

RECOMMENDATIONS FOR FUTURE WORKS

Based on this work, some future works could be done in several areas.

Experimental validation is always important to verify simulation results. Comparable results from simulation and experiments demonstrate the validity of models and force fields, while discrepancy can shed some light on model improvement. For this work, some experiments can be conducted to construct bulk TGDDM/DDS, bulk DGEBA/DETDA and interfacial system samples for mechanical tests and characterization. Experimental works were done in the past to characterize surfaces and interfaces between cured epoxy resins and metal, silicon wafer, concrete, glass substrate, etc. Technical approaches used to describe surfaces/interfaces included atomic force microscopy, neutron scattering, XPS, mechanical tests and so on [79, 80]. In most of these researches, epoxies components were peeled off from the other part to expose interfaces and make following characterization possible. However, if the depth of interfaces was large or the interface between two components was not visible, one can analyze the plane perpendicular to interfaces and perform an elemental analysis along the direction normal to interfaces to extract information about interfacial strength. The prerequisite for a successful elemental analysis depends on resolution of equipments, comparison of composition of two components, depth of interfaces and some other factors.

Some parameters with the simulation box can be changed to obtain samples with varied crosslinking density. While for interfacial system, one can change the degree of polymerization of one component to manipulate the depth of interfaces. For the water absorption part, experiments for the calculation of free volume, water uptake, change of T_g and modulus are feasible to carry out.

Another aspect for possible further investigation is more study on bridging quantum mechanics and molecular dynamics. Water diffusion and possible reaction is an area of great importance. Chapter 6 utilized empirical force field to approach this problem. Ab initio molecular dynamics may yield more reliable reaction probability for water absorbed epoxy. The difficulty lies on a long time scale of water diffusion, which cannot be captured by quantum mechanics.

The last one can be in the area of larger scale simulation. Coarse grained model or finite element analysis can be employed to explore problems such as interfacial crack mechanism.

REFERENCES

1. Varley, R.J., et al., *Toughening of a trifunctional epoxy system Part III. Kinetic and morphological study of the thermoplastic modified cure process.* Polymer, 2000. **41**(9): p. 3425-3436.
2. Dusek, K., M. Bleha, and S. Lunak, *Curing of Epoxide-Resins - Model Reactions of Curing with Amines.* Journal of Polymer Science Part a-Polymer Chemistry, 1977. **15**(10): p. 2393-2400.
3. Riccardi, C.C. and R.J.J. Williams, *Statistical Structural Model for the Buildup of Epoxy Amine Networks with Simultaneous Etherification.* Polymer, 1986. **27**(6): p. 913-920.
4. Liu, H., et al., *Influence of substituents on the kinetics of epoxy/aromatic diamine resin systems.* Journal of Polymer Science Part A: Polymer Chemistry, 2004. **42**(13): p. 3143-3156.
5. Watson, H., M.H. Kaunisto, and J.B. Rosenholm, *Ureidosilanes on E-glass fibres: deposition and surface characteristics.* Journal of Adhesion Science and Technology, 2002. **16**(4): p. 429-448.
6. Van Speybroeck, V., et al., *Ab initio and experimental study on thermally degradable polycarbonates: The effect of substituents on the reaction rates.* Journal of the American Chemical Society, 2001. **123**(43): p. 10650-10657.
7. Fromm, K.M. and W. Maudez, *Polar molecular precursors for alkali and alkaline earth metal clusters and low-dimensional polymer structures: the solid-state structures of [CaI(dme)(3)]I, and cis-[SrI2(diglyme)(2)] (dme = CH3OC2H4OCH3; diglyme = CH3(OC2H4)(2)OCH3).* European Journal of Inorganic Chemistry, 2003(18): p. 3440-3444.
8. Kalninsh, K.K. and A.F. Podolskii, *Quantum-chemical calculations of the structure of the triplet reaction complexes in anionic polymerization of butadiene.* Journal of Structural Chemistry, 2001. **42**(6): p. 894-905.
9. Fernandez, E.J., et al., *Heteropolynuclear complexes with the ligand Ph(2)PCH(2)SPh: Theoretical evidence for metallophilic Au-M attractions.* Chemistry-a European Journal, 2000. **6**(4): p. 636-644.
10. Halpin, J.C. and J.L. Kardos, *Halpin-Tsai equations:A review.* Polymer Engineering and Science, 1976. **16**(5): p. 344-352.
11. Mori, T. and K. Tanaka, *Average stress in matrix and average elastic energy of materials with misfitting inclusions.* Acta Metallurgica, 1973. **21**(5): p. 571-574.
12. *Amber*. Available from: http://ambermd.org/.
13. MacKerell, A.D., et al., *All-atom empirical potential for molecular modeling and dynamics studies of proteins.* Journal of Physical Chemistry B, 1998. **102**(18): p. 3586-3616.
14. Dauberosguthorpe, P., et al., *Structure and Energetics of Ligand-Binding to Proteins - Escherichia-Coli Dihydrofolate Reductase Trimethoprim, a Drug-Receptor System.* Proteins-Structure Function and Genetics, 1988. **4**(1): p. 31-47.
15. Warshel, A., *Quantum-Mechanical Consistent Force-Field (Qcff/Pi) Method - Calculations of Energies, Conformations and Vibronic Interactions of Ground and Excited-States of Conjugated Molecules.* Israel Journal of Chemistry, 1973. **11**(5): p. 709-717.

16. Warshel, A., M. Levitt, and S. Lifson, *Consistent Force Field for Calculation of Vibrational Spectra and Conformations of Some Amides and Lactam Rings.* Journal of Molecular Spectroscopy, 1970. **33**(1): p. 84-&.
17. Huo, S., I. Massova, and P.A. Kollman, *Computational alanine scanning of the 1 : 1 human growth hormone-receptor complex.* Journal of Computational Chemistry, 2002. **23**(1): p. 15-27.
18. Kollman, P.A. and B. Kuhn, *Binding of a diverse set of ligands to avidin and streptavidin: An accurate quantitative prediction of their relative affinities by a combination of molecular mechanics and continuum solvent models.* Journal of Medicinal Chemistry, 2000. **43**(20): p. 3786-3791.
19. Barth, P., T. Alber, and P.B. Harbury, *Accurate, conformation-dependent predictions of solvent effects on protein ionization constants.* Proceedings of the National Academy of Sciences of the United States of America, 2007. **104**(12): p. 4898-4903.
20. Frenkel, D. and B. Smit, *Understanding molecular simulation : from algorithms to applications*. 2nd ed. Computational science series2002, San Diego: Academic Press. xxii, 638 p.
21. Mccammon, J.A., B.R. Gelin, and M. Karplus, *Dynamics of Folded Proteins.* Nature, 1977. **267**(5612): p. 585-590.
22. Gee, R.H. and R.H. Boyd, *Small Penetrant Diffusion in Polybutadiene - a Molecular-Dynamics Simulation Study.* Polymer, 1995. **36**(7): p. 1435-1440.
23. Han, H., C.C. Gryte, and M. Ree, *Water Diffusion and Sorption in Films of High-Performance Poly(4,4'-Oxydiphenylene Pyromellitimide) - Effects of Humidity, Imidization History and Film Thickness.* Polymer, 1995. **36**(8): p. 1663-1672.
24. Helfand, E., Z.R. Wasserman, and T.A. Weber, *Brownian Dynamics Study of Polymer Conformational Transitions.* Macromolecules, 1980. **13**(3): p. 526-533.
25. Mayo, S.L., B.D. Olafson, and W.A. Goddard, *Dreiding - a Generic Force-Field for Molecular Simulations.* Journal of Physical Chemistry, 1990. **94**(26): p. 8897-8909.
26. Available from: http://accelrys.com/products/materials-studio/.
27. Sun, H., *COMPASS: An ab initio force-field optimized for condensed-phase applications - Overview with details on alkane and benzene compounds.* Journal of Physical Chemistry B, 1998. **102**(38): p. 7338-7364.
28. Andoh, H. and T. Yamamoto, *Large deformation in an amorphous polymer: Molecular dynamics simulation.* Kobunshi Ronbunshu, 1996. **53**(10): p. 660-664.
29. Ida, T., et al., *Simulation of Thermal Decomposition for Polymer Molecules.* Journal of Surface Analysis, 2005. **12**(2): p. 153-156.
30. Roe, R.J., *Md Simulation Study of Glass-Transition and Short-Time Dynamics in Polymer Liquids.* Atomistic Modeling of Physical Properties, 1994. **116**: p. 111-144.
31. Yu, K.Q., Z.S. Li, and J.Z. Sun, *Polymer structures and glass transition: A molecular dynamics simulation study.* Macromolecular Theory and Simulations, 2001. **10**(6): p. 624-633.
32. Lyulin, A.V., et al., *Strain softening and hardening of amorphous polymers: Atomistic simulation of bulk mechanics and local dynamics.* Europhysics Letters, 2005. **71**(4): p. 618-624.
33. Karlsson, G.E., U.W. Gedde, and M.S. Hedenqvist, *Molecular dynamics simulation of oxygen diffusion in dry and water-containing poly(vinyl alcohol).* Polymer, 2004. **45**(11): p. 3893-3900.
34. Yang, H., et al., *Computer simulation studies of the miscibility of poly(3-hydroxybutyrate)-based blends.* European Polymer Journal, 2005. **41**(12): p. 2956-2962.

35. Aabloo, A., M. Klintenberg, and J.O. Thomas, *Molecular dynamics simulation of a polymer-inorganic interface.* Electrochimica Acta, 2000. **45**(8-9): p. 1425-1429.
36. Abrams, C.F., N.K. Lee, and S.P. Obukhov, *Collapse dynamics of a polymer chain: Theory and simulation.* Europhysics Letters, 2002. **59**(3): p. 391-397.
37. Hamerton, I., C.R. Heald, and B.J. Howlin, *Molecular modelling of the physical and mechanical properties of two polycyanurate network polymers.* Journal of Materials Chemistry, 1996. **6**(3): p. 311-314.
38. Doherty, D.C., et al., *Polymerization molecular dynamics simulations. I. Cross-linked atomistic models for poly(methacrylate) networks.* Computational and Theoretical Polymer Science, 1998. **8**(1-2): p. 169-178.
39. Yarovsky, I. and E. Evans, *Atomistic simulation of the sol formation during synthesis of organic/inorganic hybrid materials.* Molecular Simulation, 2002. **28**(10-11): p. 993-1004.
40. Wu, C. and W. Xu, *Atomistic molecular modelling of crosslinked epoxy resin.* Polymer, 2006. **47**(16): p. 6004-6009.
41. Fan, H.B. and M.M.F. Yuen, *Material properties of the cross-linked epoxy resin compound predicted by molecular dynamics simulation.* Polymer, 2007. **48**(7): p. 2174-2178.
42. Komarov, P.V., et al., *Highly cross-linked epoxy resins: an atomistic molecular dynamics simulation combined with a mapping/reverse mapping procedure.* Macromolecules, 2007. **40**(22): p. 8104-8113.
43. Varshney, V., et al., *A molecular dynamics study of epoxy-based networks: Cross-linking procedure and prediction of molecular and material properties.* Macromolecules, 2008. **41**(18): p. 6837-6842.
44. Stevens, M.J., *Interfacial fracture between highly cross-linked polymer networks and a solid surface: Effect of interfacial bond density.* Macromolecules, 2001. **34**(8): p. 2710-2718.
45. Chiang, C.M., et al., *Etching, insertion, and abstraction reactions of atomic deuterium with amorphous silicon hydride films.* Journal of Physical Chemistry B, 1997. **101**(46): p. 9537-9547.
46. Woo, T.K., et al., *Static and ab initio molecular dynamics study of the titanium(IV)-constrained geometry catalyst (CpSiH2NH)Ti-R+ .2. Chain termination and long chain branching.* Organometallics, 1997. **16**(15): p. 3454-3468.
47. Peluso, A., R. Improta, and A. Zambelli, *Mechanism of isoprene and butadiene polymerization in the presence of CpTiCl3-MAO initiator: A theoretical study.* Macromolecules, 1997. **30**(8): p. 2219-2227.
48. Aust, J.F., et al., *Fourier-Transform Raman-Spectroscopic Studies of a Polyimide Curing Reaction.* Analytica Chimica Acta, 1994. **293**(1-2): p. 119-128.
49. Holmen, A., A. Broo, and B. Albinsson, *Ir Transition Moments of 1,3-Dimethyluracil - Linear Dichroism Measurements and Ab-Initio Calculations.* Journal of Physical Chemistry, 1994. **98**(19): p. 4998-5009.
50. Bach, R.D., et al., *A Model for Adhesion-Producing Interactions of Zinc-Oxide Surfaces with Alcohols, Amines, and Alkenes.* Journal of Adhesion Science and Technology, 1994. **8**(3): p. 249-259.
51. Pacansky, J., R.J. Waltman, and G. Pacansky, *Electron-Beam-Induced Degradation of Poly(Perfluoroethers) and Poly(Olefin Sulfones).* Chemistry of Materials, 1993. **5**(10): p. 1526-1532.

52. Albinati, A., et al., *Reaction of H-2 with Irhcl2p2 (P = P(I)Pr(3) or P(T)Bu2ph) - Stereoelectronic Control of the Stability of Molecular H-2 Transition-Metal Complexes.* Journal of the American Chemical Society, 1993. **115**(16): p. 7300-7312.
53. Fredriksson, C., et al., *Theoretical-Studies of the Aluminum Poly(P-Phenylene Vinylene) Interface.* Synthetic Metals, 1993. **57**(2-3): p. 4632-4637.
54. Goddard, W.A., et al., *Structures, Mechanisms, and Kinetics of Ammoxidation and Selective Oxidation of Propane Over the M2 Phase of MoVNbTeO Catalysts.* Topics in Catalysis, 2011. **54**(10-12): p. 659-668.
55. Fan, H.B., et al., *Investigation of moisture diffusion in electronic packages by molecular dynamics simulation.* Journal of Adhesion Science and Technology, 2006. **20**(16): p. 1937-1947.
56. Fukuda, M. and S. Kuwajima, *Molecular-dynamics simulation of moisture diffusion in polyethylene beyond 10 ns duration.* Journal of Chemical Physics, 1997. **107**(6): p. 2149-2159.
57. Hofmann, D., et al., *Detailed-atomistic molecular modeling of small molecule diffusion and solution processes in polymeric membrane materials.* Macromolecular Theory and Simulations, 2000. **9**(6): p. 293-327.
58. Lin, Y.C. and X. Chen, *Investigation of moisture diffusion in epoxy system: Experiments and molecular dynamics simulations.* Chemical Physics Letters, 2005. **412**(4-6): p. 322-326.
59. Soles, C.L. and A.F. Yee, *A discussion of the molecular mechanisms of moisture transport in epoxy resins.* Journal of Polymer Science Part B-Polymer Physics, 2000. **38**(5): p. 792-802.
60. Tamai, Y., H. Tanaka, and K. Nakanishi, *Molecular Simulation of Permeation of Small Penetrants through Membranes .1. Diffusion-Coefficients.* Macromolecules, 1994. **27**(16): p. 4498-4508.
61. Dermitzaki, E., et al., *Structure Property Correlation of epoxy resins under the influence of moisture and comparison of Diffusion coefficient with MD-simulations*, in *9th. Int. Conf. on Thermal, Mechanical and Multiphysics Simulation and Experiments in Micro-Electronics and Micro-Systems EuroSimE*2008.
62. Comyn, J., C.L. Groves, and R.W. Saville, *Durability in High Humidity of Glass-to-Lead Alloy Joints Bonded with an Epoxide Adhesive.* International Journal of Adhesion and Adhesives, 1994. **14**(1): p. 15-20.
63. Cantor, B., P. Grant, and H. Assender, *Aerospace materials*. Series in materials science and engineering2001, Bristol ; Philadelphia: Institute of Physics. xii, 312 p.
64. Shepherd, J.E., 2006, Georgia Institue of Technology.
65. Rappe, A.K. and W.A. Goddard, *Charge Equilibration for Molecular-Dynamics Simulations.* Journal of Physical Chemistry, 1991. **95**(8): p. 3358-3363.
66. Davis, S., et al., *Molecular dynamics simulation of zirconia melting.* Central European Journal of Physics, 2010. **8**(5): p. 789-797.
67. Jones, F.R., et al., *Thermodynamic and mechanical properties of amine-cured epoxy resins using group interaction modelling.* Journal of Materials Science, 2006. **41**(20): p. 6631-6638.
68. Liu, H., *Quantitative structure–property relationships for composites: prediction of glass transition temperatures for epoxy resins.* Polymer, 2004. **45**(6): p. 2051-2060.
69. Wu, C.F. and W.J. Xu, *Atomistic molecular modelling of crosslinked epoxy resin.* Polymer, 2006. **47**(16): p. 6004-6009.

70. Frankland, S.J.V., et al., *The stress–strain behavior of polymer–nanotube composites from molecular dynamics simulation.* Composites Science and Technology, 2003. **63**(11): p. 1655-1661.
71. Liu, J., et al., *Molecular dynamics simulation for insight into microscopic mechanism of polymer reinforcement.* Physical Chemistry Chemical Physics, 2011. **13**(2).
72. Plimpton, S., *Fast Parallel Algorithms for Short-Range Molecular-Dynamics.* Journal of Computational Physics, 1995. **117**(1): p. 1-19.
73. Humphrey, W., A. Dalke, and K. Schulten, *VMD - Visual Molecular Dynamics.* Journal of Molecular Graphics and Modelling, 1996. **14**: p. 33-38.
74. Clancy, T.C., et al., *Molecular modeling for calculation of mechanical properties of epoxies with moisture ingress.* Polymer, 2009. **50**(12): p. 2736-2742.
75. Chen, Z., J.C. Fothergill, and S.W. Rowe, *The effect of water absorption on the dielectric properties of epoxy nanocomposites.* Dielectrics and Electrical Insulation, IEEE Transactions on, 2008. **15**(1): p. 106-117.
76. Dhakal, H.N., Z.Y. Zhang, and M.O.W. Richardson, *Effect of water absorption on the mechanical properties of hemp fibre reinforced unsaturated polyester composites.* Composites Science and Technology, 2007. **67**(7-8): p. 1674-1683.
77. Erickson, K.L., *Thermal decomposition mechanisms common to polyurethane, epoxy, poly(diallyl phthalate), polycarbonate and poly(phenylene sulfide).* Journal of Thermal Analysis and Calorimetry, 2007. **89**(2): p. 427-440.
78. Levchik, S.V., et al., *Epoxy resins cured with aminophenylmethylphosphine oxide-II. Mechanism of thermal decomposition.* Polymer Degradation and Stability, 1998. **60**: p. 169-183.
79. Woerdeman, D.L., et al., *Interpreting the signal from a localized fluorescence sensor: a study by angle-resolved XPS and dynamic SIMS.* Journal of Colloid and Interface Science, 2003. **262**(2): p. 594-602.
80. Li, L. and X. Wenting. *XPS study on epoxy/Ni interface*. in *Electronic Packaging Technology & High Density Packaging, 2009. ICEPT-HDP '09. International Conference on*. 2009.